SURFACE DISTURBANCES GENERATED BY FLUID FLOW PAST AN OBSTACLE OR OVER TOPOGRAPHY AS PREDICTED BY THE KORTEWEG-DE VRIES AND THE EULER EQUATIONS

Quentin A. Robinson

A dissertation submitted to the faculty at the University of North Carolina at Chapel Hill in partial fulfillment of the requirements for the degree of Doctor of Philosophy in the Department of Mathematics.

Chapel Hill
2018

Approved by:

Roberto Camassa

Jeremy Marzuoula

Richard McLaughlin

David Adalsteinsson

Gregory Forest

ABSTRACT

Quentin A. Robinson: SURFACE DISTURBANCES GENERATED BY
FLUID FLOW PAST AN OBSTACLE OR OVER TOPOGRAPHY AS
PREDICTED BY THE KORTEWEG-DE VRIES AND THE EULER
EQUATIONS
(Under the direction of Roberto Camassa, Jeremy Marzuola, and Richard
McLauglin)

The linearized Euler equations and the forced Korteweg-de Vries equation are investigated analytically and numerically as models for the behavior of the surface of a fluid flowing over topography and past an obstacle. Dispersionless and linearized variations of the fKdV equation are compared with the full fKdV equation in various parameter regimes. Ways in which information gained from various approximations to the forced Korteweg-de Vries (fKdV) equations predict the behavior of the solution of the full equation are explored. A critical Froude number parameter value above, which stationary solutions exist, is determined and the stability of the stationary solutions is investigated.

The behavior of the dispersionless fKdV equation, which is equivalent to a forced, inviscid Burgers equation, is investigated extensively using the method of characteristics. An exact, analytically obtained solution to the dispersionless, nonlinear approximation to fKdV is derived as well as the amplitude and propagation speed of the shocks obtained from the same approximation.

The behaviors of the fKdV equation and its variants are investigated and compared for forcing constant in time and forcing with oscillating amplitude and position. A Wentzel, Kramers, Brillouin approximation is given for dispersionless KdV with low frequency amplitude oscillation in the forcing function. An averaging approximation is given for dispersionless KdV with high frequency amplitude oscillation in the forcing function.

The Inverse Scattering Transform is investigated as a diagnostic tool for the behavior of the fKdV equation. The numerical results indicate the emergence of negative eigenvalues of the Schrödinger operator correspond with the emergence of solitons in the solution of the fKdV equation. WKB analysis is used as an application of inverse scattering theory to determine a relationship between

the amplitude of the shock in the dispersionless approximation to fKdV and the amplitude of the upstream propagating solitary waves generated by the full equation. All of this information together provides a means of predicting which combinations of parameter values will result in the generation of upstream propagating solitons as well as a novel means of predicting the frequency of soliton generation. Multiple numerical methods and their implementations for solving these equations are discussed.

Experiments are carried out in a water recirculating flume and a wave tank. Phenomena predicted by the equations are observed in the experiments and results are compared quantitatively.

To Mom and Dad.

ACKNOWLEDGMENTS

I would like to thank my advisors Roberto Camassa, Jeremy Marzuola, and Richard McLaughlin for their guidance and mentorship. I would also like to thank my committee members David Adalsteinsson and Gregory Forest for their encouragement and support throughout this process.

TABLE OF CONTENTS

LIST OF FIGURES

LIST OF TABLES

CHAPTER 1

Introduction

Studies of surface disturbances generated by fluid flow past obstacles or over topography of various forms is a rather classical problem, and we attempt to give a broad overview of the history of the problem here. Note that this reference list is by no means complete and that many articles included in this discussion contain many other relevant citations to important works on the topics. The linear response to a background current for water waves driven by gravity and surface tension was studied long ago and is present in now classical texts including [16, 24]. We will derive and perform the bulk of our analysis on the forced Korteweg-de Vries equation (fKdV) and approximations to this equation. Flows in shallow water of variable bottoms have been studied in various contexts as a forced Korteweg-de Vries equation in [2, 10, 22, 7, 6], with a greater focus on numerical studies in [5, 13]. Analysis was done for flow past cylindrical obstacles using the method of successive images in for instance Havelock [11, 12], and further nonlinear studies in the gravity wave case were undertaken in works such as [23, 4, 21]. Here we will also derive a dispersion relation for water waves that includes effects from surface tension. Capillary effects have been considered in [8, 18, 9] and others.

1.1   The Dispersion Relation

To begin, we will define the material derivative $\frac{D}{Dt}$ as follows:

$$\frac{DF}{Dt} \equiv \frac{\partial F}{\partial t} + \underline{u} \cdot \nabla F$$

where t is time and $\underline{u}$ is the velocity vector. Newton's second law of motion for a fluid modeled as a continuum, considering forces that arise from action at a distance without physical contact and forces that are exerted on an area element by the surroundings through direct contact (body forces

1

and surface forces, respectively), can be written as

$$\rho \frac{Du_i}{Dt} = \rho g_i + \frac{\partial \tau_{ij}}{\partial x_j}$$

where ρ is density, g is gravity, and τ_{ij} represent the force in the j direction on a surface with a normal in the i direction. If we consider an inviscid, incompressible, constant density, Newtonian fluid, the dominant surface force (the only force we will consider in this section) comes from pressure, and $\frac{\partial \tau_{ij}}{\partial x_j}$ becomes $-\nabla p$. The negative sign arises because the normal is positive in the outward direction, whereas positive pressure is generally regarded as a compression force pushing inward. So now we have

$$\rho \frac{D\underline{u}}{Dt} = -\nabla p + \rho \mathbf{g}.$$

We now abandon our use of the material derivative notation and write

$$\rho \left(\frac{\partial \underline{u}}{\partial t} + \underline{u} \cdot \nabla \underline{u} \right) = -\nabla p + \rho \mathbf{g}.$$

We will consider small amplitude waves and assume that all nonlinear terms will be negligibly small, so we disregard them and write

$$\rho \frac{\partial \underline{u}}{\partial t} = -\nabla p + \rho \mathbf{g}.$$

We define our coordinate system so that gravity acts only in the negative z direction and assuming hydrostatic equilibrium we come to

$$\rho \frac{\partial \underline{u}}{\partial t} = -\nabla p - \rho g \hat{z}.$$

We may also include our incompressible assumption as another equation

$$\nabla \cdot \underline{u} = 0.$$

We will call $z = 0$ the undisturbed surface height and $z = h(x,t)$ will represent the position of the free surface in two spatial dimensions. We will take the pressure at the free surface to be atmospheric

$$p\Big(x, h(x,t), t\Big) = p_{atm}.$$

Say that at the surface the velocity of the fluid is equal to the change in h with respect to time for any fixed x, and that all movement is strictly in the vertical direction. This is equivalent to a kinematic boundary condition, in which a fluid particle at the surface never leaves the surface,

$$\underline{u}_{surface} = h_t \hat{k} = \begin{pmatrix} 0 \\ h_t \end{pmatrix} = \underline{u}\big|_{z=h(x,t)\forall x}.$$

It follows that at the surface

$$(h_t \hat{k}) \cdot \hat{n} = \begin{pmatrix} u \\ w \end{pmatrix} \cdot \hat{n}.$$

The slope of the surface at a point is given by

$$\Big(1, \frac{dh}{dx}\Big).$$

We normalize this vector quantity using a Euclidian norm so that the resulting magnitude is one,

$$\frac{(1, \frac{dh}{dx})}{\sqrt{1 + (\frac{dh}{dx})^2}}.$$

The unit vector normal to the fluid surface is thus given by

$$\hat{n} = \frac{(-\frac{dh}{dx}, 1)}{\sqrt{1 + (\frac{dh}{dx})^2}}.$$

Given

$$(h_t \hat{k}) \cdot \hat{n} = \begin{pmatrix} u \\ w \end{pmatrix} \cdot \hat{n},$$

we find

$$\frac{\partial h}{\partial t} = -u \frac{\partial h}{\partial x} + w.$$

3

Therefore at the surface,

$$\frac{\partial h}{\partial t} + u \frac{\partial h}{\partial x} = w\left(x, h(t), t\right),$$

and we now have the system

$$\begin{cases} \rho \frac{\partial \underline{u}}{\partial t} = -\nabla p - \rho g \hat{z}, \\ \quad \nabla \cdot \underline{u} = 0, \\ \frac{\partial h}{\partial t} + u \frac{\partial h}{\partial x} = w \qquad \text{at } z = h. \end{cases}$$

Here we introduce a velocity potential,

$$u = \frac{\partial \varphi}{\partial x}, \qquad w = \frac{\partial \varphi}{\partial z}.$$

Our incompressibility condition becomes Laplace's equation,

$$\nabla^2 \varphi = 0,$$

and the surface condition becomes

$$\frac{\partial h}{\partial t} + \frac{\partial \varphi}{\partial x} \frac{\partial h}{\partial x}\bigg|_{z=h} = \frac{\partial \varphi}{\partial z}\bigg|_{z=h}.$$

Continuing with our small amplitude assumption, we drop the nonlinear term,

$$\frac{\partial h}{\partial t} = \frac{\partial \varphi}{\partial z}\bigg|_{z=h},$$

and evaluate this expression at $z = 0$. We now integrate over the depth of the fluid and obtain Bernoulli's equation,

$$\rho \varphi_t + p = -\rho g h + p_a,$$

where p_a is atmospheric pressure. At the surface $p = p_a$ and for convenience we will say that $p_a = 0$. Here we will impose an infinite depth boundary condition. Our system is now given by

$$
\begin{cases}
\nabla^2 \varphi = 0 \\
\frac{\partial h}{\partial t} = \frac{\partial \varphi}{\partial z} & \text{at } z = 0 \\
\varphi_t = -gh & \text{at } z = 0 \\
\varphi \to 0 & z \to -\infty
\end{cases}
$$

We will solve this system by separation of variables. We begin by inserting the assumption that the solution $\varphi(x, z, t)$ can be written as the product of functions that depend on x, z, and t only,

$$
\varphi = F(t)G(x)H(z),
$$

and apply the Laplace operator,

$$
\nabla^2 \varphi = F(t)H(z)G''(x) + F(t)G(x)H''(z) = 0.
$$

Seeking a nontrivial solution we assume $F(t) \neq 0$,

$$
H(z)G''(x) + G(x)H''(z) = 0,
$$

and arrive at an equation in which a function of one variable is equal to a function of a single, different variable. We conclude both functions must be equal to the same constant λ,

$$
\frac{G''(x)}{G(x)} = -\frac{H''(z)}{H(z)} = \lambda,
$$

and solve the resulting equations separately

$$
G''(x) - \lambda G(x) = 0, \qquad H''(z) + \lambda H(z) = 0.
$$

Beginning with $G(x)$, we choose to let $\lambda = -k^2$ and find

$$
G(x) = A \cos kx + B \sin kx.
$$

5

We now solve for $H(z)$:

$$H(z) = Ce^{kz} + De^{-kz}.$$

The infinite depth boundary condition demands $D = 0$. Taking surface conditions into account gives

$$\frac{\partial h}{\partial t} = kF(t)\Big[A\cos kx + B\sin kx\Big]Ce^{kz} \tag{1.1}$$

and

$$F'(t)Ce^{kz}\Big[A\cos kx + B\sin kx\Big] = -gh(x,z,t). \tag{1.2}$$

Differentiating (1.2) with respect to t and combining it with (1.1) obtains

$$kF(t)\Big[A\cos kx + B\sin kx\Big]Ce^{kz} = \frac{-Ce^{kz}}{g}F''(t)\Big[A\cos kx + B\sin kx\Big],$$

which simplifies to

$$F''(t) + kgF(t) = 0,$$

and has solution

$$F(t) = E\cos\left(t\sqrt{kg}\right) + I\sin\left(t\sqrt{kg}\right).$$

We now know $\varphi(x,z,t)$ is given by

$$\varphi(x,z,t) = \left(E\cos\left(\sqrt{kg}t\right) + I\sin\left(\sqrt{kg}t\right)\right)\left(A\cos kx + B\sin kx\right)(Ce^{kz}),$$

which can be written as

$$\varphi(x,z,t) = \frac{Ce^{kz}}{2}\Big(\tilde{A}\cos\left(kx - \sqrt{kg}t\right) + \tilde{B}\cos\left(kx + \sqrt{kg}t\right)$$
$$+ \tilde{C}\sin\left(kx - \sqrt{kg}t\right) + \tilde{D}\sin\left(kx + \sqrt{kg}t\right)\Big)$$

where

$$\tilde{A} = AE + BI, \qquad \tilde{B} = AE - BI,$$
$$\tilde{C} = BE - AI, \qquad \tilde{D} = BE + AI.$$

We now have an expression for φ that satisfies Laplace's equation and the infinite depth boundary

condition. To find h and $\underline{u}$ we use our surface boundary condition and the definition of φ. Recall that at $z = 0$

$$\frac{\partial h}{\partial t} = \frac{Ck}{2}\left(\tilde{A}\cos(kx - \sqrt{kg}t) + \tilde{B}\cos\left(kx + \sqrt{kg}t\right)\right.$$
$$\left. + \tilde{C}\sin\left(kx - \sqrt{kg}t\right) + \tilde{D}\sin\left(kx + \sqrt{kg}t\right)\right),$$

which implies

$$h = \frac{C}{2}\sqrt{\frac{k}{g}}\left[\tilde{B}\sin\left(kx + \sqrt{kg}t\right) - \tilde{D}\cos\left(kx + \sqrt{kg}t\right)\right.$$
$$\left. - \tilde{A}\sin\left(kx - \sqrt{kg}t\right) + \tilde{C}\cos\left(kx - \sqrt{kg}t\right)\right].$$

It follows from the definition of φ that

$$u = \frac{Cke^{kz}}{2}\left[\tilde{C}\cos(kx - \omega t) + \tilde{D}\cos\left(kx + \omega t\right)\right.$$
$$\left. - \tilde{A}\sin\left(kx - \omega t\right) - \tilde{B}\sin\left(kx + \omega t\right)\right]$$

and

$$w = \frac{Cke^{kz}}{2}\left[\tilde{A}\cos(kx - \omega t) + \tilde{B}\cos\left(kx + \omega t\right)\right.$$
$$\left. + \tilde{C}\sin\left(kx - \omega t\right) + \tilde{D}\sin\left(kx + \omega t\right)\right],$$

where the dispersion relation for deep water gravity waves is $\omega(k) = \sqrt{kg}$.

1.1.1 Surface Tension

In the previous section when deriving equations for fluid motion we considered only body forces and surface forces. In this section we shall also consider forces that sometimes appear at the interface between fluids and act along a line (line forces). To begin our discussion, let us consider a taught string with some curvature. Near a point x, the tension in the string is given by $T(x - \delta x)$ to the left of the string and $T(x + \delta x)$ to the right of the point. The direction of the force is given by the vector

$$\pm\begin{pmatrix} 1 \\ f'(x \pm \delta x) \end{pmatrix}$$

where f represents the position of the string. We normalize this and get a force vector

$$F_T = \frac{\pm 1}{\sqrt{1 + f'^2}} \begin{pmatrix} 1 \\ f'(x \pm \delta x) \end{pmatrix} T(x \pm \delta x).$$

The sum of the forces a distance δx to the left and right of the point x is given by

$$\sum F_T = T \begin{pmatrix} \frac{-1}{\sqrt{1+f'^2}} - \frac{\delta x f' f''}{(1+f'^2)^{3/2}} + \cdots \\ \frac{-f'}{\sqrt{1+f'^2}} + \delta x \frac{\sqrt{1+f'^2}f'' + f' \frac{2f' f''}{2\sqrt{1+f'^2}}}{1+f'^2} + \cdots \end{pmatrix}$$
$$+ T \begin{pmatrix} \frac{1}{\sqrt{1+f'^2}} - \frac{\delta x f' f''}{(1+f'^2)^{3/2}} + \cdots \\ \frac{f'}{\sqrt{1+f'^2}} + \delta x \frac{\sqrt{1+f'^2}f'' - f' \frac{2f' f''}{2\sqrt{1+f'^2}}}{1+f'^2} + \cdots \end{pmatrix},$$

which simplifies to

$$\sum F_T \approx 2T\, \delta x\, \frac{f''}{(1 + f'^2)^{3/2}} \begin{pmatrix} -f' \\ 1 \end{pmatrix}.$$

At this point we note that the function f is analogous to the position of our fluid surface and replace it with h,

$$2T\, \delta x\, \frac{\frac{\partial^2 h}{\partial x^2}}{(1 + (\frac{\partial h}{\partial x})^2)^{3/2}} \begin{pmatrix} -\frac{\partial h}{\partial x} \\ 1 \end{pmatrix}.$$

We dot the tension vector with the unit vector normal to the fluid surface,

$$\hat{n} = \frac{(-\frac{dh}{dx}, 1)}{\sqrt{1 + (\frac{dh}{dx})^2}},$$

and get

$$2T\, \delta x\, \frac{h_{xx}}{1 + h_x^2}.$$

We absorb the dimensionless denominator and the coefficient 2 into the term T, and our system becomes

$$\begin{cases} \nabla^2 \varphi = 0 \\ \frac{\partial h}{\partial t} = \frac{\partial \varphi}{\partial z} & \text{at } z = 0 \\ \varphi_t = -gh + \frac{T}{\rho} h_{xx} & \text{at } z = 0 \\ \varphi \to 0 & z \to -\infty \end{cases}$$

8

We will again assume separability. Before taking into account the new boundary condition we still have

$$\varphi(x, z, t) = F(t)G(x)H(z),$$

$$G(x) = A\cos kx + B\sin kx,$$

and

$$H(z) = Ce^{kz}.$$

We next incorporate the boundary condition affected by the inclusion of surface tension,

$$F'(t)Ce^{kz}\Big[A\cos kx + B\sin kx\Big] = -gh(x, z, t) + \frac{T}{\rho}\frac{\partial^2 h}{\partial x^2},$$

and solve for h:

$$h = -\frac{C\rho}{g\rho + k^2 T}e^{kz}F'(t)\Big[A\cos kx + B\sin kx\Big] + \alpha e^{\sqrt{\frac{g\rho}{T}}x} + \beta e^{-\sqrt{\frac{g\rho}{T}}x}.$$

Applying the other surface boundary condition reveals

$$F(t) = \gamma\cos\left(t\sqrt{gk + \frac{T}{\rho}k^3}\right) + \varepsilon\sin\left(t\sqrt{gk + \frac{T}{\rho}k^3}\right),$$

and we have a solution

$$\varphi = \left[\gamma\cos\left(t\sqrt{gk + \frac{T}{\rho}k^3}\right) + \varepsilon\sin\left(t\sqrt{gk + \frac{T}{\rho}k^3}\right)\right]\cdot\Big[A\cos kx + B\sin kx\Big]\cdot\Big[Ce^{kz}\Big],$$

which we can write

$$\varphi = \frac{Ce^{kz}}{2}\Big[\tilde{A}\cos(kx - \omega t) + \tilde{B}\cos(kx + \omega t) + \tilde{C}\sin(kx - \omega t) + \tilde{D}\sin(kx + \omega t)\Big].$$

This implies

$$u = \frac{Cke^{kz}}{2}\Big[-\tilde{A}\sin(kx - \omega t) - \tilde{B}\sin(kx + \omega t) + \tilde{C}\cos(kx - \omega t) + \tilde{D}\cos(kx + \omega t)\Big]$$

9

and

$$w = \frac{Cke^{kz}}{2}\left[\tilde{A}\cos{(kx - \omega t)} + \tilde{B}\cos{(kx + \omega t)} + \tilde{C}\sin{(kx - \omega t)} + \tilde{D}\sin{(kx + \omega t)}\right],$$

where now

$$\tilde{A} = A\gamma + B\varepsilon \qquad \tilde{B} = A\gamma - B\varepsilon$$

$$\tilde{C} = B\gamma - A\varepsilon \qquad \tilde{D} = B\gamma + A\varepsilon$$

and

$$\omega(k) = \sqrt{gk + \frac{T}{\rho}k^3},$$

where $\omega(k) = \sqrt{gk + \frac{T}{\rho}k^3}$ is our dispersion relation for gravity-capillary water waves [24].

1.2   Korteweg-de Vries

1.2.1   Derivation

Following work by Newell [20], let us consider a fluid in a coordinate system with a horizontal (x) direction and a vertical (z) direction. We will assume flow to be irrotational and a velocity field $\underline{u}(x, z, t)$ in a domain bounded by $z = -h$ and a free surface $z = \zeta(x, t)$. We introduce a velocity potential $\underline{u} = \nabla\phi$.

We assume a typical wavelength λ is large when compared to the undisturbed fluid depth, $h^2/\lambda^2 = \varepsilon \ll 1$. We also assume a typical wave amplitude a is small compared with the undisturbed fluid depth i.e., $a/h = \alpha \ll 1$. We rescale the following variables:

$$x = \lambda x^*, \qquad z = hz^*, \qquad t = \frac{\lambda}{\sqrt{gh}}t^*, \qquad \zeta = a\zeta^*, \qquad \phi = \frac{a}{h}\lambda\sqrt{gh}\phi^*, \qquad h = hh^* \qquad (1.3)$$

where asterisks denote rescaled, dimensionless quantities. These asterisks will be dropped going forward. With these scalings, the equations of continuity, the boundary condition on the normal velocity at $z = -h$, the continuity of normal stress (pressure) at the free surface (Bernoulli's equation), and the free surface condition that equates the normal velocity of a particle at the surface

10

with the normal velocity of the surface are:

$$\phi_{zz} + \varepsilon\phi_{xx} = 0, \tag{1.4}$$

$$\phi_z = 0, \quad \text{at } z = -1, \tag{1.5}$$

$$\phi_t + \zeta + \frac{1}{2}\alpha\phi_x^2 + \frac{1}{2}\frac{\alpha}{\varepsilon}\phi_z^2 = 0 \quad \text{at } z = \alpha\zeta, \tag{1.6}$$

$$\zeta_t + \alpha\phi_x\zeta_x = \frac{1}{\varepsilon}\phi_z \quad \text{at } z = \alpha\zeta \tag{1.7}$$

The rescaled Laplace equation admits a power series solution. We will write ϕ as a power series in $(z+1)$,

$$\phi = \sum_{n=0}^{\infty}(z+1)^n\varphi_n(x,t).$$

Note here that $\varphi_n(x,t)$ does not depend on z. Recall the boundary condition $\phi_z = 0$ at $z = -1$. With this in mind we consider

$$\phi_z = \sum_{n=1}^{\infty}n(z+1)^{n-1}\varphi_n(x,t),$$

and can conclude that $\varphi_1(x,t) = 0$. We now plug this series into the Laplace equation,

$$\sum_{n=0}^{\infty}\left[(n+2)(n+1)(z+h)^n\varphi_{n+2} + \varepsilon(z+h)^n\varphi_{n_{xx}}\right] = 0.$$

This equation implies the recursive relationship,

$$(n+2)(n+1)\varphi_{n+2} + \varepsilon\varphi_{n_{xx}} = 0,$$

which, together with our discovery that $\varphi_1 = 0$, implies that all odd terms in the series are zero. Using this relation we obtain

$$\varphi_2 = \frac{-\varepsilon\varphi_{0_{xx}}}{(0+2)(0+1)} = \frac{-\varepsilon\varphi_{0_{xx}}}{2}$$

and

$$\varphi_4 = \frac{-\varepsilon\varphi_{2_{xx}}}{(2+2)(2+1)} = \frac{\varepsilon^2\varphi_{0_{xxxx}}}{2(2+2)(2+1)} = \frac{\varepsilon^2\varphi_{0_{xxxx}}}{24}.$$

11

Now let

$$F(x,t) = \varphi_0(x,t).$$

This gives us a series expression for ϕ,

$$\phi(x,z,t) = F(x,t) - \frac{\varepsilon}{2}(z+h)^2 F_{xx}(x,t) + \frac{\varepsilon^2}{24}(z+h)^4 F_{xxxx} + \cdots . \qquad (1.8)$$

Here we are interested in the limit in which nonlinearity (measured by α) and dispersion (measured by ε) are both small and balance. First we expand ϕ about $z = 0$. The value of ϕ at the fluid surface is given by

$$\phi(x,z=\alpha\zeta,t) = \phi|_{z=0} + (\alpha\zeta)\phi_z|_{z=0} + \frac{(\alpha\zeta)^2}{2}\phi_{zz}|_{z=0} + \cdots .$$

Setting $O(\alpha) = O(\varepsilon)$, keeping in mind that ζ is $O(1)$ and that α and ε are small, plugging this expansion into (1.6) and (1.7), using (1.8) to substitute for ϕ_z in the first equation, and dropping all terms $O(\varepsilon^2)$ or higher yields

$$\phi_t + \zeta + \frac{1}{2}\alpha\phi_x^2 = 0, \quad z = 0 \qquad (1.9)$$

and

$$\zeta_t + \alpha(\phi_x\zeta)_x = \frac{1}{\varepsilon}\phi_z, \quad z = 0, \qquad (1.10)$$

where

$$\frac{1}{\varepsilon}\phi_z = -F_{xx} + \frac{\varepsilon}{6}F_{xxxx}.$$

In this limit the dispersion, which comes from the higher order derivatives on F occurs at a level which can balance the tendency of the wave to break. Note from (1.8)

$$\phi_x = F_x - \frac{\varepsilon}{2}(z+1)^2 F_{xxx} + O(\varepsilon^2).$$

Writing (1.10) in terms of F gives

$$\zeta_t + \alpha\left(\left(F_x - \frac{\varepsilon}{2}F_{xxx}\right)\zeta\right)_x = -F_{xx} + \frac{\varepsilon}{6}F_{xxxx}.$$

12

Discarding terms of order ε^2 obtains

$$\zeta_t + \alpha(\zeta F_x)_x = -F_{xx} + \frac{\varepsilon}{6} F_{xxxx}.$$

We next solve (1.9) for ζ

$$\zeta = -\phi_t - \frac{1}{2}\alpha\phi_x^2,$$

insert (1.8), and discard terms of order ε^2,

$$\zeta = -\left(F - \frac{\varepsilon}{2}F_{xx}\right)_t - \frac{1}{2}\alpha\left(F_x - \frac{\varepsilon}{2}F_{xxx}\right)^2 = -F_t + \frac{1}{2}\left(\varepsilon F_{xxt} - \alpha F_x^2\right).$$

Substituting this and (1.8) into (1.10) gives

$$\left(-F_t + \frac{1}{2}(\varepsilon F_{xxt} - \alpha F_x^2)\right)_t + \alpha\left(\left(-F_t + \frac{\varepsilon}{2}(F_{xxt} - F_x^2)\right)F_x\right)_x = -F_{xx} + \frac{\varepsilon}{6}F_{xxxx}.$$

After applying derivatives we arrive at

$$-F_{tt} + \left(\frac{\varepsilon}{2}F_{xxtt} - \alpha F_x F_{xt}\right) + \alpha\left(-F_x F_t + \frac{\varepsilon}{2}\left(F_x F_{xxt} - F_x^3\right)\right)_x = -F_{xx} + \frac{\varepsilon}{6}F_{xxxx}.$$

We drop higher order terms

$$-F_{tt} + \left(\frac{\varepsilon}{2}F_{xxtt} - \alpha F_x F_{xt}\right) - \alpha(F_x F_t)_x = -F_{xx} + \frac{\varepsilon}{6}F_{xxxx},$$

and simplify

$$F_{tt} - F_{xx} = -2\alpha F_x F_{xt} - \alpha F_{xx} F_t + \varepsilon\left(\frac{1}{2}F_{xxtt} - \frac{1}{6}F_{xxxx}\right).$$

It is evident here that at first order F obeys the wave equation, and $F_{xx} - F_{tt} = O(\varepsilon)$. To move forward we use this to substitute F_{xxxx} for F_{xxtt} in the above equation and note that any resulting error term would be of the same order as terms already discarded,

$$F_{tt} - F_{xx} = -2\alpha F_x F_{xt} - \alpha F_{xx} F_t + \varepsilon\frac{1}{3}F_{xxxx}. \tag{1.11}$$

Now to derive the equation which describes the long time behavior of F, we seek unidirectional

traveling wave solutions. Let $F = f + \varepsilon F_1 + \cdots$ where $f = f(\xi = x - t, T = \varepsilon t)$. We plug this in and, keeping only terms up to $O(\varepsilon)$ our equation becomes

$$f_{tt} + \varepsilon F_{1tt} - f_{xx} - \varepsilon F_{1xx} = -2\alpha f_x f_{xt} - \alpha f_{xx} f_t + \varepsilon \frac{1}{3} f_{xxxx}.$$

We next apply the chain rule

$$f_{\xi\xi} - 2\varepsilon f_{\xi T} + \varepsilon F_{1tt} - f_{\xi\xi} - \varepsilon F_{1xx} = 2\alpha f_\xi f_{\xi\xi} + \alpha f_{\xi\xi} f_\xi + \varepsilon \frac{1}{3} f_{\xi\xi\xi\xi}.$$

At leading order (1.11) is clearly satisfied. At $O(\varepsilon)$ we have

$$\varepsilon F_{1tt} - \varepsilon F_{1xx} = 2\varepsilon f_{\xi T} + 3\alpha f_\xi f_{\xi\xi} + \frac{\varepsilon}{3} f_{\xi\xi\xi\xi}. \tag{1.12}$$

In terms of the variables $\xi = x - t$ and $\xi_- = t + x$,

$$\frac{\partial}{\partial t} = -\frac{\partial}{\partial \xi} + \frac{\partial}{\partial \xi_-} \qquad\qquad \frac{\partial}{\partial x} = \frac{\partial}{\partial \xi} + \frac{\partial}{\partial \xi_-},$$

so

$$F_{1tt} = F_{1\xi\xi} - 2F_{1\xi_-\xi} + F_{1\xi_-\xi_-}, \qquad\qquad F_{1xx} = F_{1\xi\xi} + 2F_{1\xi_-\xi} + F_{1\xi_-\xi_-},$$

which imply

$$F_{1tt} - F_{1xx} = -4\frac{\partial^2 F_1}{\partial \xi_- \xi}.$$

We insert this into (1.12) to get

$$\varepsilon F_{1tt} - \varepsilon F_{1xx} = -4\varepsilon \frac{\partial^2 F_1}{\partial \xi_- \partial \xi} = 2\varepsilon f_{\xi T} + 3\alpha f_\xi f_{\xi\xi} + \frac{\varepsilon}{3} f_{\xi\xi\xi\xi}.$$

Since the RHS of this equation does not depend on ξ_-, to keep F_1 from growing linearly with ξ_- (or growing linearly in time) we must insist that

$$2\varepsilon f_{\xi T} + 3\alpha f_\xi f_{\xi\xi} + \frac{\varepsilon}{3} f_{\xi\xi\xi\xi} = 0. \tag{1.13}$$

To leading order $f = F$ and $\zeta = -F_t$. Also to leading order $-F_t = f_\xi$. Thus $f_\xi = \zeta$ and we have

$$2\varepsilon\zeta_T + 3\alpha\zeta\zeta_\xi + \frac{\varepsilon}{3}\zeta_{\xi\xi\xi} = 0.$$

Switching back from slow time and returning to a stationary frame of reference yields the Korteweg-de Vries equation

$$\zeta_t + \left(1 + \frac{3\alpha}{2}\zeta\right)\zeta_x + \frac{\varepsilon}{6}\zeta_{xxx} = 0.$$

Here analysis of KdV will be in a frame of reference that moves at nondimensional speed F

$$\zeta_t + \left(F - 1 - \frac{3\alpha}{2}\zeta\right)\zeta_x - \frac{\varepsilon}{6}\zeta_{xxx} = 0, \tag{1.14}$$

where we define the Froude number $F = \frac{U}{\sqrt{gh}}$ to be the ratio of velocity to the natural shallow water wave speed. The case involving flow over a bottom topography, or (equivalently) topography moving through the fluid at the speed of the frame of reference F, is described by forced problem [25],

$$\zeta_t + \left(F - 1 - \frac{3\alpha}{2}\zeta\right)\zeta_x - \frac{\varepsilon}{6}\zeta_{xxx} = f_x(x), \tag{1.15}$$

where the function f gives the non-dimensionalized height of the topography.

1.2.2 The Hydraulic Approximation

We insert the forcing function $f(x) = f'(x')$ into equation (1.15), where $x' = \kappa'x$. We next rescale the equation in the variables x' and $t' = \kappa't$,

$$\kappa'\zeta_{t'} + \kappa'\left(F - 1 - \frac{3\alpha}{2}\zeta\right)\zeta_{x'} - \kappa'^3\frac{\varepsilon}{6}\zeta_{x'x'x'} = \kappa'f'_{x'}(x').$$

Taking κ' to be small, dropping the $O(\kappa'^2)$ term and dropping the primes obtains the hydraulic (dispersionless) approximation to equation (1.15),

$$\zeta_t + \left(F - 1 - \frac{3\alpha}{2}\zeta\right)\zeta_x = f_x(x). \tag{1.16}$$

15

This equation can serve as a valid approximation of the fKdV equation for a fluid with an initially smooth, flat surface flowing over a wide obstacle [10]. This is equivalent to the inviscid Burgers equation with a forcing term. We will also consider the linearized fKdV equation,

$$\zeta_t + (F - 1)\zeta_x - \frac{\varepsilon}{6}\zeta_{xxx} = f_x(x). \tag{1.17}$$

CHAPTER 2

Soliton Generation in fKdV due to steady forcing

The case of resonant flow (F close to 1) was studied in [10] and in [22]. It is known that in this case, the forced equation generates upstream propagating solitary waves [25, 17]. For large enough F, equation 1.15 has stationary solutions, the stability of which has been studied in [2].

Here we will give a means for predicting the critical Froude number that defines the resonant regime (semi-analytically), and the frequency of soliton generation (analytically). We will begin with analysis of the hydraulic approximation studied in [10]. We will then examine stationary solutions for super critical Froude values, use the eigenvalues of the Schrödinger operator to predict the frequency of soliton generation, and finally look at the inverse scattering transform (IST) to justify our prediction.

2.1 The Hydraulic Approximation

2.1.1 Exact Solution

Equation (1.16) can be solved by the method of characteristics, thus we consider the system

$$
\begin{aligned}
\frac{\mathrm{d}x}{\mathrm{d}t} &= F - 1 - \frac{3\alpha}{2}\zeta, \\
\frac{\mathrm{d}\zeta}{\mathrm{d}t} &= f_x(x),
\end{aligned}
\tag{2.1}
$$

on

$$ x \in \mathbb{R}, \qquad t \geq 0 $$

with initial conditions

$$ x(t = 0) = \xi, \qquad u(t = 0) = 0. $$

17

We can convert this system to a single second order equation,

$$\frac{d^2x}{dt^2} = -\frac{3\alpha}{2}\frac{d\zeta}{dt} = -\frac{3\alpha}{2}f_x(x).$$

Notice here we have the second derivative of x with respect to time (analogous to acceleration) equal to the negative of the derivative of some function with respect to position. We can think of this as an equation relating force and potential in a closed system in which energy is conserved,

$$\text{Force} = ma = m\ddot{x} = -\frac{d}{dx}\text{Potential},$$

where the potential is some function of space, defined at every point in space, whose value is the potential energy at the given point. Since energy is conserved, the change in total energy (kinetic plus potential) will be zero. We seek to arrange the terms of the equation in a way that allows us to use this. We multiply both sides by $\frac{dx}{dt}$ and get

$$\frac{d^2x}{dt^2}\frac{dx}{dt} = -\frac{3\alpha}{2}f_x(x)\frac{dx}{dt}.$$

We then rearrange the equation as follows:

$$\frac{d}{dt}\left[\frac{1}{2}\left(\frac{dx}{dt}\right)^2 + \frac{3\alpha}{2}f(x)\right] = 0,$$

and integrate

$$\frac{1}{2}\left(\frac{dx}{dt}\right)^2 + \frac{3\alpha}{2}f(x) = \text{constant}.$$

At this point we insert initial conditions to solve for the unknown constant

$$\text{constant} = \frac{1}{2}(F-1)^2 + \frac{3\alpha}{2}f(\xi),$$

and next solve for ζ. Recall $\frac{dx}{dt} = (F-1) - \frac{3\alpha}{2}\zeta$, so

$$\frac{1}{2}\left((F-1) - \frac{3\alpha}{2}\zeta\right)^2 + \frac{3\alpha}{2}f(x) = \frac{1}{2}(F-1)^2 + \frac{3\alpha}{2}f(\xi),$$

18

and
$$\frac{3\alpha}{2}\zeta = (F-1) \mp \sqrt{(F-1)^2 + 3\alpha\big(f(\xi) - f(x)\big)}.$$

To choose between the positive and negative branches, again consider the initial conditions

$$x = \xi, \quad \zeta = 0 \quad \text{at} \quad t = 0.$$

Doing so we arrive at

$$0 = F - 1 \mp \sqrt{(F-1)^2} = F - 1 \mp |(F-1)|.$$

To satisfy the initial conditions when $(F-1)$ is both positive and negative, we insert a signum function in the solution. Also, since by convention $\text{sgn}(0) = 0$, we write the solution piecewise. Considering the case $(F-1) = 0$ along with a positive, even forcing function that is maximized at $x = 0$, the sign of the rate of change of x with respect to time must depend on the sign of the initial position ξ in order for the solution to remain well-defined. Therefore,

$$\frac{3\alpha}{2}\zeta = \begin{cases} (F-1) - \text{sgn}(F-1)\sqrt{(F-1)^2 - 3\alpha\big(f(x) - f(\xi)\big)}, & F \neq 1 \\ \text{sgn}(\xi)\sqrt{3\alpha\big(f(\xi) - f(x)\big)}, & F = 1. \end{cases} \tag{2.2}$$

Now to find x as a function of t, we must consider as separate cases when $(F-1)$ does and does not equal zero. Beginning with the case in which $(F-1) = 0$, we seek to solve the equation

$$\frac{\mathrm{d}x}{\mathrm{d}t} = (F-1) - \frac{3\alpha}{2}\zeta.$$

Inserting our expression for ζ with $F = 1$,

$$\frac{\mathrm{d}x}{\mathrm{d}t} = \text{sgn}(\xi)\sqrt{3\alpha\big(f(\xi) - f(x)\big)}, \tag{2.3}$$

we then solve the separable ODE for t and use the initial condition $x(0) = \xi$ to determine the bounds of integration

$$t = \frac{\text{sgn}(\xi)}{\sqrt{3\alpha}} \int_\xi^x \frac{1}{\sqrt{f(\xi) - f(y)}}\, \mathrm{d}y.$$

19

We choose a forcing function f with compact support

$$f(x) = \begin{cases} p_m(1 - \kappa^2 x^2), & -\frac{1}{\kappa} < x < \frac{1}{\kappa} \\ 0, & |x| \geq \frac{1}{\kappa}. \end{cases} \tag{2.4}$$

Note that unless otherwise stated, numerical simulations were run using

$$f(x) = p_m \operatorname{sech}^2(\kappa x) \tag{2.5}$$

as a forcing function. KdV solutions exhibit comparable behavior for a wide class of forcing functions with similar shapes [10]. We take $p_m > 0$ and $\kappa > 0$. With this choice of forcing function, when $-\frac{1}{\kappa} < x < \frac{1}{\kappa}$ we have

$$t = \frac{\operatorname{sgn}(\xi)}{\sqrt{3\alpha}} \int_\xi^x \frac{1}{\sqrt{p_m(1 - \kappa^2\xi^2 - 1 + \kappa^2 y^2)}} \, \mathrm{d}y,$$

which simplifies to

$$t = \frac{\operatorname{sgn}(\xi)}{\kappa\sqrt{3\alpha p_m}} \int_\xi^x \frac{\mathrm{d}y}{|\xi|\sqrt{(y/\xi)^2 - 1}}.$$

We now introduce a change of variables,

$$z = y/\xi \quad \Rightarrow \quad \mathrm{d}z = \frac{\mathrm{d}y}{\xi},$$

and drop the $\operatorname{sgn}(\xi)$ term. This is done without loss of generality, as in the case where $\xi < 0$, x will decrease with time and, therefore $x \leq \xi$ will always be true. As a consequence of this inequality, the bounds of integration should be switched, which must be accompanied by an overall sign change,

$$t = \frac{1}{\kappa\sqrt{3\alpha p_m}} \int_1^{x/\xi} \frac{\mathrm{d}z}{\sqrt{z^2 - 1}}.$$

We now introduce a second change of variables. We choose hyperbolic cosine instead of cosine to ensure that the argument of the square root is always nonnegative

$$z = \cosh w \quad \Rightarrow \quad \mathrm{d}z = \sinh w \, \mathrm{d}w.$$

20

Inserting the change of variables gives

$$t = \frac{1}{\kappa\sqrt{3\alpha p_m}} \int_0^{\cosh^{-1}(x/\xi)} \mathrm{d}w,$$

which evaluates to

$$t = \frac{w}{\kappa\sqrt{3\alpha p_m}} \Big|_0^{\cosh^{-1}(x/\xi)} = \frac{1}{\kappa\sqrt{3\alpha p_m}} \cosh^{-1}(x/\xi).$$

The inverse function notation is inconvenient, so we consider the definition of the cosh function

$$\cosh x = \frac{e^x + e^{-x}}{2}.$$

Let $t = e^v$, and let $w = \cosh v$. Substituting these variables gives

$$\cosh v = w = \frac{t + 1/t}{2}.$$

We solve this expression for t

$$t = w \pm \sqrt{w^2 - 1},$$

then rewrite t in terms of v and solve,

$$e^v = w \pm \sqrt{w^2 - 1} \quad \rightarrow \quad v = \ln(w \pm \sqrt{w^2 - 1}).$$

Thus

$$\cosh^{-1} x = \ln\left(x \pm \sqrt{x^2 - 1}\right),$$

and

$$t = \frac{1}{\kappa\sqrt{3\alpha p_m}} \ln\left(x/\xi + \sqrt{(x/\xi)^2 - 1}\right). \tag{2.6}$$

Note that we consider only positive values of t, so we choose the positive branch. Again, note that this is valid for $|x| < \frac{1}{\kappa}$. Solving for x gives

$$x = \xi \cosh\left(\kappa\sqrt{3\alpha p_m}\, t\right).$$

When $|x| \geq \frac{1}{\kappa}$, $f(x) = 0$. This implies that $\frac{\mathrm{d}u}{\mathrm{d}t} = 0$, which implies that u is constant with respect to

21

time t, and $\frac{\mathrm{d}x}{\mathrm{d}t}$ is equal to a constant. Thus, the characteristic curves become straight lines. The slopes of these lines are given by (2.3), where $|x| \geq \frac{1}{\kappa}$ and $f(x) = 0$, *i.e.* $\frac{\mathrm{d}x}{\mathrm{d}t} = \mathrm{sgn}(\xi)\sqrt{3\alpha f(\xi)}$, given $|\xi| < \frac{1}{\kappa}$. We now solve for the additive constant in order to define these lines.

$$t = \mathrm{sgn}(\xi)\frac{x}{\sqrt{3\alpha f(\xi)}} + d_1.$$

At the boundary of the forced region we substitute (2.6) evaluated at $x = \frac{\mathrm{sgn}(\xi)}{\kappa}$ and determine that

$$d_1 = \frac{1}{\kappa\sqrt{3\alpha p_m}} \ln\left(\frac{1}{\kappa|\xi|} + \sqrt{(1/\kappa\xi)^2 - 1}\right) - \frac{1}{\sqrt{3\alpha f(\xi)}}.$$

If $|\xi| > \frac{1}{\kappa}$, the characteristics are vertical lines. Figure (2.1.1) shows the characteristic curves plotted for the case where $p_m = \kappa = 1$, $\alpha = 4$. Now we consider the case $F \neq 1$. For simplicity we will
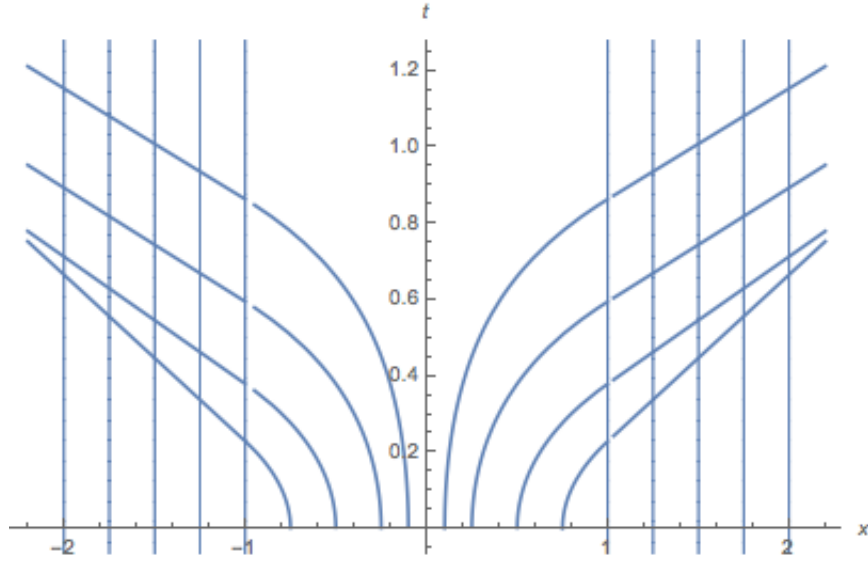

Figure 2.1: Characteristic curves for the equation (1.16) for the case $\kappa = F = 1$

assume $F > 1$, but the case in which $F < 1$ follows similarly. We now have

$$\frac{3\alpha}{2}\zeta = F - 1 - \sqrt{(F-1)^2 - 3\alpha(f(x) - f(\xi))},$$

and

$$\frac{\mathrm{d}x}{\mathrm{d}t} = F - 1 - \frac{3\alpha}{2}\zeta = \sqrt{(F-1)^2 - 3\alpha(f(x) - f(\xi))}.$$

22

This system has as a solution

$$t = \int_\xi^x \frac{\mathrm{d}y}{\sqrt{(F-1)^2 - 3\alpha\big(f(y) - f(\xi)\big)}}. \tag{2.7}$$

We again insert (2.4) into the integral

$$t = \int_\xi^x \frac{\mathrm{d}y}{\sqrt{(F-1)^2 - 3\alpha\kappa^2 p_m\big(\xi^2 - y^2\big)}},$$

to now arrive at

$$t = \int_\xi^x \frac{\mathrm{d}y}{\sqrt{3\alpha\kappa^2 p_m y^2 + (F-1)^2 - 3\alpha\kappa^2 p_m\xi^2}}.$$

Let us first assume that $(F-1)^2 > 3\alpha\kappa^2 p_m\xi^2$, which leads to

$$t = \frac{1}{\sqrt{(F-1)^2 - 3\alpha\kappa^2 p_m\xi^2}} \int_\xi^x \frac{\mathrm{d}y}{\sqrt{3\alpha\kappa^2 p_m y^2/((F-1)^2 - 3\alpha\kappa^2 p_m\xi^2) + 1}}.$$

Now let

$$z = y\sqrt{\frac{3\alpha\kappa^2 p_m}{(F-1)^2 - 3\alpha\kappa^2 p_m\xi^2}} \quad \Rightarrow \quad \mathrm{d}z = \mathrm{d}y\sqrt{\frac{3\alpha\kappa^2 p_m}{(F-1)^2 - 3\alpha\kappa^2 p_m\xi^2}},$$

which gives

$$t = \frac{1}{\sqrt{3\alpha\kappa^2 p_m}} \int_a^b \frac{\mathrm{d}z}{\sqrt{z^2 + 1}}.$$

We introduce

$$z = \sinh u \quad \to \quad \mathrm{d}z = \cosh u \, \mathrm{d}u$$

and substitute the new variables into our expression, which ultimately yields

$$t = \frac{1}{\sqrt{3\alpha\kappa^2 p_m}} \sinh^{-1}\left[x\sqrt{\frac{3\alpha\kappa^2 p_m}{(F-1)^2 - 3\alpha\kappa^2 p_m\xi^2}}\right]$$
$$- \frac{1}{\sqrt{3\alpha\kappa^2 p_m}} \sinh^{-1}\left[\xi\sqrt{\frac{3\alpha\kappa^2 p_m}{(F-1)^2 - 3\alpha\kappa^2 p_m\xi^2}}\right]$$

in terms of the original variables. Note that if we take

$$\sinh v = w = \frac{e^v - e^{-v}}{2} = \frac{t - 1/t}{2},$$

23

then

$$v = \ln\left(w \pm \sqrt{w^2 + 1}\right).$$

This is only defined for the positive branch, so we take

$$\sinh^{-1} x = \ln\left(x + \sqrt{x^2 + 1}\right),$$

and thus

$$t = \frac{1}{\kappa\sqrt{3\alpha p_m}} \ln\left[x\sqrt{\frac{3\alpha\kappa^2 p_m}{(F-1)^2 - 3\alpha\kappa^2 p_m \xi^2}} + \sqrt{\frac{(F-1)^2 + 3\alpha\kappa^2 p_m(x^2 - \xi^2)}{(F-1)^2 - 3\alpha\kappa^2 p_m \xi^2}}\right]$$
$$- \frac{1}{\kappa\sqrt{3\alpha p_m}} \ln\left[\xi\sqrt{\frac{3\alpha\kappa^2 p_m}{(F-1)^2 - 3\alpha\kappa^2 p_m \xi^2}} + \sqrt{\frac{(F-1)^2}{(F-1)^2 - 3\alpha\kappa^2 p_m \xi^2}}\right].$$

while $|x| < \frac{1}{\kappa}$. Simplified we have

$$t = \frac{1}{\kappa\sqrt{3\alpha p_m}} \ln\left[\frac{x}{\xi} \cdot \frac{\kappa\sqrt{3\alpha p_m} + \sqrt{(F-1)^2 + 3\alpha\kappa^2 p_m(x^2 - \xi^2)}}{\kappa\sqrt{3\alpha p_m} + F - 1}\right]. \tag{2.8}$$

We proceed to solve this expression for x,

$$x = \left(\xi + \frac{F-1}{\kappa\sqrt{3\alpha p_m}}\right) e^{t\kappa\sqrt{3\alpha p_m}} + \left(\xi - \frac{F-1}{\kappa\sqrt{3\alpha p_m}}\right) e^{-t\kappa\sqrt{3\alpha p_m}},$$

and from this we see that

$$\frac{dx}{dt} = \left(\xi\kappa\sqrt{3\alpha p_m} + F - 1\right) e^{t\kappa\sqrt{3\alpha p_m}} - \left(\xi\kappa\sqrt{3\alpha p_m} - (F-1)\right) e^{-t\kappa\sqrt{3\alpha p_m}}. \tag{2.9}$$

Substituting this into the first equation of (2.1) gives

$$\frac{3\alpha}{2}\zeta = F - 1 - \left(\xi\kappa\sqrt{3\alpha p_m} + F - 1\right) e^{t\kappa\sqrt{3\alpha p_m}} + \left(\xi\kappa\sqrt{3\alpha p_m} - (F-1)\right) e^{-t\kappa\sqrt{3\alpha p_m}}.$$

We next seek the solution outside of the forced region. For $|\xi| < \frac{1}{\kappa}$ and $|x| > \frac{1}{\kappa}$, $f(x) = 0$ and (still assuming $F > 1$), it follows from (2.1) and (2.2) that the constant slope of the characteristic curves

24

is given by

$$\frac{dx}{dt} = \sqrt{(F-1)^2 + 3\alpha f(\xi)}.$$

Writing it as such after plugging in the forcing function used (2.4) gives

$$t = \frac{x}{\sqrt{(F-1)^2 + 3\alpha p_m(1 - \kappa^2\xi^2)}} + d_2.$$

Treating t as a function of x, we use the time value at the boundary of the forced region to solve for the unknown constant using (2.8). Note that from (2.9) we can conclude that x always increases for $t > 0$, so no characteristic curves with $\xi > -\frac{1}{\kappa}$ will reach $x = -\frac{1}{\kappa}$. Thus we consider only $x = \frac{1}{\kappa}$

$$t|_{x=1/\kappa} = \frac{1}{\kappa\sqrt{(F-1)^2 + 3\alpha p_m(1 - \kappa^2\xi^2)}} + d_2$$
$$= \frac{1}{\kappa\sqrt{3\alpha p_m}} \ln\left(\frac{1}{\kappa\xi} \cdot \frac{\kappa\sqrt{3\alpha p_m} + \sqrt{(F-1)^2 + 3\alpha p_m(1 - \kappa^2\xi^2)}}{\kappa\sqrt{3\alpha p_m} + F - 1}\right),$$

and find

$$d_2 = \frac{1}{\kappa\sqrt{3\alpha p_m}} \ln\left(\frac{\kappa\sqrt{3\alpha p_m} + \sqrt{(F-1)^2 + 3\alpha p_m(1 - \kappa^2\xi^2)}}{\kappa\xi(\kappa\sqrt{3\alpha p_m} + F - 1)}\right)$$
$$- \frac{1}{\kappa\sqrt{(F-1)^2 + 3\alpha p_m(1 - \kappa^2\xi^2)}}.$$

For $|\xi| > \frac{1}{\kappa}$ and $|x| > \frac{1}{\kappa}$, the characteristic curves are straight lines given by

$$t = \frac{x - \xi}{F - 1}. \tag{2.10}$$

For $\xi < -\frac{1}{\kappa}$ and $|x| < \frac{1}{\kappa}$, following steps similar to those given above, but solving on the interval $x \in \left(-\frac{1}{\kappa}, \frac{1}{\kappa}\right)$ for $t > \frac{-1/\kappa - \xi}{F-1}$, treating $x\left(\frac{-1/\kappa - \xi}{F-1}\right) = -\frac{1}{\kappa}$ and $\zeta\left(\frac{-\frac{1}{\kappa} - \xi}{F-1}\right) = 0$ as our new boundary values, we find (2.1) has solution

$$t = \int_{-1/\kappa}^{x} \frac{dy}{\sqrt{(F-1)^2 - 3\alpha f(y)}} - \frac{1/\kappa + \xi}{F - 1},$$

which evaluates to

$$t = \frac{1}{\kappa\sqrt{3\alpha p_m}} \ln\left(\frac{\kappa x\sqrt{3\alpha p_m} + \sqrt{(F-1)^2 + 3\alpha p_m(\kappa^2 x^2 - 1)}}{F - 1 - \sqrt{3\alpha p_m}}\right) - \frac{1/\kappa + \xi}{F - 1}.$$

This describes the characteristic curve until $x = \frac{1}{\kappa}$, at which point

$$t|_{x=1/\kappa} = \frac{1}{\kappa\sqrt{3\alpha p_m}} \ln\left(\frac{F - 1 + \sqrt{3\alpha p_m}}{F - 1 - \sqrt{3\alpha p_m}}\right) - \frac{1/\kappa + \xi}{F - 1},$$

and the slope is given by

$$\frac{\mathrm{d}t}{\mathrm{d}x}\bigg|_{x=1/\kappa} = \frac{1}{F - 1}.$$

Thus for $\xi < -\frac{1}{\kappa}$ and $x > \frac{1}{\kappa}$

$$t = \frac{x - 2/\kappa - \xi}{F - 1} + \frac{1}{\kappa\sqrt{3\alpha p_m}} \ln\left(\frac{F - 1 + \sqrt{3\alpha p_m}}{F - 1 - \sqrt{3\alpha p_m}}\right).$$

This analysis assumes $(F - 1)^2 > 3\alpha\kappa^2 p_m\xi^2$, which is true for all ξ values inside the forced region, given $(F - 1)^2 > 3\alpha p_m$. Thus we can conclude that all characteristics maintain a nonnegative slope for all time. Characteristics originating in the forced region, upon exiting this region, have a slope that depends on their initial positions ξ. The slopes of the characteristic curves originating inside the forced region near $\frac{1}{\kappa}$ will have a slope less than that of the characteristics originating downstream of the forced region, so these will intersect. Furthermore, for $\xi \in (0, 1/\kappa)$ the slope of the characteristics upon exiting the forced region is an increasing function of ξ. For $\xi \in (-1/\kappa, 0)$, the slope of the characteristics outside the forced region ($x > 1/\kappa$) is a decreasing function of ξ, so the characteristics fan out. For large values of F, these differences in slope will be small, as things are quickly swept out of the forced region and moved downstream. The slopes of the characteristics originating upstream of the forced region do not depend on ξ. Each of these will have a slope equal to that of its neighboring characteristic curves. The slope does, however, depend on x inside the forced region. Inside this region the curves steepen around $x = 0$, resulting in a gap between these characteristics and those originating inside and downstream of the forced region.

This likely corresponds with the depressed region immediately downstream of the forcing seen in numerical solutions of the fKdV equation (1.15). For values of F closer to one that still satisfy $(F - 1)^2 > 3\alpha p_m$ this gap can become large. Figure (2.1.1) shows the characteristic curves plotted for the case where $p_m = \kappa = 1$, $\alpha = 4$, and $F = 8$.

From the above lines it is clear that this approach is rather cumbersome. It is considerably more so for the case $(F - 1)^2 < 3\alpha\kappa^2 p_m\xi^2$. Looking back to the characteristic system of equations (2.1),
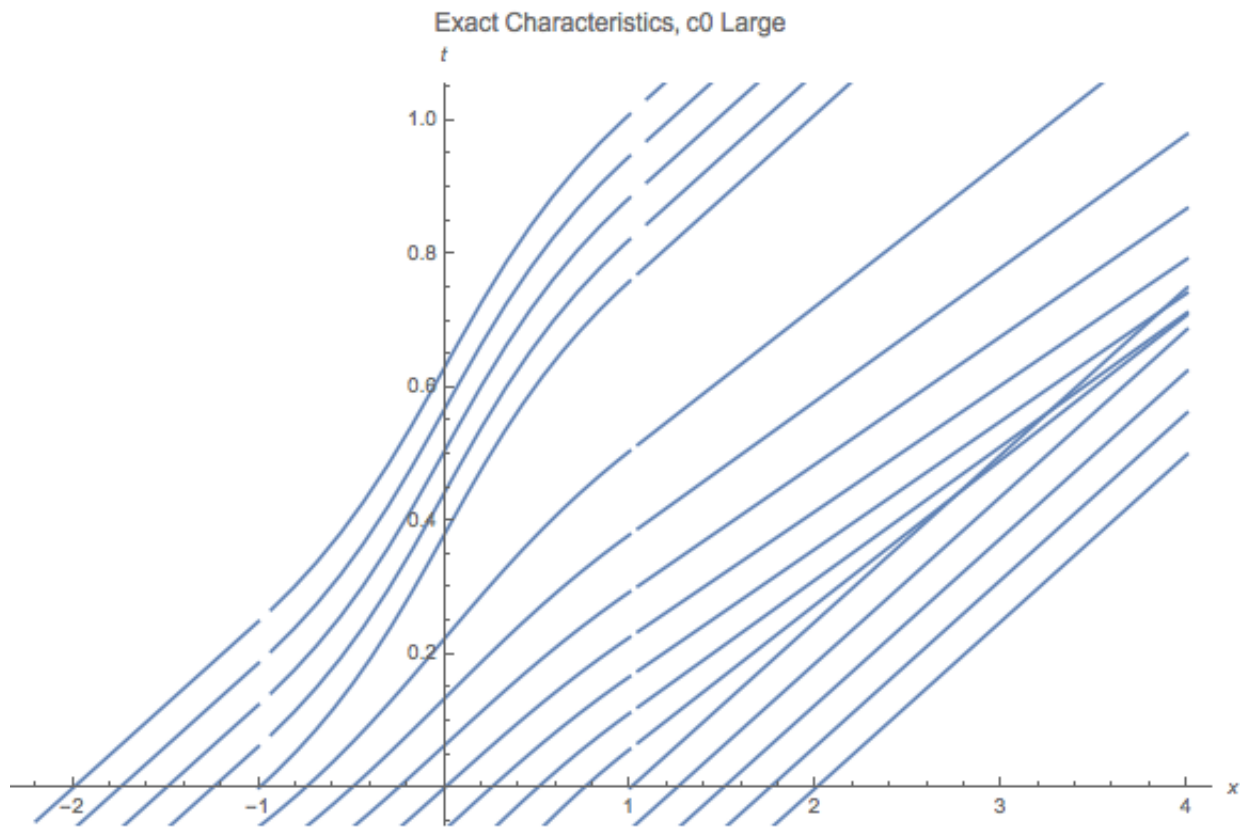
Figure 2.2: Characteristic curves for the equation (1.16) plotted in space-time for $p_m = \kappa = 1$, $\alpha = 4$, and $F = 8$.

if we insert the forcing function (2.4) directly, then when $|x| < \frac{1}{\kappa}$

$$\frac{\mathrm{d}x}{\mathrm{d}t} = (F - 1) - \frac{3\alpha}{2}\zeta,$$

$$\frac{\mathrm{d}\zeta}{\mathrm{d}t} = -2\kappa^2 p_m x.$$

This is a system of linear first order equations. We can rewrite this system as a matrix equation of the form $\vec{x}' = A\vec{x} + \vec{b}$,

$$\vec{x}' = \begin{pmatrix} 0 & -\frac{3\alpha}{2} \\ -2\kappa^2 p_m & 0 \end{pmatrix} \vec{x} + \begin{pmatrix} F - 1 \\ 0 \end{pmatrix},$$

where $\vec{x} = \begin{pmatrix} x \\ \zeta \end{pmatrix}$. Let us begin by finding a particular solution

$$\vec{x}_p = \begin{pmatrix} a_1 \\ a_2 \end{pmatrix} \qquad \vec{x}_p{}' = \begin{pmatrix} 0 \\ 0 \end{pmatrix}.$$

Inserting this solution form into equation (2.1.1), we find

$$\begin{pmatrix} 0 \\ 0 \end{pmatrix} = \begin{pmatrix} 0 & -\frac{3\alpha}{2} \\ -2\kappa^2 p_m & 0 \end{pmatrix} \begin{pmatrix} a_1 \\ a_2 \end{pmatrix} + \begin{pmatrix} F - 1 \\ 0 \end{pmatrix},$$

and

$$\vec{x}_p = \begin{pmatrix} 0 \\ 2(F - 1)/3\alpha \end{pmatrix}.$$

The matrix A has eigenvalues $\pm \kappa \sqrt{3\alpha p_m}$ and eigenvectors

$$\vec{v} = \begin{pmatrix} \mp 1 \\ \frac{\sqrt{3\alpha p_m}}{2\kappa p_m} \end{pmatrix},$$

so the solution is given by

$$\vec{x} = d_3 \begin{pmatrix} -1 \\ \frac{\sqrt{3\alpha p_m}}{2\kappa p_m} \end{pmatrix} e^{t\kappa\sqrt{3\alpha p_m}} + d_4 \begin{pmatrix} 1 \\ \frac{\sqrt{3\alpha p_m}}{2\kappa p_m} \end{pmatrix} e^{-t\kappa\sqrt{3\alpha p_m}} + \begin{pmatrix} 0 \\ 2(F - 1)/3\alpha \end{pmatrix}.$$

We now insert initial conditions to solve for the unknown constants d_3 and d_4

$$\begin{pmatrix} \xi \\ 0 \end{pmatrix} = d_3 \begin{pmatrix} -1 \\ \frac{\sqrt{3\alpha p_m}}{2\kappa p_m} \end{pmatrix} + d_4 \begin{pmatrix} 1 \\ \frac{\sqrt{3\alpha p_m}}{2\kappa p_m} \end{pmatrix} + \begin{pmatrix} 0 \\ 2(F - 1)/3\alpha \end{pmatrix},$$

and find

$$d_3 = \frac{2\kappa(1-F)\sqrt{3\alpha p_m}}{9\alpha^2} - \frac{1}{2}\xi \qquad d_4 = \frac{2\kappa(F-1)\sqrt{3\alpha p_m}}{9\alpha^2} + \frac{1}{2}\xi.$$

Thus

$$x(t) = \frac{1}{2}\left(\frac{F-1}{\kappa\sqrt{3\alpha p_m}} + \xi\right)e^{\kappa t\sqrt{3\alpha p_m}} - \frac{1}{2}\left(\frac{F-1}{\kappa\sqrt{3\alpha p_m}} - \xi\right)e^{-\kappa t\sqrt{3\alpha p_m}}, \qquad (2.11)$$

and

$$\zeta(t) = -\left(\frac{F-1}{3\alpha} + \kappa\xi\sqrt{\frac{p_m}{3\alpha}}\right)e^{\kappa t\sqrt{3\alpha p_m}} - \left(\frac{F-1}{3\alpha} - \kappa\xi\sqrt{\frac{p_m}{3\alpha}}\right)e^{-\kappa t\sqrt{3\alpha p_m}} + \frac{2}{3\alpha}(F-1).$$

Note this matches the results of integrating the separable equation in the case $(F-1)^2 > 3\alpha\kappa^2 p_m\xi^2$. Similarly, this is only valid when $|\xi| < \frac{1}{\kappa}$ and $|x| < \frac{1}{\kappa}$.

To construct the characteristic curves outside of this region we solve the x equation for t. Let

$$x = -d_5 z + \frac{d_6}{z} \quad \text{where} \quad z = e^{t\kappa\sqrt{3\alpha p_m}}.$$

Solving for z and then reinserting the original variables gives

$$e^{t\kappa\sqrt{3\alpha p_m}} = \frac{x \pm \sqrt{x^2 + 4d_5 d_6}}{-2d_5},$$

which we solve for t,

$$t = \frac{1}{2\sqrt{3\alpha}}\ln\left(\frac{x \pm \sqrt{x^2 + 4d_5 d_6}}{-2d_5}\right).$$

Inserting appropriate values for d_5 and d_6,

$$t = \frac{1}{2\sqrt{3\alpha}}\ln\left[\frac{x \pm \sqrt{x^2 + 4\left(\frac{-(F-1)\sqrt{3\alpha}}{3\alpha p_m} - \frac{1}{2}\xi\right)\left(\frac{-(F-1)\sqrt{3\alpha}}{3\alpha p_m} + \frac{1}{2}\xi\right)}}{-2\left(\frac{-(F-1)\sqrt{3\alpha}}{3\alpha p_m} - \frac{1}{2}\xi\right)}\right],$$

and then simplifying leads to

$$t = \frac{1}{\kappa\sqrt{3\alpha p_m}}\ln\left(\frac{x \pm \sqrt{x^2 + \frac{(F-1)^2}{\kappa^2 3\alpha p_m} - \xi^2}}{\frac{F-1}{\kappa\sqrt{3\alpha p_m}} + \xi}\right).$$

Characteristic curves for $\frac{-(F-1)}{2\sqrt{3\alpha}} < \xi < \frac{1}{\kappa}$ exit the forced region at position $x = \frac{1}{\kappa}$ and at time

$$t = \frac{1}{2\sqrt{3\alpha}} \ln \left(\frac{\frac{1}{\kappa} + \sqrt{(1/\kappa)^2 + \frac{(F-1)^2}{3\alpha p_m} - \xi^2}}{\frac{(F-1)\sqrt{3\alpha}}{6\alpha} + \xi} \right).$$

Note that in this case we take the positive branch of the square root so that everything is well-defined for the entire range of ξ values. The curve is defined by the positive branch until reaching a turning point (if the curve overturns), after which it follows the negative branch. Examining the derivative of this time function with respect to x,

$$\frac{\mathrm{d}t}{\mathrm{d}x} = \frac{\pm 1}{\sqrt{(F-1)^2 + 3\alpha\kappa^2 p_m(x^2 - \xi^2)}},$$

we find that within the region for which the above expression is valid, the slopes of the characteristic curves become undefined when

$$x = -\sqrt{\xi^2 - \frac{(F-1)^2}{3\alpha\kappa p_m}},$$

given $-\frac{1}{\kappa} < \xi < \frac{1-F}{\kappa\sqrt{3\alpha p_m}}$ and $F > 1$ (The case in which $F < 1$ follows similarly). Here the characteristic curves reach a turning point and change direction. Thus characteristic curves overturn only when $(F-1)^2 < 3\alpha p_m$. At the left boundary of the forced region $x = -\frac{1}{\kappa}$, the negative branch of the square root gives a non-negative value for t,

$$t = \frac{1}{2\sqrt{3\alpha}} \ln \left(\frac{-\frac{1}{\kappa} - \sqrt{(1/\kappa)^2 + \frac{(F-1)^2}{3\alpha p_m} - \xi^2}}{\frac{(F-1)}{2\sqrt{3\alpha}} + \xi} \right).$$

As in the previous case, the characteristic curves are straight lines outside the forced region. To determine their slopes we plug the solution $\zeta(t)$ into the characteristic equation for $\frac{\mathrm{d}x}{\mathrm{d}t}$,

$$\frac{\mathrm{d}x}{\mathrm{d}t} = (F-1) - \frac{3\alpha}{2}\zeta = \left(\frac{(F-1)}{2} + \xi\sqrt{3\alpha p_m} \right) e^{t\kappa\sqrt{3\alpha p_m}} + \left(\frac{(F-1)}{2} - \xi\sqrt{3\alpha p_m} \right) e^{-2t\sqrt{3\alpha}}.$$

We can plug the above value of t into this expression to find the slope (and from that, the equation)

of the characteristic curves for $x \leq -\frac{1}{\kappa}$,

$$x = -\sqrt{(F-1)^2 + 3\alpha p_m (1 - \kappa^2 \xi^2)} \left[t - \frac{1}{\kappa \sqrt{3\alpha p_m}} \ln \left(\frac{-1 \pm \sqrt{1 + \frac{(F-1)^2}{3\alpha p_m} - \kappa^2 \xi^2}}{\frac{F-1}{\sqrt{3\alpha p_m}} + \kappa \xi} \right) \right] - \frac{1}{\kappa}.$$

For $|x|, |\xi| > \frac{1}{\kappa}$ the characteristics are given by

$$t = \frac{x - \xi}{(F-1)}.$$

The characteristic curves for the case $p_m = \kappa = (F-1) = 1$ are plotted in Figure (2.1.1).
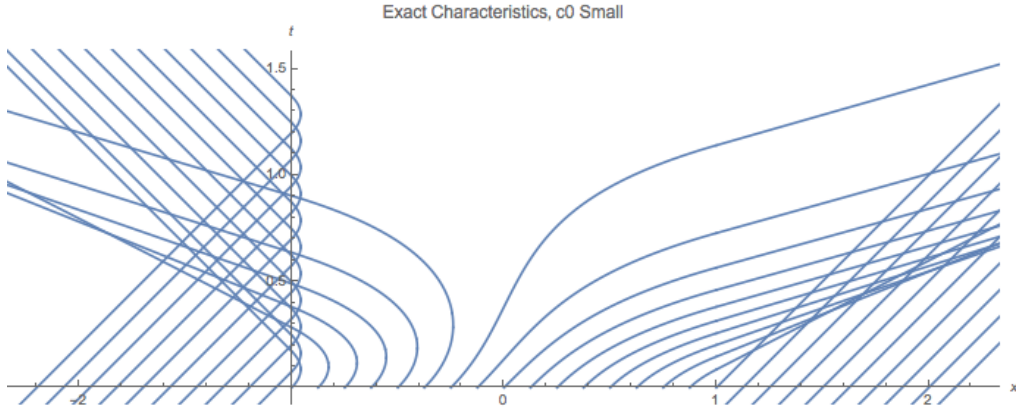

Figure 2.3: Characteristic curves for the equation (1.16) with parameter values $p_m = \kappa = 1$, $F = 2$.

Figure 2.1.1 shows the fluid surface for various Froude values, given $\alpha = 2/3$, $p_m = 3/4$ and compares results from the full KdV equation (1.15) with $\varepsilon = 1$ and the dispersionless equation.

2.1.2 Shocks

Characteristic curves for the system (2.1) cross both up and downstream of the forced region when $(F-1)^2 < 3\alpha p_m$, and they cross downstream of the forced region when $(F-1)^2 \geq 3\alpha p_m$. Multiple characteristic curves occupying the same point in space-time (i.e. intersection of the characteristic curves) corresponds to multivaluedness in the solution. To remedy this we insert shocks. To determine when and where these shocks first appear, we consider the Jacobian of our change of variables

$$J = \begin{vmatrix} \frac{\partial x}{\partial \xi} & \frac{\partial x}{\partial \tau} \\ \frac{\partial t}{\partial \xi} & \frac{\partial t}{\partial \tau} \end{vmatrix} = \frac{\partial x}{\partial \xi} \frac{\partial t}{\partial \tau} - \frac{\partial x}{\partial \tau} \frac{\partial t}{\partial \xi} = \frac{\partial x}{\partial \xi}$$
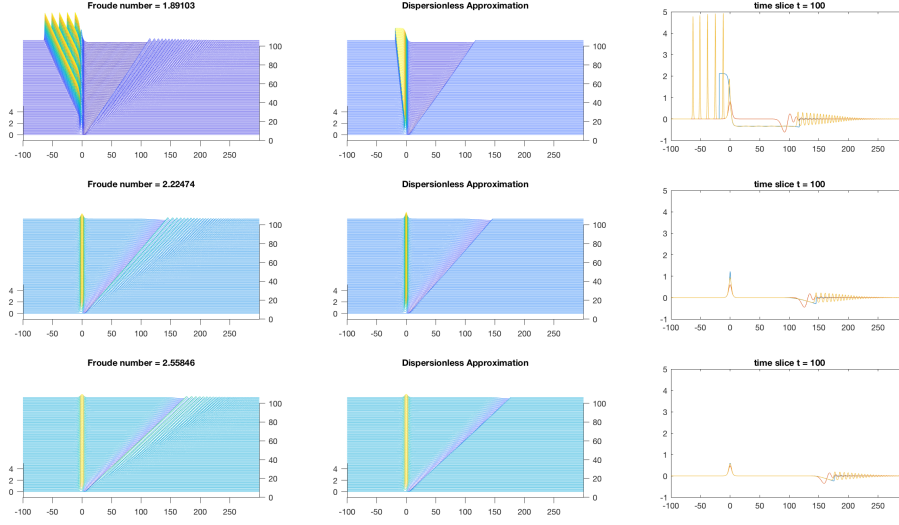
31

Figure 2.4: Numerical solutions to equation (1.15) and (1.16) shown evolving in time for Froude numbers $F = 1.89103$, $F = 2.22474$, and $F = 2.55846$; and parameter values $\alpha = 2/3$, $p_m = 3/4$, and $\varepsilon = 1$, using (2.5) as a forcing function with $\kappa = 0.3$. The left column overlays the solutions at time $t = 100$ for the full fKdV equation (1.15), the dispersionless approximation (1.16), and the linearized equation (1.17).

where $t = \tau$. Solving for when this is equal to zero or undefined also indicates the time and initial value ξ for which breaking occurs. For $-\frac{1}{\kappa} < \xi < \frac{1}{\kappa}$

$$\frac{\partial x}{\partial \xi} = \cosh\left[\kappa t \sqrt{3\alpha p_m}\right].$$

This expression is never equal to zero, indicating characteristic curves originating within the forced region do not intersect within the forced region. For $\xi < -\frac{1}{\kappa}$, characteristic curves approach the forced region with a constant slope. After entering the forced region, they are overturned and exit from the same side they entered (for sufficiently small $(F - 1)$ or sufficiently large forcing p_m). While inside the forced region, the characteristic curve is given by

$$x(\xi, t) = \left(\frac{(F - 1)}{2\kappa\sqrt{3\alpha p_m}} - \frac{1}{2\kappa}\right) e^{\kappa\sqrt{3\alpha p_m}\left(t - \frac{-1/\kappa - \xi}{(F-1)}\right)} - \left(\frac{(F - 1)}{2\kappa\sqrt{3\alpha p_m}} + \frac{1}{2\kappa}\right) e^{-\kappa\sqrt{3\alpha p_m}\left(t - \frac{-1/\kappa - \xi}{(F-1)}\right)}. \quad (2.12)$$

We next find

$$\frac{\partial x}{\partial \xi} = \left(\frac{1}{2} - \frac{\sqrt{3\alpha p_m}}{2(F - 1)}\right) e^{\kappa\sqrt{3\alpha p_m}\left(t - \frac{-1/\kappa - \xi}{(F-1)}\right)} + \left(\frac{1}{2} + \frac{\sqrt{3\alpha p_m}}{2(F - 1)}\right) e^{-\kappa\sqrt{3\alpha p_m}\left(t - \frac{-1/\kappa - \xi}{(F-1)}\right)}.$$

Solving this expression for t when $\frac{\partial x}{\partial \xi} = 0$ gives

$$t(\xi) = \frac{1}{2\kappa\sqrt{3\alpha p_m}} \ln\left(\frac{\sqrt{3\alpha p_m} + (F-1)}{\sqrt{3\alpha p_m} - (F-1)}\right) + \frac{-1/\kappa - \xi}{(F-1)}. \tag{2.13}$$

The infimum t value for which $\frac{\partial x}{\partial \xi}$ is equal to zero occurs when $\xi = -\frac{1}{\kappa}$. Since $\xi < -\frac{1}{\kappa}$ for this expression we consider $\xi = -\frac{1}{\kappa} - h$, solve for t, and take the limit as $h \to 0$. Doing so gives the time of initial upstream shock formation,

$$t_B = \frac{1}{2\kappa\sqrt{3\alpha p_m}} \ln\left(\frac{\sqrt{3\alpha p_m} + (F-1)}{\sqrt{3\alpha p_m} - (F-1)}\right).$$

Plugging this time into the expression for x when $\xi = -\frac{1}{\kappa}$ gives

$$x\left(\frac{-1}{\kappa}, t_B\right) = \frac{1}{2}\left(\frac{F-1}{\kappa\sqrt{3\alpha p_m}} - \frac{1}{\kappa}\right) e^{\kappa t_B \sqrt{3\alpha p_m}} - \frac{1}{2}\left(\frac{F-1}{\kappa\sqrt{3\alpha p_m}} + \frac{1}{\kappa}\right) e^{-\kappa t_B \sqrt{3\alpha p_m}}$$

$$x\left(\frac{-1}{\kappa}, t_B\right) = -\sqrt{\frac{1}{\kappa^2} - \frac{(F-1)^2}{3\alpha\kappa^2 p_m}}$$

By plugging time t_B into the characteristics solution for $\xi = -\frac{1}{\kappa}$, one also finds that this is the time at which the slope of the characteristic curve becomes vertical. For the downstream shock, we consider characteristic curves for $\frac{-(F-1)}{\kappa\sqrt{3\alpha p_m}} < \xi < \frac{1}{\kappa}$ after they have exited the forced region. These are given by

$$x = \sqrt{(F-1)^2 + 3\alpha p_m(1 - \kappa^2\xi^2)} \cdot \left[t - \frac{1}{\kappa\sqrt{3\alpha p_m}} \ln\left(\frac{-1 + \sqrt{1 + \frac{(F-1)^2}{3\alpha p_m} - \kappa^2\xi^2}}{\frac{F-1}{\sqrt{3\alpha p_m}} + \kappa\xi}\right)\right] + \frac{1}{\kappa}. \tag{2.14}$$

We next find the Jacobian,

$$
J = \frac{\kappa\xi\left(\ln\left(\frac{\sqrt{-3\alpha p_m(\kappa^2\xi^2 - 1) + (F-1)^2} + \sqrt{3\alpha p_m}}{\kappa\xi\sqrt{3\alpha p_m} + (F-1)}\right) - \sqrt{3\alpha p_m}\kappa t\right)}{\sqrt{1 + \frac{(F-1)^2}{3\alpha p_m} - \kappa^2\xi^2}}
$$

$$
+ \frac{\left(3\alpha p_m\sqrt{1 + \frac{(F-1)^2}{3\alpha p_m} - \kappa^2\xi^2} + F\left(\kappa\xi\sqrt{3\alpha p_m} + F - 2\right) - \kappa\xi\sqrt{3\alpha p_m} + 3\alpha p_m + 1\right)}{\left(\kappa\xi\sqrt{3\alpha p_m} + F - 1\right)\left(\sqrt{(F-1)^2 - 3\alpha p_m(\kappa^2\xi^2 - 1)} + \sqrt{3\alpha p_m}\right)}
$$

$$\tag{2.15}$$

Similarly, the infimum t value for which this is equal to zero occurs when $\xi = \frac{1}{\kappa}$. Since $\xi < \frac{1}{\kappa}$ for

33

this expression, we consider $\xi = \frac{1}{\kappa} - h$, solve for t, and again take the limit as $h \to 0$. Doing so, taking p_m, κ, and $(F-1)$ all positive, gives

$$t_B = \frac{(F-1)}{3\alpha\kappa p_m}.$$

Plugging this time into the expression for x when $\xi = \frac{1}{\kappa}$ gives the position of initial downstream shock formation

$$x\left(\frac{1}{\kappa}, t_B\right) = \frac{1}{\kappa} + \frac{(F-1)^2}{3\alpha\kappa p_m}$$

Envelope   Whitham, in [24], outlines a procedure for finding the envelope containing crossing characteristic curves. We shall follow that procedure here. The condition that two neighboring characteristics ξ, and $\xi + h$ intersect at a point (x, t) is that

$$x = x(\xi, t)$$

and

$$x = x(\xi + h, t)$$

hold simultaneously. In the limit $h \to 0$ these give

$$x = x(\xi, t) \quad \text{and} \quad 0 = \lim_{h \to 0} \frac{x(\xi + h, t) - x(\xi, t)}{h} = \frac{\partial x}{\partial \xi}$$

as the implicit equations of an envelope. Note that the second equation here is equivalent to what was done above utilizing the Jacobian determinant. In the present case there are a few ranges of ξ that make sense to consider using this approach. If we consider applicable expressions for x on either side of the upstream edge of the forced region, this limit is undefined unless you fix $\xi = -\frac{1}{\kappa}$. Doing so gives a single time value equal to the one given as the time of initial upstream breaking above. If we consider the characteristic curves for values $\xi < -\frac{1}{\kappa}$ and $|x| < \frac{1}{\kappa}$, we again have equation (2.12) and (2.13). Eliminating ξ causes a cancellation of t and we're left with the vertical line

$$x = -\sqrt{\frac{1}{\kappa^2} - \frac{(F-1)^2}{3\alpha\kappa^2 p_m}}.$$

34

This is consistent with the previous result. Since this expression applies when $\xi < -\frac{1}{\kappa}$, the minimum t value is given by

$$t_{\min} = \frac{1}{2\kappa\sqrt{3\alpha p_m}} \ln \left(\frac{\sqrt{3\alpha p_m} + (F-1)}{\sqrt{3\alpha p_m} - (F-1)} \right).$$

and $t \to \infty$ as $\xi \to -\infty$.

We now consider the characteristic curves for values $-\frac{1}{\kappa} < \xi < \frac{-(F-1)}{\kappa\sqrt{3\alpha p_m}}$. These characteristics cross after exiting the forced region upstream. Following Whitham we arrive at the equations

$$x = -\sqrt{(F-1)^2 + 3\alpha p_m(1 - \kappa^2\xi^2)} \cdot \left[t - \frac{1}{\kappa\sqrt{3\alpha p_m}} \ln \left(\frac{-1 \pm \sqrt{1 + \frac{(F-1)^2}{3\alpha p_m} - \kappa^2\xi^2}}{\frac{F-1}{\sqrt{3\alpha p_m}} + \kappa\xi} \right) \right] - \frac{1}{\kappa}.$$

and

$$t(\xi) = \frac{1}{\sqrt{3\alpha p_m}} \left[\frac{\left(\sqrt{1 - \kappa^2\xi^2 + \frac{(F-1)^2}{3\alpha p_m}} + \kappa\xi\frac{F-1}{\sqrt{3\alpha p_m}} + \frac{(F-1)^2}{3\alpha p_m} + 1 \right) \left(\kappa^2(x^2 - \xi^2) + \frac{(F-1)^2}{3\alpha p_m} \right)}{\kappa\xi \left(\kappa\xi + \frac{F-1}{\sqrt{3\alpha p_m}} \right) \sqrt{1 - \kappa^2\xi^2 + \frac{(F-1)^2}{3\alpha p_m}} \left(\sqrt{1 - \kappa^2\xi^2 + \frac{(F-1)^2}{3\alpha p_m}} + 1 \right)} \right. $$
$$\left. + \ln \left(\frac{-1 - \sqrt{\frac{(F-1)^2}{3\alpha p_m} - \kappa^2\xi^2 + 1}}{\frac{F-1}{\sqrt{3\alpha p_m}} + \kappa\xi} \right) \right].$$

These expressions are a bit messier than the previous, but we can parametrically plot t vs. x on top of the characteristic curves. Similarly, downstream we have

$$x = \sqrt{(F-1)^2 + 3\alpha p_m(1 - \kappa^2\xi^2)} \cdot \left[t - \frac{1}{\kappa\sqrt{3\alpha p_m}} \ln \left(\frac{-1 + \sqrt{1 + \frac{(F-1)^2}{3\alpha p_m} - \kappa^2\xi^2}}{\frac{F-1}{\sqrt{3\alpha p_m}} + \kappa\xi} \right) \right] + \frac{1}{\kappa}.$$

and

$$t = \frac{\ln \left(\frac{\sqrt{3\alpha p_m(1 - \kappa^2\xi^2) + (F-1)^2} + \sqrt{3\alpha p_m}}{\kappa\xi\sqrt{3\alpha p_m} + (F-1)} \right)}{\kappa\sqrt{3\alpha p_m}} - \frac{1}{\kappa\sqrt{3\alpha p_m(1 - \kappa^2\xi^2) + (F-1)^2}}.$$

As an upper bound we take the line $t = \frac{x - \frac{1}{\kappa}}{(F-1)}$. The upstream and downstream shocks will travel within these envelopes. Figure (2.1.2) shows the characteristic curves with the envelopes containing intersecting curves and initial shock formation highlighted for the case $p_m = \kappa = (F-1) = 1$. Consider again the integral equation (2.7) for the characteristics system (2.1). This expression holds for an arbitrary forcing function $f(x)$. If we take f to be positive when $|x| < \frac{1}{\kappa}$ and zero elsewhere,
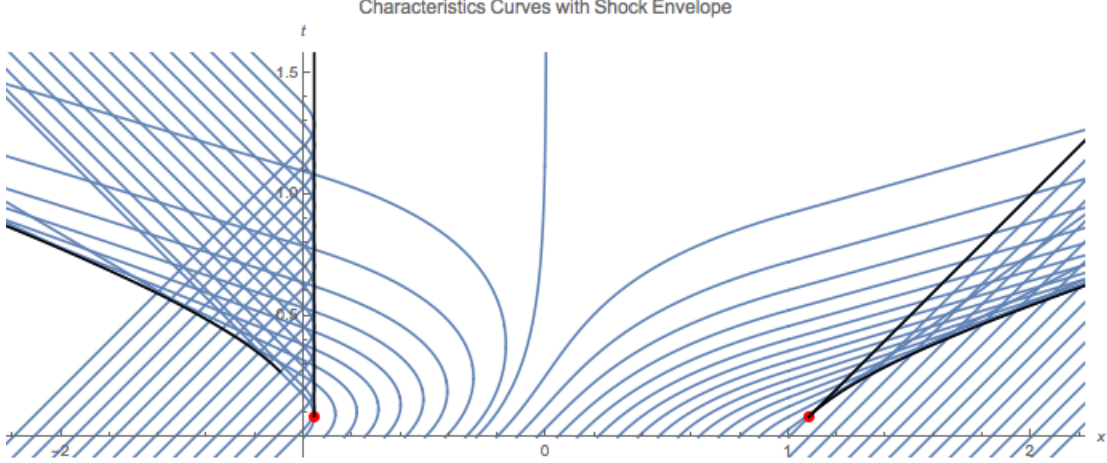
Figure 2.5: Characteristic curves for the system (2.1) with envelopes containing all crossings of characteristic curves pictured in black and red dots highlighting the time and position of initial shock formation. Curves were determined using parameter values $p_m = \kappa = 1$, $F = 2$, $\alpha = 4$.

characteristic curves $x(t)$ for $x, \xi < -\frac{1}{\kappa}$ are given by (2.10). Here we shall assume f_0, the maximum value of f, occurs when $x = 0$. These characteristic curves for $x, \xi < -\frac{1}{\kappa}$ are straight lines, all with the same slope for any $x, \xi < -\frac{1}{\kappa}$. For $\xi \leq -\frac{1}{\kappa}$ and $-\frac{1}{\kappa} < x$ the curves are given by

$$t = \frac{1}{F-1}\left(-\frac{1}{\kappa} - \xi\right) + \int_{-\frac{1}{\kappa}}^{x} \frac{1}{\sqrt{(F-1)^2 - 3\alpha f(y)}}\, \mathrm{d}y.$$

These curves have the same slope for all values x, given $\xi \leq -\frac{1}{\kappa}$, and thus will intersect only if they overturn (assuming continuity). Characteristic curves overturn only if $(F-1)^2 < 3\alpha f_0$, [10]. As the characteristic curves in the case $\xi \leq -\frac{1}{\kappa}$ all have the same slope for all x values, and it can be shown that characteristic curves with $|\xi| < \frac{1}{\kappa}$ do not intersect inside the forced region for a non-negative, symmetric forcing function with compact support that is continuous and concave down, the characteristic curves all have a turning point at the same x value when $(F-1)^2 < 3\alpha f_0$ and this x value corresponds to one leg of the envelope containing all crossings of characteristic curves for $x < 0$. The time of initial upstream shock formation is given by

$$t_B = \frac{1}{2\kappa\sqrt{3\alpha p_m}} \ln\left(\frac{\sqrt{3\alpha p_m} + (F-1)}{\sqrt{3\alpha p_m} - (F-1)}\right). \tag{2.16}$$

Thus for a non-negative, symmetric forcing function with compact support that is continuous and concave down, one leg of the envelope containing all crossings of characteristic curves on the

36

upstream side of the forcing region will be perfectly vertical.

Amplitude and Speed   The velocity of shocks in the solution to (1.16) must be equal to the average of the velocities (given by $\frac{dx}{dt}$) of the solution just behind and ahead of the shock. Recall that in the case $(F-1)^2 < 3\alpha p_m$, characteristics exit the forced region moving both up and downstream. In this case a stationary solution u_s develops over the forced region and extends outward at the speed of the up and downstream shocks. This stationary solution is determined by the characteristic curve that is not swept downstream and does not reach a turning point in finite time. This characteristic curve does not exit the forced region but asymptotically approaches the line $x = 0$, and emanates from $\xi = \frac{1-F}{\kappa\sqrt{3\alpha p_m}}$. Plugging this into the solution of the characteristics system, for long time outside of the forced region but still behind the shock, gives

Following the work outlined by Grimshaw and Smyth, we can find the long time limiting values of the shock speeds up and downstream of the forced region. The shock velocity must be equal to the average of the velocities (i.e. $\frac{dx}{dt}$) of the solution just behind and just ahead of the shock. Recall

$$\frac{dx}{dt} = F - 1 - \frac{3\alpha}{2}u.$$

Letting u_1 and u_2 be the values of the solution just upstream and downstream (respectively) of the shock gives a shock speed $\dot{s}$ of

$$\dot{s} = F - 1 - \frac{3\alpha}{4}(u_1 + u_2). \tag{2.17}$$

The stationary solution that develops over the forced region and emanates outward is given by

$$u_s = \frac{2}{3\alpha}\left(F - 1 - \text{sgn}(x)\sqrt{3\alpha p_m}\right) \tag{2.18}$$

for long times, outside of the forced region where $f(x) = 0$, but still behind the shocks. Ahead of the shocks we still have $u = 0$. Using this in equation (2.17) gives us the long time limiting values of the shock speeds up and downstream of the forced region, where the plus and minus signs denote evaluation at large positive and negative x values (respectively).

$$\dot{s}_\pm = \frac{1}{2}\left[(F-1) \pm \sqrt{3\alpha p_m}\right],$$
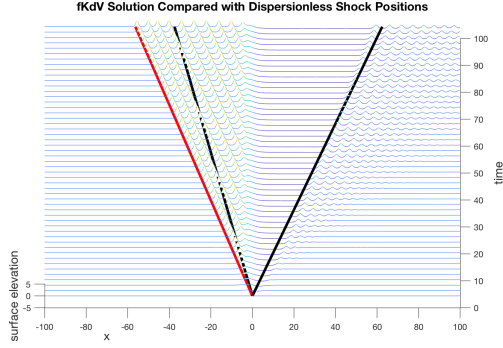
37

Figure 2.6: Waterfall plot of the forced KdV equation (1.15) with black lines representing the limiting shock speed prediction from the analysis in [10] and a red line representing a prediction from analysis presented here. The numerical solution was computed using parameter values $\alpha = \frac{2}{3}$, $\varepsilon = 1$, $F = 1.25$, $p_m = 0.5$, $\kappa = 0.3$, a time step $dt = $ 5e-6, and spatial grid spacing $dx = .0976562$. Using the shock speed of the dispersionless problem does reasonably well in predicting the position of the downstream dispersive shock wave, but a poor job of predicting the position of the leading upstream traveling soliton.

	$\alpha = \sqrt[2]{3}$	$\alpha = \sqrt[5]{3}$	$\alpha = 3$	$\alpha = 4$
$F = 1$	-0.49988	-0.79102	-1.06079	-1.22437
$F = 1.25$	-0.37476	-0.66589	-0.93567	-1.09985
$F = 1.5$	-0.25024	-0.54077	-0.81547	-0.97473
$F = 1.75$	-0.12878	-0.41565	-0.68542	-0.84961

Table 2.1: Shock speeds computed numerically by determining the change in location of the greatest increase in surface elevation from time $t = 40$ to $t = 50$ for various values of the nonlinear parameter α and Froude number F. For simulations the forcing function (2.5) was used with $\kappa = 0.3$ and $p_m = \frac{1}{2}$, on a domain with $dx = 0.00610352$ and $dt = $ 2e $- 5$.

For example, given $p_m = 0.5$, $F = 1.25$, and $\alpha = \frac{2}{3}$, the value of the solution just behind the shock moving upstream is 1.25. Expression (2.18) gives the amplitude of the shock formed by equation (1.16), which we can use to determine its velocity. Lines corresponding to the propagation speeds of upstream and downstream moving shocks for these parameter values are plotted in Figure (2.6) along with the solution of the full forced KdV equation (1.15). We find the quantities that describe the shocks are affected by the maximum amplitude of a wide class of forcing functions which are localized such that $f(x) \to 0$ as $x \to \pm\infty$, and not only those with compact support [10]. Numerical simulations in this paper will use the forcing function

$$\tilde{f}(x) = p_m \operatorname{sech}^2(\kappa x). \tag{2.19}$$

Exact stationary solutions to the forced KdV equation (1.15) for elements in this class of forcing functions are reported in [2].

38
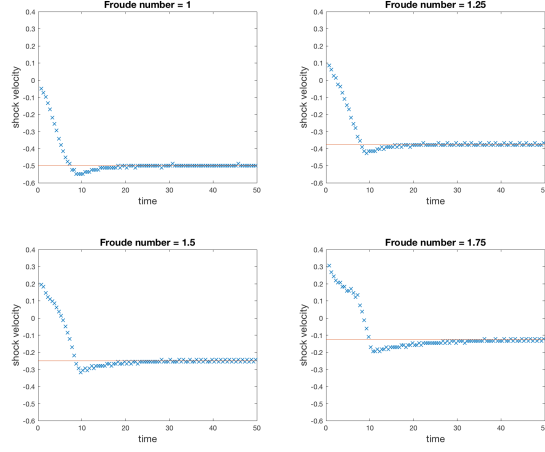
Figure 2.7: Numerically computed upstream shock propagation speeds for various Froude number values. The analytically obtained long time limit prediction (2.20) of upstream shock propagation speed for equation (1.16) is plotted as a solid line for comparison.
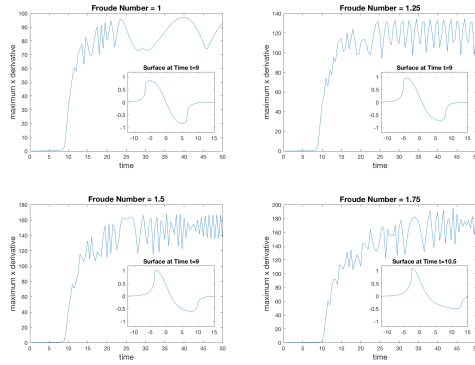
Figure 2.8: The maximum value of the x-derivative of the fluid surface in the simulations from Figure 2.7 is plotted against time for Froude values 1, 1.25, 1.5, and 1.75. The inset shows the fluid surface at the time of shock formation. The time of shock formation for simulations was taken to be the initial time at which the x-derivative of the dispersionless solution at a point reached a magnitude of at least one twelfth of the maximum of this value for the entire simulation. This seemed to correspond to the time value at which the curve began its steep upward trend.

	$\alpha = \, ^2\!/_3$	$\alpha = \, ^5\!/_3$	$\alpha = 3$	$\alpha = 4$
$F = 1$	-0.50000	-0.79057	-1.06066	-1.22474
$F = 1.25$	-0.37500	-0.66557	-0.93566	-1.09974
$F = 1.5$	-0.25000	-0.54057	-0.81066	-0.97474
$F = 1.75$	-0.12500	-0.41557	-0.68566	-0.84974

Table 2.2: Upstream shock speeds for various values of the nonlinear parameter α and Froude number F as predicted by (2.20)

Numerical simulations using a shock capturing method described by [15] with parameters listed above give a solution with amplitude approximately equal to 1.5142 behind the upstream moving shock for $dt = 5e - 4$ and $dx = 0.048828125$. Ahead of the shocks we still have $u = 0$. Using the analytically obtained expression in our equation for shock speed $\dot{s}$ gives the long time limiting values of the shock speed. Upstream we have

$$\dot{s} = \frac{(F - 1) - \sqrt{3\alpha p_m}}{2}. \tag{2.20}$$

For tested parameter values, the prediction in (2.20) appears to agree well with numerical results; with percent differences ranging from 0.001% for $F = 1.5$ and $\alpha = 4$, to 0.593% for $F = 1.5$ and $\alpha = 3$. Results are reported in Tables (2.1.2) and (2.1.2). The agreement is also clear from plotting numerical shock speed against time in Figure 2.7. For numerical values the shock location at a given time is taken to be the midpoint of the two discrete spatial points between which there is the greatest increase in surface elevation in the computed solution. This position is stored every 0.5 time units and tracked over the duration of the simulation. The shock speed is taken to be the difference in shock position divided by 0.5 time units, and stored as the speed at the time value that is the midpoint between the two sample time values. Initially the surface begins to take the shape of the forcing function, so the location of greatest increase is at the inflection point of its derivative. This position is pushed downstream (faster for larger Froude numbers) until the amplitude of the shock becomes large enough to overcome the background flow speed and it is able to propagate upstream. Numerical simulation results pictured used forcing function (2.5), $\kappa = 0.3$, $p_m = \frac{1}{2}$, $\alpha = \frac{2}{3}$, $dx = 0.00610352$, $dt = 2e\text{-}5$. Equation (2.16) predicts that with these parameter values, using (2.4) as a forcing function, the times of initial shock formation will be $t_B = 0$ for $F = 1$, $t_B = 0.8514$ for $F = 1.25$, $t_B = 1.8310$ for $F = 1.5$, and $t_B = 3.2432$ for $F = 1.75$.

2.1.3 Comparison with KdV

The downstream depressed region of the hydraulic approximation (1.16) agrees well with that of the full, forced KdV equation (1.15). As one might expect, the agreement improves as $\varepsilon \to 0$. This is demonstrated in figure (2.1.3). The upstream moving shock front does not accurately predict
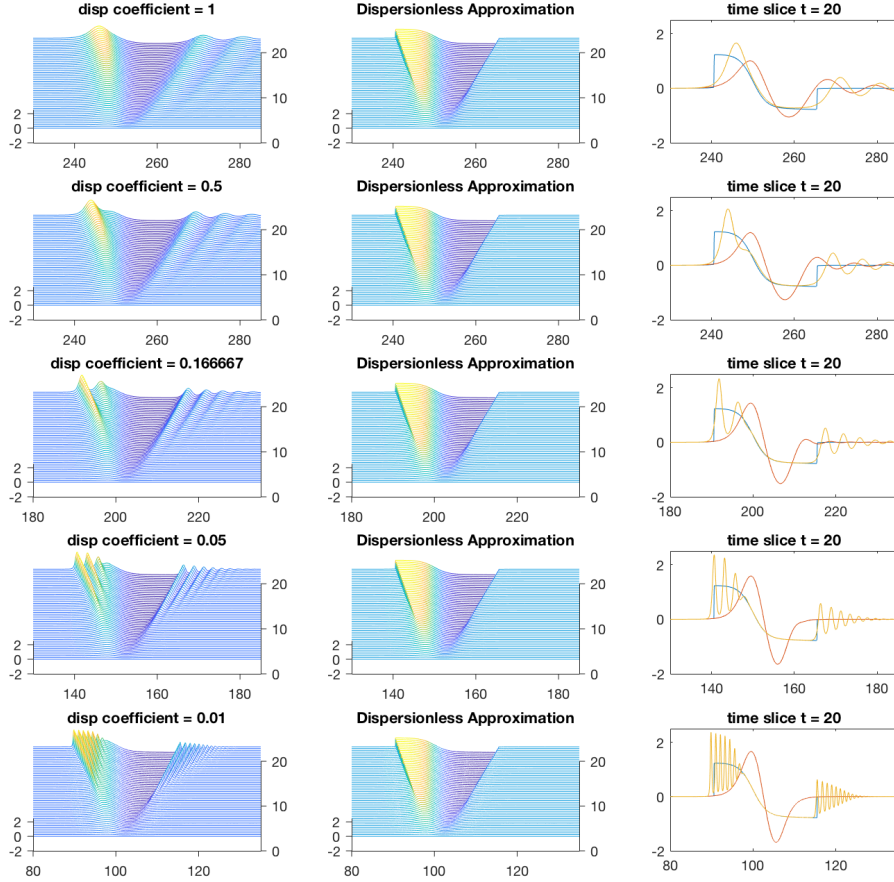
Figure 2.9: The full fKdV equation (1.15) (left) is compared with the dispersionless approximation (1.16) (middle) for varying values of the dispersion parameter ε. The solutions of (1.15), (1.16), and the linearized equation (1.17) are overlayed at time $t = 20$.

the speed of the leading soliton generated in the forced problem. The downstream portion of the solution is shaped like a rectangular potential well. The leading edge of the upstream portion of the solution to the hydraulic approximation looks like the corner of a rectangular box, thus we insert a rectangular box in the free KdV equation (1.14) as an initial condition and examine how well this

predicts upstream behavior of the forced problem (1.15) with a zero initial condition.

A numerically computed solution of the unforced KdV equation (1.14) with a rectangular box initial condition of length L compared with a solution of the forced problem (1.15) with a zero initial condition is pictured in Figure 2.10. The box was of length $L = 200$ (Figure 2.10), with height equal to the expected amplitude of the upstream shock formed by the hydraulic approximation (2.18). In the simulation the left edge of the box was positioned at $x = 0$, and the solution was computed using parameter values $\alpha = \frac{2}{3}$, $F = 1.25$, and $p_m = 0.5$. The corners of the rectangular box were rounded using the function $\cos^4(\beta x)$ with $\beta = 1$. A time step and spatial grid point spacing $1e - 5$ and $dx = 0.0305176$ for $\varepsilon = 3$, $1e - 5$ and $dx = 0.0488281$ for $\varepsilon = 1$, $1e - 5$ and $dx = 0.0183105$ for $\varepsilon = 0.3$, and $2e - 6$ with $dx = 0.0061035$ for $\varepsilon = 0.06$ were used in the computations.

The forced KdV Equation (1.15) with forcing function (2.5) and $\kappa = 0.3$ was solved using the same values for α and F. A time step of $dt = 5$e-5 was used for $\varepsilon = 3, 1$; $dt = 2$e-5 for $\varepsilon = 0.3$; and $dt = 1$e-5 for $\varepsilon = 0.06$. Spatial grid point spacing matched that of the corresponding epsilon values in the case of a box initial condition. The agreement between the two cases highlights the fact that useful information about the full forced KdV equation (1.15) can be gleaned from the study of the dispersionless problem (1.16). The results show that as we decrease ε the number of leading solitons within reasonable agreement seems to get a bit better, and suggest that a significantly longer box initial condition might yield even better agreement with the long time behavior of the solitons generated in the forced case.

2.2   Stationary Solutions

The hydraulic approximation gives insight into the dynamics of equation (1.15), but of course it ignores the effects of dispersion. To learn more about the contributions made by dispersion, we begin by looking for stationary solutions.

2.2.1   Linearized KdV Operator

Let us assume that we have an exact stationary solution to equation (1.15), $\phi(x)$. To linearize about this solution, we insert it along with a perturbation,

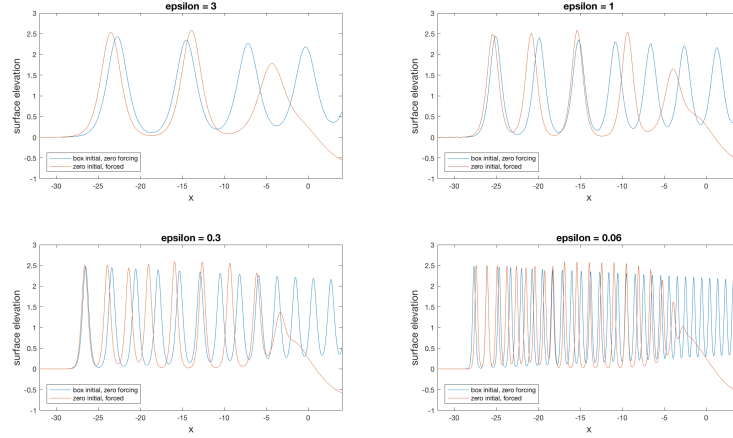$$\zeta(x,t) = \phi(x) + \eta(x,t), \tag{2.21}$$

42

Figure 2.10: Numerically computed solutions of the unforced KdV equation (1.14) with approximately rectangular box initial conditions of length $L = 200$ compared with that of the forced KdV equation (1.15) with a zero initial condition at time $t = 50$. The solutions were computed using values (from left to right) $\varepsilon = 3$, $\varepsilon = 1$, $\varepsilon = 0.3$, $\varepsilon = 0.06$, where the ε parameter determines the strength of dispersion.

into equation (1.15),

$$(\phi + \eta)_t + (F - 1)(\phi + \eta)_x - \frac{3\alpha}{2}(\phi + \eta)(\phi + \eta)_x - \frac{\varepsilon}{6}(\phi + \eta)_{xxx} = f_x(x),$$

and solve for η_t,

$$\eta_t = (1 - F)\eta_x + \frac{3\alpha}{2}\eta\phi_x + \frac{3\alpha}{2}\phi\eta_x + \frac{3\alpha}{2}\eta\eta_x + \frac{\varepsilon}{6}\eta_{xxx}$$

Assuming the perturbation to be small, we drop terms nonlinear in η

$$\eta_t = \left(1 - F + \frac{3\alpha}{2}\phi\right)\eta_x + \frac{3\alpha}{2}\phi_x\eta + \frac{\varepsilon}{6}\eta_{xxx},$$

and we can now write the linearized operator

$$\mathcal{L}_\phi(x) = \left(1 - F + \frac{3\alpha}{2}\phi\right)\partial_x + \frac{3\alpha}{2}\phi_x + \frac{\varepsilon}{6}\partial_x^3. \tag{2.22}$$

To examine the stability of this operator we consider solutions of the form

$$\eta(x, t) = e^{\lambda t}g(x),$$

and apply (2.22)

$$\mathcal{L}_\phi(x)g = \lambda g.$$

The stability of the operator (2.22) are indicated by its eigenvalues λ.

We can find the eigenvalues of (2.22) numerically. Doing so requires a stationary solution. To find one we integrate equation (1.15) with respect to x, insisting that the solution and the forcing function approach zero appropriately fast as $|x| \to \infty$,

$$(1 - F)\zeta - \frac{3\alpha}{4}\zeta^2 - \frac{\varepsilon}{6}\zeta_{xx} = f(x),$$

we can, assuming negligibly small dispersion $\varepsilon \to 0$, solve the resulting quadratic equation

$$\zeta = 2\frac{F - 1 \pm \sqrt{(1 - F)^2 - 3\alpha f(x)}}{3\alpha}.$$

Only the negative branch satisfies the boundary conditions. Furthermore we see that the strength of the nonlinearity and the forcing must be small enough (or the Froude number large enough) to ensure this expression produces a real value. We can then use this expression as an initial guess for Newton's method as we re-insert dispersion, beginning with some small value and iterating up to the desired ε.

If the requirement to ensure that the use of the square root does not produce imaginary values in generating an initial value for Newton's method is too restrictive, we can similarly use Newton's method again to iterate to desired values for amplitude of the forcing function, Froude number, or the nonlinear coefficient.

Running such a numerical method for parameter values $\varepsilon = 1$, $\alpha = \frac{2}{3}$, $\kappa = 0.3$, and $p_m = 0.5$ (with forcing function 2.5), the method finds stationary solutions for Froude values $F > 1.761$. Equation (1.15) with a zero initial condition will generate upstream propagating solitary waves for Froude numbers below this critical value. We call this the resonant regime. For the parameters above, analysis of the dispersionless case (1.16) predicts that there will be no upstream propagation for Froude numbers $F > 2$. This discrepancy suggests dispersion plays a role in determining the critical Froude value for which we see solitons traveling upstream. For super critical Froude values, we find two solution branches, as pictured in Figure 2.11. Stationary solutions to the forced KdV
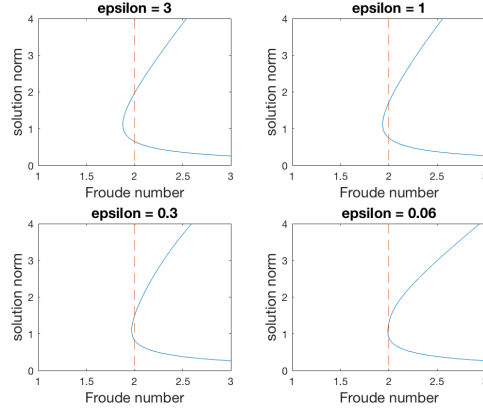
Figure 2.11: The norm of computed stationary solutions to (1.15) is plotted against the corresponding Froude numbers for various values of the dispersion parameter ε. The dashed line depicts the predicted minimum Froude value for which a stationary solution exists, obtained from analysis of the dispersionless hydraulic approximation (1.16).

equation (1.15) are computed using this numerical continuation method. The nonlinear parameter used in each computation is $\alpha = \frac{2}{3}$ and the forcing function used is given by (2.5). Derivatives are computed spectrally, with a grid spacing $dx = 0.390625$. We see that the turning point in the bifurcation diagram approaches the hydraulic approximation prediction as $\varepsilon \to 0$.

The numerically computed eigenvalues of the linearized operator (2.22) indicate that the branch corresponding to solutions with the smaller norm is stable and the other branch is unstable. Solutions on each branch of this curve for $\varepsilon = 1$ are perturbed and evolved according to (1.15) and the results are plotting in Figure 2.12. The solutions were computed on a grid $dx = 0.390625$, $dt = 1e\text{-}5$ using parameters $\alpha = \frac{2}{3}$, $\varepsilon = 1$, $p_m = \frac{1}{2}$, $\kappa = 0.3$. We see that the solution with the greater norm is indeed unstable, as when perturbed it collapses back onto the stable solution. This is consistent with the results reported in [2].

By numerically approximating and examining stationary solutions to equation (1.15) we are able to determine a critical Froude value below which solitons will develop and travel upstream. By examining the eigenvalues of the linearized KdV operator (2.22) we are able to determine the stability of these stationary solutions. Comparing our findings from this analysis with what we learned from the hydraulic approximation (1.16) we see that dispersion plays a role in determining for what Froude values upstream propagating solitons are generated by (1.15), and that this critical value approaches the prediction made using the (1.16) as the dispersion parameter $\varepsilon \to 0$.
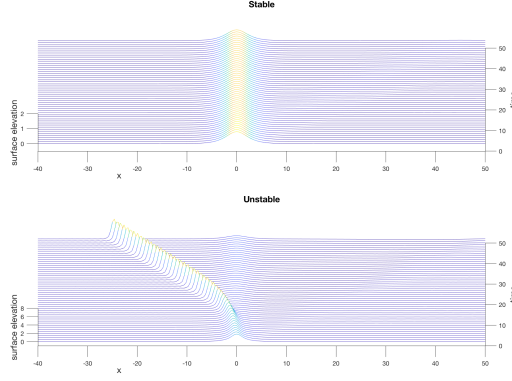
Figure 2.12: Perturbed stable and unstable stationary solutions computed via numerical continuation are inserted as initial conditions and evolved to time $t = 50$ using the ETD-RK4 method described in [14]. Stationary solutions were selected for Froude values $F \approx 2.01042$ (stable) and $F \approx 1.99140$ (unstable). To perturb the numerically computed stationary solutions they were multiplied by 1.1. Note the stable solution is plotted on a z-axis that goes to two, and the unstable solution on a z-axis that goes to eight.

2.3   The Schrödinger Operator

Important to the inverse scattering theory to follow is some analysis of the Schrödinger operator with a potential function evolved according to the KdV equation. The typical inverse scattering technique for solving the KdV equation uses

$$u_t - 6uu_{\tilde{x}} + u_{\tilde{x}\tilde{x}\tilde{x}} = 0. \tag{2.23}$$

Given the Schrödinger equation,

$$\big(-\partial_{\tilde{x}\tilde{x}} + u(\tilde{x}, t)\big)\psi = \lambda\psi,$$

if u evolves according to the KdV equation (2.23), then λ is independent of time [24]. To arrive at equation (2.23) we can rescale the variables ζ and x

$$u = -\frac{\alpha}{4}\left(\frac{6}{\varepsilon}\right)^{1/3}\zeta, \qquad \text{and} \qquad \tilde{x} = -\left(\frac{6}{\varepsilon}\right)^{1/3}\big(x - (F-1)t\big). \tag{2.24}$$

From this we see that the appropriate Schrödinger operator is

$$(\partial_{\tilde{x}\tilde{x}} - 6u) = \left[-\left(\frac{\varepsilon}{6}\right)^{2/3}\partial_{xx} - \frac{\alpha}{4}\left(\frac{6}{\varepsilon}\right)^{1/3}\zeta\right]. \tag{2.25}$$
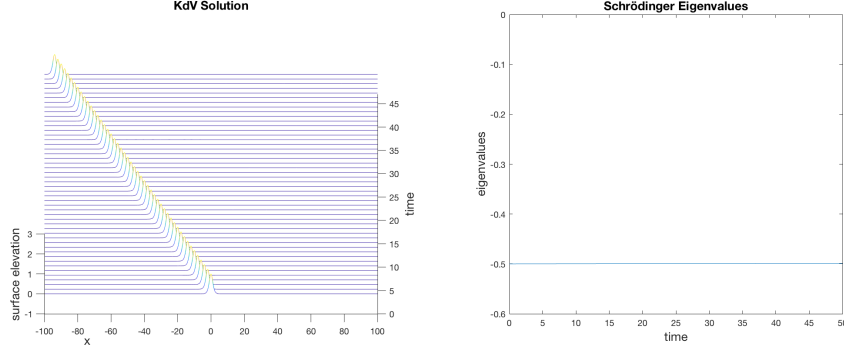
Figure 2.13: The plot on the left shows an initial soliton evolved according to (1.14). The plot on the right shows the numerically computed eigenvalue of (2.25) versus time, using the KdV soliton pictured on the left as its potential function. The spacing of grid points is 0.012207, the time step is 2e-5, $\varepsilon = 6$, $F = 1$, and $\alpha = 4$.

Inserting parameters $F = 1$, $\alpha = 4$, and $\varepsilon = -6$ also gives the 'typical' KdV equation (2.23). The KdV equation (1.14) has an exact traveling wave solution [24],

$$\zeta = \operatorname{sech}^2\left(\sqrt{\frac{3\alpha}{4\varepsilon}}(x + 2t)\right).$$

To test our numerical method we can use this as an initial condition and evolve the KdV equation (1.14) using an exponential time differencing fourth order Runge-Kutta method (ETD-RK4) [14]. To determine the eigenvalues of the Schrödinger operator with the KdV solution for a potential function we can use the Matlab function 'eigs'. We expect to find a single eigenvalue that remains constant in time. Our numerical method producing these results provides evidence that the ETD-RK4 method and the 'eigs' function are working as expected. The result is shown in Figure 2.13. For an initial soliton of unit amplitude we expect a single constant negative eigenvalue $\lambda = -\frac{1}{2}$. The solution on a grid with points spaced 0.195313 units apart was input into the 'eigs' function to calculate the eigenvalues of the Schrödinger operator (2.25).

Next, with the shock solution of the hydraulic approximation (1.16) in mind, we consider a rectangular box potential of length L, i.e. ζ equal to a constant value u_0 when $x \in \left[-\frac{L}{2}, \frac{L}{2}\right]$ and zero elsewhere. We know from WKB theory that Schrödinger's equation has nontrivial solutions only if

$$\int_0^L \sqrt{\lambda + \frac{\alpha}{4}\left(\frac{6}{\varepsilon}\right)^{1/3} u_0}\,\mathrm{d}x = \left(n + \frac{1}{2}\right)\pi \left(\frac{\varepsilon}{6}\right)^{1/3}, \tag{2.26}$$
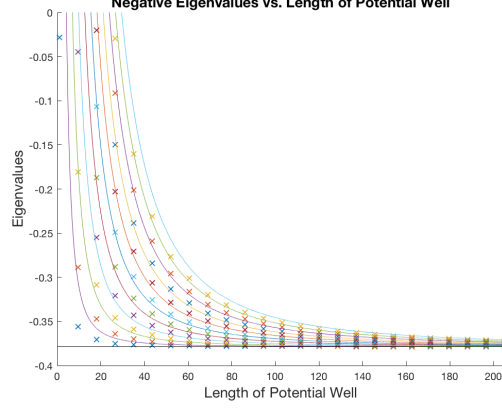
47

Figure 2.14: Eigenvalues of the Schrödinger operator with a rectangular box potential function versus the length of the box. Numerically coputed eigenvalues are marked x. The curves represent the analytically obtained predictions of the eigenvalues as functions of L. The plotted black, horizontal line represents the limit of this prediction as $L \to \infty$

$$\lambda = \frac{\pi^2}{L^2}\left(\frac{\varepsilon}{6}\right)^{2/3}\left(n+\frac{1}{2}\right)^2 - \frac{\alpha}{4}\left(\frac{6}{\varepsilon}\right)^{1/3}u_0, \tag{2.27}$$

to first order [1]. It is clear from this analytically obtained expression that the eigenvalues approach a limiting quantity $\lambda = \frac{\alpha}{4}\left(\frac{6}{\varepsilon}\right)^{1/3}u_0$ as $L \to \infty$. Multiplying $\varepsilon^{1/3}$ across the expression to account for the variable transformation (2.24), it becomes clear that the eigenvalues approach the limiting quantity as $\varepsilon \to 0$ in the same way as when $L \to \infty$. This agrees with the numerical findings presented in Figure 2.10, and again suggests that the solution of of the unforced problem (1.14) with a box initial condition will approach the solution of the forced problem (1.15) as $L \to \infty$.

For $\alpha = \frac{2}{3}$, $\varepsilon = 1$, $F = 1.25$, and $p_m = 0.5$ we can numerically find the eigenvalues with this square well potential plugged into the appropriate Schrödinger operator on a grid $x \in [-525, 525]$ with grid points spaced $dx \approx 0.5068$. We allow L to take 25 evenly spaced values from 1 to 205, find the 10 eigenvalues of the operator with the most negative real part, and plot the negative ones against L in Figure 2.14 (On finer grids or for larger values of L, fewer than 10 eigenvalues converge using the Matlab function 'eigs').

We also plot the analytically predicted eigenvalues as a function of L for $n = 1, 2, \ldots, 10$. Here we take the value from the hydraulic approximation prediction of shock amplitude (2.18) $u_0 = \frac{2}{3\alpha}(F - 1 + \sqrt{3\alpha p_m})$. For chosen parameter values we expect the eigenvalues to approach -0.378567 as L approaches infinity. This limit is also plotted.

We see in the Figure 2.14 and in the WKB expression for the eigenvalues of the Schrödinger
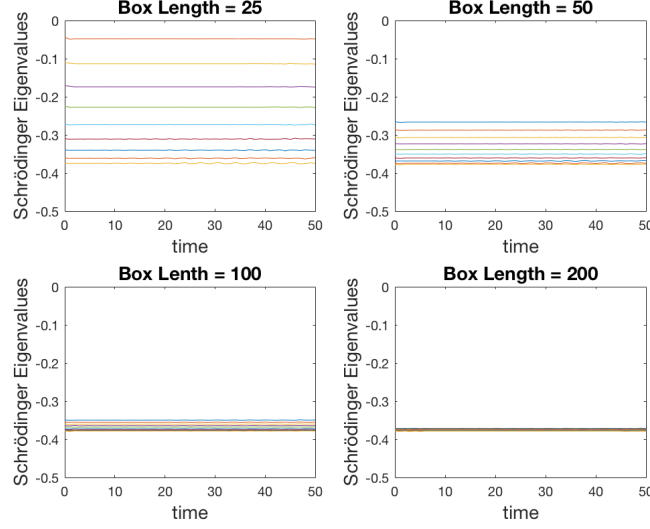
Figure 2.15: Numerically computed eigenvalues of the Schrödinger operator with an approximately rectangular box initial potential functions of various lengths evolved according to KdV plotted versus time. A time step 2e-5 was used, along with spatial grid point spacing $dx \approx 0.048828$, $\alpha = \frac{2}{3}$, $\varepsilon = 1$, $F = 1.25$, $\beta = 1.75$. The height of the initial box was $u_0 = 1.25$.

operator that as L increases, all eigenvalues converge toward the expected quantity $\lambda = \frac{\alpha}{4} \left(\frac{6}{\varepsilon} \right)^{1/3} u_0 \approx -0.378567$. If we use a rectangular well, rounded using the function $\cos^4(\beta x)$ where β represents a smoothing factor, of length L as an initial condition and evolve it according to equation (1.14), we expect the eigenvalues to remain constant in time. The results of doing so numerically are plotted in Figure 2.15. The potential used to calculate the eigenvalues of the Schrödinger operator was the numerical KdV solution evaluated on the center half of the full grid, using points spaced $dx = 0.78125$, evaluated every $dt = 1$ nondimensional time unit. For a box of length $L = 25$ the 'eigs' function only computed 9 eigenvalues (consistent with the prediction in equation (2.33)). In all other cases the 10 eigenvalues with the most negative real part are plotted. We also expect the eigenvalues to converge to the value above as L grows.

In simulations, for a rounded square potential well of length 200 initial condition evolved according to the KdV equation, the Matlab function 'eigs' fails to calculate eigenvalues when the surface elevation is calculated on 2^{11} or more points.

Exact solutions to the unforced KdV equation in the form of solitons are known,

$$\zeta_s = a \operatorname{sech}^2 \left\{ \left(\frac{3\alpha a}{4\varepsilon} \right)^{1/2} x \right\},$$

49

where the amplitude a is a free parameter. In the absence of forcing, this profile translates without changing its shape when evolved according to the KdV equation (1.14). Numerical results have demonstrated that the amplitudes of solitons that advance upstream in the time evolution of equation (1.15) are typically approximately double the amplitude of the upstream advancing shock generated in the hydraulic approximation to the equation, all parameters other than dispersion equal. The amplitude of the shock can be obtained analytically (as demonstrated above).

The area under an exact soliton solution to equation (1.14) is

$$\int_{-\infty}^{\infty} \zeta_s \, dx = \frac{8}{3\alpha} \sqrt{\varepsilon \left(F - 1 + \sqrt{3\alpha p_m} \right)} \tag{2.28}$$

We can use the analytically determined speed of the shock along with its amplitude to find the approximate area under the curve of the shock profile as a function of time. Setting this equal to the area under the curve of an exact soliton solution, the amplitude of which is double the amplitude of the upstream advancing shock, we can predict the time it takes for each new soliton to form in equation (1.15)

$$T_s = \frac{8\sqrt{\varepsilon \left(F - 1 + \sqrt{3\alpha p_m} \right)}}{3\alpha p_m - (F - 1)^2}. \tag{2.29}$$

This prediction is compared with numerical results in Figure 2.16. While it does not provide a precisely accurate count across all parameter combinations that produce upstream traveling solitons in the forced KdV equation (1.15), the expression in (2.29) is easily calculable and shows reasonable agreement with numerical results.

Equation (2.29) can also be used to predict the position of the leading upstream propagating soliton as a function of time. Expecting soliton spacing to be equal to some constant times the expression (2.28) divided by the amplitude of the solitons,

$$\text{spacing} = 2 \left(\frac{4\varepsilon}{3\alpha a} \right)^{1/2} \text{constant}, \tag{2.30}$$

we compare the results of several numerical simulations for parameter values $\alpha = \frac{2}{3}$, $p_m = \frac{1}{2}$, $F = 1.25$, and $\varepsilon = 3, 1, 0.3, 0.06$. The spacing between all soliton peaks located to the left of $x = -10$ (where the value of the forcing function was less than one percent of its maximum value) was averaged and compared with (2.30) at time $t = 100$ when $\varepsilon = 1$ and at time $t = 50$ for all other
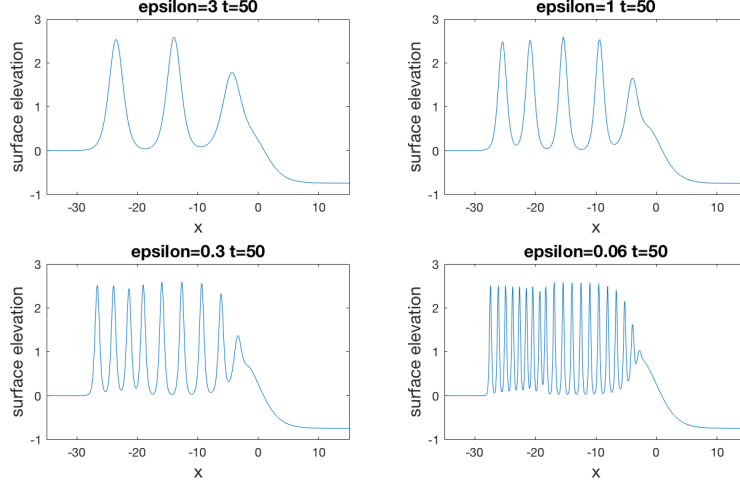
50

Figure 2.16: Numerically computed solutions of equation (1.15) for various values of ε. In each computation the forcing function (2.4) is used with parameters $\alpha = \frac{2}{3}$, $F = 1.25$, $p_m = 0.5$, $\kappa = 0.3$ and a zero initial condition. A time step of (from left to right, top to bottom) $dt = $ 5e-5, 5e-5, 2e-5, 1e-5 and grid point spacing $dx = 0.0305176, 0.0488281, 0.0183105, 0.00610352$ was used for the computations. For the values of ε shown, equation (2.29) predicts the formation of 2, 5, 10, 17 solitons.

values of ε. The constant was found to be 3.0053 (approximately 3). We expect the speed of the leading upstream propagating soliton to then be this soliton spacing divided by T_s,

$$\frac{3}{4}\left(\sqrt{3\alpha p_m} - (F - 1)\right).$$

2.4   Inverse Scattering Transform

The inverse scattering transform solution of the KdV equation (2.23) is [24]

$$u = -2\frac{\mathrm{d}^2}{\mathrm{d}\tilde{x}^2}\log|P| \tag{2.31}$$

where

$$|P| \propto \left|\frac{\gamma_m \exp\left[-2\mu_m - \left(\frac{6}{\varepsilon}\right)^{1/3}\left(x - (F - 1)t\right) + 8\mu_m^3 t\right]}{\mu_m + \mu_n}\right|,$$

normalization constants

$$\gamma_n = \left\{\int_{-\infty}^{\infty} u^2 \, \mathrm{d}\tilde{x}\right\}^{-1} = \frac{8\varepsilon}{3\alpha^2}\left\{\int_{-\infty}^{\infty} \zeta^2 \, \mathrm{d}x\right\}^{-1},$$

51

and we use the negative eigenvalues of the Schrödinger operator (2.25) with the KdV initial condition as a potential function,

$$\lambda = -\mu_n^2.$$

In terms of our variables, (2.31) can be written as

$$\zeta = -\frac{4\varepsilon}{3\alpha} \frac{\mathrm{d}^2}{\mathrm{d}x^2} \log |P|. \tag{2.32}$$

We can compute this solution to KdV (1.14) numerically for a rectangular box initial condition.

We take $F = 1.25$, $\varepsilon = 1$ and $\alpha = \frac{2}{3}$. Using the chosen solution form, for an initial box of length $L = 15$ and height from (2.18) $u_0 = \frac{2}{3\alpha}\left(F - 1 + \sqrt{3\alpha p_m}\right)$ solved on a domain $x \in [-74.25, 65.75]$ with 806 grid points, peaks formed in the solution are nearest to uniform (the standard deviation of the values of local maxima in the solution) at time $t \approx -1.844994704$. There are six peaks in the solution, consistent with the prediction in [24],

$$N = \text{largest integer} \le \frac{u_0^{1/2} L}{\pi} + 1. \tag{2.33}$$

By comparing the IST and ETD-RK4 solutions, shown in Figure 2.17, we see excellent agreement in the solitary waves traveling upstream. For the ETD-RK4 solution the corners of the rectangular box were rounded using a $\text{sech}^2(\kappa x)$ function with $\kappa = 0.7$, which minimized the 2-norm of the difference between this initial profile and that obtained from the IST, and equation (1.15) was solved using a time step 2e-6 and spatial grid point spacing $dx = 0.0244141$. The IST solution was evolved according to (2.32) in which $|P|$, γ_n, and λ were computed numerically. Time values in the IST solution were uniformly shifted so that the time at which solution peaks were most uniform was used as the starting time $t = 0$. Both box heights were set by (2.18) using parameter values $\alpha = \frac{2}{3}$, $\varepsilon = 1$, $p_m = 0.5$ and $F = 1.25$. Matlab failed to produce a smooth solution for a significantly longer initial box on the grid used and, using the Matlab function 'eigs', the expected number of eigenvalues failed to converge on finer grids.

Note that here our IST solution ignores any contributions from the continuous spectrum of the operator, so we may conclude that such contributions are small and do not significantly affect the behavior of the solitons traveling upstream.
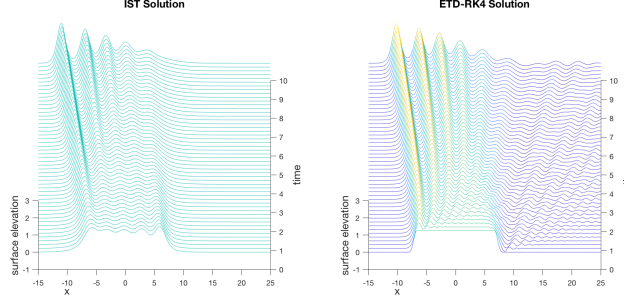
Figure 2.17: Numerically computed solutions to equation (1.14) for an approximately rectangular box initial condition are shown evolving over 10 nondimensional time units in the top two plots in the figure. The left solution is obtained using the inverse scattering transform, and the right solution using the ETD-RK4 method from [14].

One might expect this, in combination with results from analysis of the inviscid equation (1.16), presents a way to predict the frequency of soliton generation in the full forced problem (1.15). If we treat the upstream or downstream traveling shock as a potential function of constant amplitude that grows in length at the speed of shock propagation, (2.33) can be used to predict a period for soliton emission. For solitons traveling upstream this prediction would be given by

$$T_s = \left| \frac{2\pi}{(F - 1 - \sqrt{3\alpha p_m})\sqrt{\frac{2}{3\alpha}(F - 1 + \sqrt{3\alpha p_m})}} \right|.$$

As this method does not include dispersion, one might expect this estimate becomes more accurate as ε decreases. In actuality, the number of upstream propagating solitons generated in a given amount of time increases as ε decreases (all other paramters held constant), and is not bounded by this method of prediction. For the parameter values $\alpha = \frac{2}{3}$, $F = 1.25$, and $p_m = \frac{1}{2}$, this method predicts approximately seven solitons will form in 50 nondimensional time units regardless of the value of ε. It is clear from Figure 2.16 that the number of solitons produced by (1.15) does not approach the prediction obtained using this method as $\varepsilon \to 0$.

2.5 Numerical Methods

2.5.1 Integrating Factor, Fourth Order Runge-Kutta

To numerically solve the KdV equation

$$-\zeta_t + \left(1 - F + \frac{3\alpha}{2}\zeta\right)\zeta_x + \frac{\varepsilon}{6}\zeta_{xxx} = 0, \qquad x \in [x_{\min}, x_{\max}], \quad t \in (t_0, t_{\max}), \tag{2.34}$$

we utilize an integrating factor method as described in [14]. For our problem we make use of the Fourier transform, which allows us to evaluate derivatives via multiplication with the imaginary unit and the frequency variable k. We will denote the Fourier transformed variable $\hat{\zeta}(k, t)$. Our equation becomes

$$\hat{\zeta}_t = ik(1 - F)\hat{\zeta} - ik^3\frac{\varepsilon}{6}\hat{\zeta} + ik\frac{3\alpha}{4}\widehat{(\zeta^2)}, \tag{2.35}$$

At this point we can define a linear operator $\mathbf{L} = ik(1 - F) - ik^3\frac{\varepsilon}{6}$ and a nonlinear operator $\mathbf{N}(\zeta) = ik\frac{3\alpha}{4}\widehat{(\zeta^2)}$, and write our equation

$$\hat{\zeta}_t = \mathbf{L}\hat{\zeta} + \mathbf{N}(\zeta). \tag{2.36}$$

Multiplication by an integrating factor $e^{-\mathbf{L}t}$ gives

$$e^{-\mathbf{L}t}\hat{\zeta}_t = \mathbf{L}e^{-\mathbf{L}t}\hat{\zeta} + e^{-\mathbf{L}t}\mathbf{N}(\zeta). \tag{2.37}$$

Use the integrating factor to define a new variable

$$v(k, t) = e^{-Lt}\hat{\zeta}(k, t). \tag{2.38}$$

And we find

$$v_t = e^{-Lt}N(e^{Lt}v). \tag{2.39}$$

54

We use a standard fourth-order Runge-Kutta time stepping method to solve this equation. Let $t_n = t_0 + n \cdot dt$ and let $v_n = v(k, t_n)$

$$a = dt\, e^{-Lt_n}\, N\left(e^{Lt_n}\, v_n\right) \tag{2.40}$$

$$b = dt\, e^{-L(t_n + dt/2)}\, N\left(e^{L(t_n + dt/2)}\, (v_n + a/2)\right) \tag{2.41}$$

$$c = dt\, e^{-L(t_n + dt/2)}\, N\left(e^{L(t_n + dt/2)}\, (v_n + b/2)\right) \tag{2.42}$$

$$d = dt\, e^{-Lt_{n+1}}\, N\left(e^{Lt_{n+1}}\, (v_n + c)\right) \tag{2.43}$$

$$v_{n+1} = v_n + \frac{1}{6}(a + 2b + 2c + d) \tag{2.44}$$

2.5.2 Exponential Time Differencing Fourth-Order Runge-Kutta

The solution to the Kortewig de-Vries equation is approximated using a method developed by Kassam and Trefethen in a 2005 paper [14]. The method evaluates the spatial derivatives pseudo spectrally and uses an exponential time-differencing fourth-order Runge Kutta (ETD-RK4) time stepping method. Pseudo spectral methods to evaluate derivatives make use of the Fourier transform

$$\mathcal{F}\{u(x)\} = \hat{u}(k) = \int_{-\infty}^{\infty} u(x)e^{-ikx}\, \mathrm{d}x.$$

If we consider the inverse Fourier transform,

$$\mathcal{F}^{-1}\{\hat{u}(k)\} = u(x) = \int_{-\infty}^{\infty} \hat{u}(k)e^{ikx}\, \mathrm{d}k,$$

along with the Fourier transform of the derivative of the function u, we find that

$$\mathcal{F}\left\{\frac{\partial}{\partial x}u(x)\right\} = \int_{-\infty}^{\infty} ik\left[\int_{-\infty}^{\infty} \hat{u}(k)e^{ikx}\, \mathrm{d}k\right]e^{-ikx}\, \mathrm{d}x = ik\,\hat{u}(k).$$

Thus, using the Fast Fourier Transform (FFT) and operating in Fourier space can allow us to do calculation quickly and easily. The ETD-RK4 time stepping method is well suited for evolution equations with both linear and nonlinear terms, making it a natural choice for evaluating the KdV

equation. Consider an equation of the form

$$u_t = \mathbf{L}u + \mathbf{N}(u, t) \tag{2.45}$$

where $\mathbf{L}$ and $\mathbf{N}$ are discretized forms of linear and nonlinear operators (respectively). Define

$$v = e^{-\mathbf{L}t}u$$

and differentiate the equation with respect to t to obtain

$$v_t = -e^{-\mathbf{L}t}\mathbf{L}u + e^{-\mathbf{L}t}u_t.$$

Notice that if we multiply Equation (2.45) by $e^{-\mathbf{L}t}$ we obtain

$$e^{-\mathbf{L}t}u_t = e^{-\mathbf{L}t}\mathbf{L}u + e^{-\mathbf{L}t}\mathbf{N}(u, t).$$

This allows us to substitute v_t into the result, yielding

$$v_t = e^{-\mathbf{L}t}\mathbf{N}(e^{\mathbf{L}t}v, t).$$

If we now integrate over a single time step of length h we arrive at

$$v_{n+1} = v_n + \int_0^h e^{-\mathbf{L}(t_n+\tau)}\mathbf{N}(e^{\mathbf{L}(t_n+\tau)}v(t_n+\tau), t_n+\tau)\,\mathrm{d}\tau.$$

Re-writing the equation in terms of u gives

$$e^{-\mathbf{L}t_{n+1}}u_{n+1} = e^{-\mathbf{L}t_n}u_n + \int_0^h e^{-\mathbf{L}(t_n+\tau)}\mathbf{N}(u(t_n+\tau), t_n+\tau)\,\mathrm{d}\tau.$$

We may now multiply by $e^{\mathbf{L}t_{n+1}}$ to reach

$$u_{n+1} = e^{\mathbf{L}h}u_n + e^{\mathbf{L}h}\int_0^h e^{-\mathbf{L}\tau}\mathbf{N}(u(t_n+\tau), t_n+\tau)\,\mathrm{d}\tau.$$

The exponential time differencing described in [3] is similar to the integrating factor method.

re-write the equation in terms of and solve for $\hat{\zeta}$

$$\hat{\zeta}_{n+1} = e^{\mathbf{L}dt}\hat{\zeta}_n + e^{\mathbf{L}dt}\int_0^{dt} e^{-\mathbf{L}\tau}\mathbf{N}\Big(\hat{\zeta}(t_n + \tau), t_n + \tau\Big)\,\mathrm{d}\tau \tag{2.46}$$

In [3] authors Cox and Matthews give a set of fourth-order Runge-Kutta time stepping formulae. Following Kassam & Trefethen, for a time step of length h we can write these formulae in terms of the coefficients

$$\alpha = h^{-2}\mathbf{L}^{-3}\Big[-4 - \mathbf{L}h + e^{\mathbf{L}h}\big(4 - 3\mathbf{L}h + (\mathbf{L}h)^2\big)\Big] \tag{2.47}$$

$$\beta = h^{-2}\mathbf{L}^{-3}\Big[2 + \mathbf{L}h + e^{\mathbf{L}h}(-2 + \mathbf{L}h)\Big] \tag{2.48}$$

$$\gamma = h^{-2}\mathbf{L}^{-3}\Big[-4 - 3\mathbf{L}h - (\mathbf{L}h)^2 + e^{\mathbf{L}h}(4 - \mathbf{L}h)\Big] \tag{2.49}$$

for a dependent variable u

$$a_n = e^{\mathbf{L}h/2}u_n + \mathbf{L}^{-1}\big(e^{\mathbf{L}h/2} - \mathbf{I}\big)\mathbf{N}(u_n, t_n), \tag{2.50}$$

$$b_n = e^{\mathbf{L}h/2}u_n + \mathbf{L}^{-1}\big(e^{\mathbf{L}h/2} - \mathbf{I}\big)\mathbf{N}(a_n, t_n + h/2), \tag{2.51}$$

$$c_n = e^{\mathbf{L}h/2}a_n + \mathbf{L}^{-1}\big(e^{\mathbf{L}h/2} - \mathbf{I}\big)\big(2\mathbf{N}(b_n, t_n + h/2) - \mathbf{N}(u_n, t_n)\big), \tag{2.52}$$

$$u_{n+1} = e^{\mathbf{L}h}u_n + h^{-2}\mathbf{L}^{-3}\Big\{\alpha\mathbf{N}(u_n, t_n) + 2\beta\Big[\mathbf{N}(a_n, t_n + h/2) + \mathbf{N}(b_n, t_n + h/2)\Big] + \gamma\mathbf{N}(c_n, t_n + h)\Big\}. \tag{2.53}$$

To circumvent numerical instability, we evaluate elements of this expression via an integral over a circle of unit radius in the complex plane centered at the $\mathbf{L}$ using the Cauchy integral formula for a diagonal matrix $\mathbf{L}$

$$f(\mathbf{L}) = \frac{1}{2\pi i}\oint_C f(z)(z\mathbf{I} - \mathbf{L})^{-1}\,\mathrm{d}z. \tag{2.54}$$

Numerically, for our purposes, the contour integral reduces to a mean of the function prone to numerical error over the contour. Functions evaluated in this way include the expressions for α, β, γ, and

$$f(\mathbf{L}) = \mathbf{L}^{-1}\big(e^{\mathbf{L}h/2} - \mathbf{I}\big). \tag{2.55}$$

Either this or the previous method may be used to solve the linearized problem

$$\zeta_t = (1 - F)\zeta_x + \frac{\varepsilon}{6}\zeta_{xxx}.$$

2.5.3 Shock Capturing

To numerically solve the dispersionless, hydraulic approximation to KdV (1.16), we employ a method discussed in [15] by authors Kurganov and Tadmor. We begin by writing this in the form of a nonlinear conservation law

$$\frac{\partial}{\partial t}\zeta + \frac{\partial}{\partial x}g\Big(\zeta(x,t)\Big) = 0, \tag{2.56}$$

where the flux function

$$g\big(\zeta(x,t)\big) = (F - 1)\zeta - \frac{3}{4}\alpha\zeta^2. \tag{2.57}$$

The Kurganov-Tadmor scheme we seek to use here is given by

$$
\begin{aligned}
\frac{d}{dt}u_j(t) = &-\frac{\Big(g\big(u_{j+1/2}^+(t)\big) + g\big(u_{j+1/2}^-(t)\big)\Big) - \Big(g\big(u_{j-1/2}^+(t)\big) + g\big(u_{j-1/2}^-(t)\big)\Big)}{2\Delta x} \\
&+ \frac{1}{2\Delta x}\Big\{a_{j+1/2}(t)\big[u_{j+1/2}^+(t) - u_{j+1/2}^-(t)\big] - a_{j-1/2}(t)\big[u_{j-1/2}^+(t) - u_{j-1/2}^-(t)\big]\Big\},
\end{aligned}
\tag{2.58}
$$

for a dependent variable u where, in the generic case, one may take

$$a_{j+1/2}(t) := \max\left\{\left|\frac{\partial g}{\partial u}\big(u_{j+1/2}^+(t)\big)\right|, \left|\frac{\partial g}{\partial u}\big(u_{j+1/2}^-(t)\big)\right|\right\}. \tag{2.59}$$

Note that $u_{j+1/2}^+ := u_{j+1}^n - \frac{\Delta x}{2}(u_x)_{j+1}^n$, $u_{j+1/2}^- := u_j^n + \frac{\Delta x}{2}(u_x)_j^n$, and $u_j^n = u(x_j, t_n)$; where u_x is given by

$$(u_x)_j^n = \text{minmod}\left(\frac{u_j^n - u_{j-1}^n}{\Delta x}, \frac{u_{j+1}^n - u_j^n}{\Delta x}\right), \tag{2.60}$$

and $\text{minmod}(a,b) := \frac{1}{2}[\text{sgn}(a) + \text{sgn}(b)] \cdot \min(|a|, |b|)$. The equation is evolved in time using a standard fourth-order Runge-Kutta scheme. We can evolve the forced KdV equation (1.15) and the dispersionless approximation to forced KdV (1.16) from a zero initial condition numerically and observe how time dependence in the forcing function affects the behavior of the solutions. The solution to equation (1.15) is approximated using the method described by Kassam and Trefethen in [14]. The solution to equation (1.16) is approximated using the method described by Kurganov

and Tadmor in [15].

2.6 Conclusions

In summary, we have presented an exact solution to the hydraulic approximation to the forced Korteweg-de Vries equation for a special forcing function. We use numerical continuation to numerically approximate stationary solutions (one stable and one unstable) to (1.15) and a critical Froude value above which stationary solutions exist. We demonstrate that the eigenvalues of the Schrödinger operator with a rectangular box potential function converge to a value that we predict analytically as the length of the box increases.

We use analysis of the dispersionless approximation to KdV (1.16) the results of WKB analysis to predict the frequency of soliton generation and demonstrate that this method is accurate. This method for analytically predicting the rate of soliton generation gives a frequency around which we can tune oscillation in a time dependent forcing function to create interesting and surprising resonant behavior in the solution. Study of the case of time dependent forcing is currently underway.

CHAPTER 3

Time Dependent Forcing

Here we present an anlytic study of time dependent oscillations in the dispersionless approximation to KdV (1.16) studied in [10] and a numerical study of the resonant regime as well as the asymptotic high and low frequency limits.

3.1 Forcing Amplitude Modulation

Suppose now we consider forcing whose amplitude oscillates in time. Our system becomes

$$\begin{aligned}
\frac{\mathrm{d}x}{\mathrm{d}t} &= F - 1 - \frac{3\alpha}{2}\zeta \\
\frac{\mathrm{d}\zeta}{\mathrm{d}t} &= \Omega^2(\omega t) f_x(x)
\end{aligned} \tag{3.1}$$

Where $f(x) = p_m(1 - \kappa^2 x^2)$ where $|x| < \frac{1}{\kappa}$ and zero elsewhere, and $\Omega^2(\omega t) = 1 - \varepsilon_F^2 \sin(\omega t)$. We will assume $\varepsilon_F < 1$. We can re-write this system as a single second order equation

$$\frac{\mathrm{d}^2 x}{\mathrm{d}t^2} = -\frac{3\alpha}{2}\Omega^2(\omega t) f_x(x).$$

Inserting our chosen function definitions we get

$$\frac{\mathrm{d}^2 x}{\mathrm{d}t^2} = 3\alpha\kappa^2 p_m\left(1 - \varepsilon_F^2 \sin(\omega t)\right)x. \tag{3.2}$$

Consider the Mathieu equation

$$\frac{\mathrm{d}^2 x}{\mathrm{d}t^2} + \left(a - 2q\cos(2t)\right)x = 0,$$

which has solutions,

$$x(z) = c_1 C(a, q, z) + c_2 S(a, q, z),$$

where C and S are the Mathieu cosine and sine functions (respectively). We can determine an exact solution to (3.2) in terms of Mathieu functions by introducing a change of variables

$$\omega t = \frac{\pi}{2} - 2z \quad \Leftrightarrow \quad z = \frac{\pi}{4} - \frac{\omega t}{2},$$

under which (3.2) becomes

$$\frac{d^2 x}{dz^2} + \left[\frac{-12\alpha\kappa^2 p_m}{\omega^2} - 2\left(\frac{-6\alpha\varepsilon^2\kappa^2 p_m}{\omega^2}\right)\cos(2z)\right]x = 0.$$

This equation has solutions

$$x(z) = c_1 C\left(\frac{-12\alpha\kappa^2 p_m}{\omega^2}, \frac{-6\alpha\varepsilon_F^2\kappa^2 p_m}{\omega^2}, z\right) + c_2 S\left(\frac{-12\alpha\kappa^2 p_m}{\omega^2}, \frac{-6\alpha\varepsilon_F^2\kappa^2 p_m}{\omega^2}, z\right)$$

Inserting our initial conditions gives

$$c_2 = \frac{2(F-1)C^* + \omega\xi C'^*}{\omega(S^*C'^* - C^*S'^*)},$$

$$c_1 = \frac{2(F-1)S^* + \omega\xi S'^*}{\omega(C^*S'^* - S^*C'^*)},$$

where a star superscript denote the evaluation of a Mathieu function or its derivative at $z = \pi/4$ for parameter values $a = -12\alpha\kappa^2 p_m/\omega^2$ and $q = -6\alpha\varepsilon_F^2\kappa^2 p_m/\omega^2$.

3.1.1 Low Frequency Modulation

To generate approximate solutions to (3.2) we can introduce the change of variables $\tau = \omega t$, which yields the expression

$$\omega^2 \frac{d^2 x}{d\tau^2} = 3\alpha p_m \kappa^2 (1 - \varepsilon_F^2 \sin\tau)x$$

$$\omega^2 x'' = 3\alpha p_m \kappa^2 \Omega^2(\tau)x.$$

For small omega, $0 < \omega \ll 1$, we can find a WKB approximation to the solution of the equation. We assume an exponential power series expansion for x

$$x(\tau) \sim \exp\left[\frac{1}{\delta}\sum_{n=0}^{\infty}\delta^n S_n(\tau)\right], \quad \delta \to 0.$$

We now find the first derivative,

$$x' \sim \left(\frac{1}{\delta}\sum_{n=0}^{\infty}\delta^n S_n'\right)\exp\left(\frac{1}{\delta}\sum_{n=0}^{\infty}\delta^n S_n\right),$$

and the second,

$$x'' \sim \left[\frac{1}{\delta^2}\left(\sum_{n=0}^{\infty}\delta^n S_n'\right)^2 + \frac{1}{\delta}\sum_{n=0}^{\infty}\delta^n S_n''\right]\exp\left(\frac{1}{\delta}\sum_{n=0}^{\infty}\delta^n S_n\right),$$

and substitute the series expressions for x and x'' into the equation

$$\omega^2\left[\frac{1}{\delta^2}\left(\sum_{n=0}^{\infty}\delta^n S_n'\right)^2 + \frac{1}{\delta}\sum_{n=0}^{\infty}\delta^n S_n''\right]\exp\left(\frac{1}{\delta}\sum_{n=0}^{\infty}\delta^n S_n\right)$$
$$= 3\alpha\kappa^2 p_m\Omega^2(\tau)\exp\left(\frac{1}{\delta}\sum_{n=0}^{\infty}\delta^n S_n(\tau)\right).$$

We next simplify and expand the summations. The first several equations are:

$$\frac{\omega^2}{\delta^2}S_0'^2 + \frac{2\omega^2}{\delta}S_0'S_1' + \omega^2 S_1'^2 + 2\omega^2 S_0'S_2' + 2\omega^2\delta S_1'S_2' + 2\omega^2\delta S_0'S_3'$$
$$+ \frac{\omega^2}{\delta}S_0'' + \omega^2 S_1'' + \omega^2\delta S_2'' + \cdots = 3\alpha\kappa^2 p_m\Omega^2(\tau).$$

Here we choose $\delta = \omega$ and match powers of ω,

$$S_0'^2 = 3\alpha\kappa^2 p_m\Omega^2(\tau)$$

$$2S_0'S_1' + S_0'' = 0$$

$$S_1'^2 + 2S_0'S_2' + S_1'' = 0$$

$$\cdots$$

We now solve these equations. From the zeroeth order equation,

$$S_0' = \pm \kappa \sqrt{3\alpha p_m} \Omega(\tau),$$

we obtain

$$S_0 = \pm \kappa \sqrt{3\alpha p_m} \int^\tau \Omega(y) \mathrm{d}y.$$

We find the second derivative of this expression,

$$S_0'' = \mp \frac{\varepsilon_F^2 \kappa \sqrt{3\alpha p_m}}{2} \left(1 - \varepsilon_F^2 \sin \tau\right)^{-1/2} \cos \tau,$$

and insert the result into the first order equation,

$$\pm 2\kappa \sqrt{3\alpha p_m} \Omega(\tau) S_1' \pm \kappa \sqrt{3\alpha p_m} \Omega'(\tau) = 0.$$

We solve for S_1 and find

$$S_1 = -\frac{1}{2} \ln \left[\Omega(\tau)\right]$$

Neglecting higher order terms for now we combine S_0 and S_1 to get

$$x(\tau) \sim c_1 \exp\left[\frac{\kappa\sqrt{3\alpha p_m}}{\omega} \int^\tau \Omega(y)\mathrm{d}y - \frac{1}{2}\ln\Omega(\tau)\right]$$
$$+ c_2 \exp\left[\frac{-\kappa\sqrt{3\alpha p_m}}{\omega} \int^\tau \Omega(y)\mathrm{d}y - \frac{1}{2}\ln\Omega(\tau)\right],$$

which simplifies to

$$x(\tau) \sim c_1 \Omega^{-1/2}(\tau) \exp\left[\frac{\kappa\sqrt{3\alpha p_m}}{\omega} \int^\tau \Omega(y)\mathrm{d}y\right] + c_2 \Omega^{-1/2}(\tau) \exp\left[\frac{-\kappa\sqrt{3\alpha p_m}}{\omega} \int^\tau \Omega(y)\mathrm{d}y\right].$$

We now consider the derivative of our WKB solution

$$x'(\tau) \sim c_1 \left[\frac{-1}{2}\Omega^{-3/2}(\tau)\Omega'(\tau) + \frac{\kappa\sqrt{3\alpha p_m}}{\omega}\Omega^{1/2}(\tau)\right] \exp\left[\frac{\kappa\sqrt{3\alpha p_m}}{\omega} \int^\tau \Omega(y)\mathrm{d}y\right]$$
$$+ c_2 \left[\frac{-1}{2}\Omega^{-3/2}(\tau)\Omega'(\tau) - \frac{\kappa\sqrt{3\alpha p_m}}{\omega}\Omega^{1/2}(\tau)\right] \exp\left[\frac{-\kappa\sqrt{3\alpha p_m}}{\omega} \int^\tau \Omega(y)\mathrm{d}y\right].$$

Inserting initial conditions yields the system

$$x(0) = \xi = c_1 + c_2$$

$$x'(0) = \frac{F-1}{\omega} = c_1 \left(\frac{\varepsilon_F^2}{4} + \frac{\kappa\sqrt{3\alpha p_m}}{\omega} \right) + c_2 \left(\frac{\varepsilon_F^2}{4} - \frac{\kappa\sqrt{3\alpha p_m}}{\omega} \right),$$

and we find our coefficients to be

$$c_1 = \frac{4\kappa\sqrt{3\alpha p_m} - \varepsilon_F^2 \omega}{8\kappa\sqrt{3\alpha p_m}} \xi + \frac{F-1}{2\kappa\sqrt{3\alpha p_m}}$$

and

$$c_2 = \frac{4\kappa\sqrt{3\alpha p_m} + \varepsilon_F^2 \omega}{8\kappa\sqrt{3\alpha p_m}} \xi - \frac{F-1}{2\kappa\sqrt{3\alpha p_m}}.$$

Thus,

$$x(\tau) \sim \left(\frac{8\sqrt{3p_m\kappa^2} - \varepsilon_F^2\omega}{8\sqrt{\kappa^2}} \xi + \frac{F-1}{\sqrt{\alpha\kappa^2}} \right) \frac{\Omega^{-1/2}(\tau)}{2\sqrt{3p_m}} \exp\left[\frac{\sqrt{3\alpha p_m \kappa^2}}{\omega} \int^\tau \Omega(y)\mathrm{d}y \right]$$
$$+ \left(\frac{8\sqrt{3p_m\kappa^2} + \varepsilon_F^2\omega}{8\sqrt{\kappa^2}} \xi - \frac{F-1}{\sqrt{\alpha\kappa^2}} \right) \frac{\Omega^{-1/2}(\tau)}{2\sqrt{3p_m}} \exp\left[\frac{-\sqrt{3\alpha p_m \kappa^2}}{\omega} \int^\tau \Omega(y)\mathrm{d}y \right]$$

for $|x|, |\xi| < \frac{1}{\kappa}$. In the limit as $\varepsilon_F \to 0$ and $\Omega^2(\omega t) = \left(1 - \varepsilon_F^2 \sin(\omega t)\right) \to 1$, the above expression simplifies to the exact solution of the case with steady forcing.

Outside the range $-\frac{1}{\kappa} < x < \frac{1}{\kappa}$ the characteristics continue as lines with constant slope. We can use numerical root finding to approximate the value t^* at which the WKB solution approximation $x_{WKB}(t^*) = \pm\frac{1}{\kappa}$. The solutions continue with slope equal to that at $x_{WKB}(t^*)$ and for $t > t^*$, the characteristic curves are given by

$$x(t) = x'_{WKB}(t^*)(t - t^*) + \operatorname{sgn}\left(x_{WKB}(t^*)\right)\frac{1}{\kappa}.$$

The resulting characteristic curves for parameter values $p_m = \kappa = 1$, $F = 2$, $\varepsilon_F = 0.8$, $\omega = 0.15$ are shown in Figure 3.1.1

Turning points in the characteristic curves occur when the derivative of the solution with respect
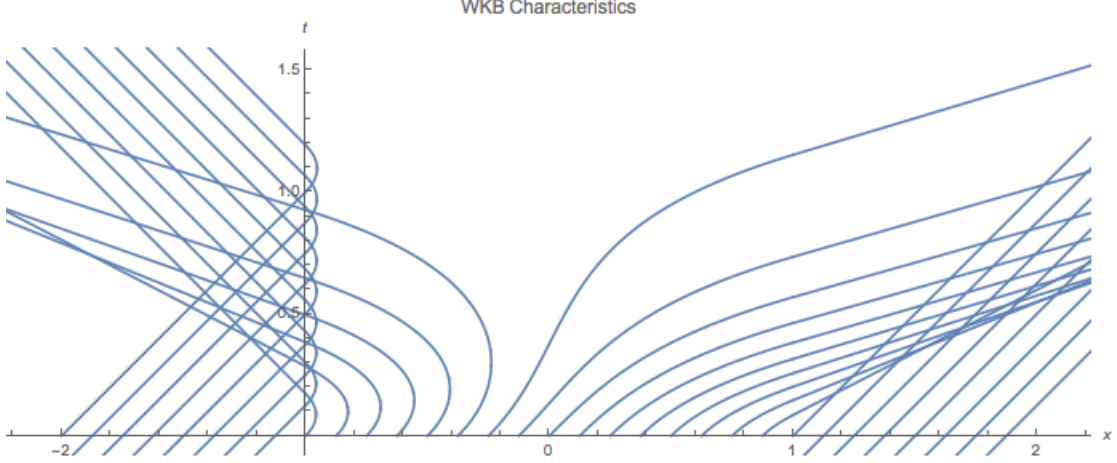
Figure 3.1: Characteristic curves for the system (3.1) for parameter values $p_m = \kappa = 1$, $F = 2$, $\varepsilon_F = 0.8$, $\omega = 0.15$. For small values of ω and ε_F, the curves look very similar to those for the case of steady forcing

to time is equal to zero,

$$
\frac{\mathrm{d}x}{\mathrm{d}t} = \frac{\Omega^{1/2}(\tau)}{2\sqrt{3\alpha}} \left[\left(\frac{24 - \frac{\varepsilon_F^2 \omega \sqrt{3}}{\kappa \sqrt{p_m}}}{4\sqrt{3}} \xi + \frac{F-1}{\kappa \sqrt{p_m}} \right) \left(\frac{\varepsilon_F^2 \cos \tau}{4\Omega^3(\tau)} + \frac{\kappa \sqrt{3\alpha p_m}}{\omega} \right) e^{\frac{\kappa \sqrt{3\alpha p_m}}{\omega} \int^\tau \Omega(y) \mathrm{d}y} + \right.
$$
$$
\left. + \left(\frac{24 + \frac{\varepsilon_F^2 \omega \sqrt{3}}{\kappa \sqrt{p_m}}}{4\sqrt{3}} \xi - \frac{F-1}{\kappa \sqrt{p_m}} \right) \left(\frac{\varepsilon_F^2 \cos \tau}{4\Omega^3(\tau)} - \frac{\kappa \sqrt{3\alpha p_m}}{\omega} \right) e^{\frac{-\kappa \sqrt{3\alpha p_m}}{\omega} \int^\tau \Omega(y) \mathrm{d}y} \right] = 0
$$

(note that for $0 < \varepsilon_F < 1$, the function $\Omega(\tau)$ is positive and bounded for all time). We solve the equation above for ξ and arrive at

$$
\xi = \left[\frac{\varepsilon_F^2 \kappa \sqrt{3 p_m} \left(\frac{2 \cos \tau}{\Omega(\tau)} - \sqrt{\alpha} \Omega^2(\tau) \right) \cosh \left[\frac{\kappa \sqrt{3\alpha p_m}}{\omega} \int^\tau \Omega(y) \, \mathrm{d}y \right]}{4(F-1) \left(\frac{2\sqrt{3 p_m \kappa^2}}{\omega} \Omega^2(\tau) - \frac{\varepsilon_F^2 \cos \tau}{4\Omega(\tau)} \right) \sinh \left[\frac{\kappa \sqrt{3\alpha p_m}}{\omega} \int^\tau \Omega(y) \, \mathrm{d}y \right]} \right.
$$
$$
\left. + \frac{\left(\frac{24\kappa^2 p_m \sqrt{\alpha}}{\omega} \Omega^2(\tau) - \frac{\varepsilon_F^4 \omega \cos \tau}{4\Omega(\tau)} \right)}{4(F-1) \left(\frac{2\sqrt{3 p_m \kappa^2}}{\omega} \Omega^2(\tau) - \frac{\varepsilon_F^2 \cos \tau}{4\Omega(\tau)} \right)} \right]^{-1}
$$

Seeking the critical ξ value which reaches its turning point as $\tau \to \infty$, we seek the long time limit of this expression. The integrands in the exponential functions are strictly positive, thus the arguments of the exponential functions monotonically increase in magnitude, and long time behavior will be
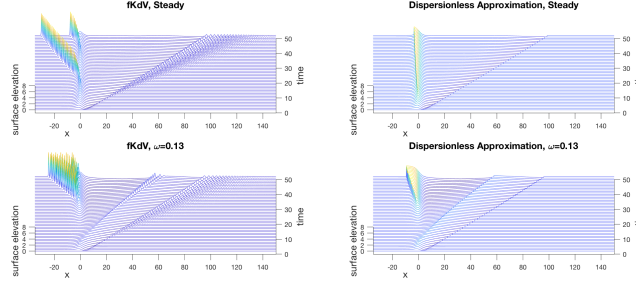
65

Figure 3.2: Waterfall plots of solutions to the fKdV equation (1.15) (left), and the dispersionless approximation to the fKdV equation (1.16) (right) for steady forcing (2.5) (top), and a forcing function with modulating amplitude (3.3) (bottom). Parameter values are $F = 2.6$, $\varepsilon = 0.2$, $\alpha = {}^2\!/_3$, $dx = 0.0305176$, $dt = $ 1e-5, $p_m = 1.4$, $\kappa = 0.3$, $\varepsilon_F = 1$, and $\omega = {}^{2\pi}\!/_{50}$.

dominated by the exponentials with positive arguments

$$\lim_{\tau \to \infty} \frac{4(F-1)\left(\omega\Omega'(\tau) - 2\kappa\Omega^2(\tau)\sqrt{3\alpha p_m}\right)\exp\left[B(\tau)\right]}{\left(\left(24\alpha\kappa^2 p_m\Omega^2(\tau) + \varepsilon_F^2\omega^2\Omega'(\tau)\right) - 2\kappa\omega\sqrt{3\alpha p_m}\left(\varepsilon_F^2\Omega^2(\tau) + 2\Omega'(\tau)\right)\right)\exp[B(\tau)]},$$

where

$$B(\tau) = \frac{\kappa\sqrt{3\alpha p_m}}{\omega}\int^\tau \Omega(y)\,\mathrm{d}y,$$

and we ultimately find

$$\xi_c = \frac{-(F-1)}{\sqrt{3\alpha p_m \kappa^2 - \omega\frac{\varepsilon_F^2}{4}}}$$

The critical ξ value is shifted from the time independent case by a small amount that depends on both ω and ε_F.

For numerical comparisons in Figures (3.1.1) and (3.1.1) the forcing function

$$f(x) = \left(1 - \varepsilon_F \sin(\omega t)\right)p_m \operatorname{sech}^2\left(\kappa x\right), \qquad \varepsilon_F \leq 1 \tag{3.3}$$

was used. The frequency of forcing modulation was set so that the forcing would undergo one complete cycle in the simulation time. Solution behavior seems to agree well for short times, but for long times at points where the effective magnitude of the forcing function is significantly different from that in the steady case the solution exhibits drastically different behavior.
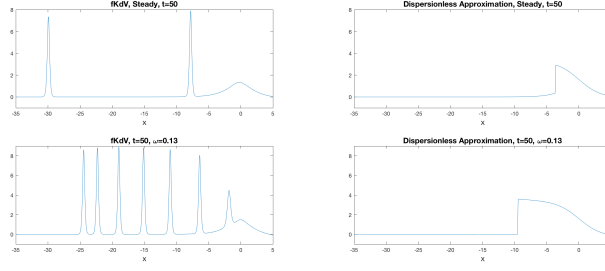
66

Figure 3.3: Numerical solutions to fKdV (1.15) (left) and the dispersionless approximation to fKdV (1.16) (right) at time $t = 50$. The solution obtained from a steady forcing function (2.5) is shown in the top two plots. The bottom two plots were generated using (3.3) as a forcing function. Parameter values are $F = 2.6$, $\varepsilon = 0.2$, $\alpha = 2/3$, $dx = 0.030517$, $dt = $ 1e-5, $p_m = 1.4$, $\kappa = 0.3$, $\varepsilon_F = 1$, and $\omega = 2\pi/50$.

3.1.2   High Frequency Modulation

To find an averaging approximation to the solution of (3.2) in the case of large ω, we consider a vector equation in the form

$$\dot{x} = \varepsilon f(x, t) \qquad x \in \mathbb{R}^n, \ t \in \mathbb{T}^1, \tag{3.4}$$

and make a near identity transformation

$$x = y + \varepsilon g(y, t).$$

We insert this transformation into (3.4),

$$\dot{x} = \frac{\mathrm{d}y}{\mathrm{d}t} + \varepsilon \left(\frac{\partial g}{\partial t} + D_y g \cdot \frac{\mathrm{d}y}{\mathrm{d}t} \right) = \varepsilon f(y + \varepsilon g, t),$$

and expand f in its Taylor series

$$\frac{\mathrm{d}y}{\mathrm{d}t} + \varepsilon \left(\frac{\partial g}{\partial t} + D_y g \cdot \frac{\mathrm{d}y}{\mathrm{d}t} \right) = \varepsilon \left[f(y, t) + \varepsilon D_y f \cdot g + O(\varepsilon^2) \right].$$

We next group terms

$$(\mathbb{1} + \varepsilon D_y g) \cdot \frac{\mathrm{d}y}{\mathrm{d}t} = \varepsilon \left[f(y, t) - \frac{\partial g}{\partial t} + \varepsilon D_y f \cdot g \right] + O(\varepsilon^3).$$

67

Note that

$$(\mathbb{1} - \varepsilon A)(\mathbb{1} + \varepsilon A) = \mathbb{1} - O(\varepsilon^2) \quad \Rightarrow \quad (\mathbb{1} + \varepsilon A)^{-1} = (\mathbb{1} - \varepsilon A) + O(\varepsilon^2)$$

which allows us to approximately invert the operator acting on $\frac{\mathrm{d}y}{\mathrm{d}t}$,

$$\dot{y} = \varepsilon(\mathbb{1} - \varepsilon D_y g)\left[f(y,t) - \frac{\partial g}{\partial t} + \varepsilon D_y f \cdot g\right] + O(\varepsilon^3).$$

We add and subtract $\varepsilon \bar{f} = \varepsilon \frac{1}{T}\int_0^T f(y,s)\,\mathrm{d}s$,

$$\dot{y} = \varepsilon \bar{f}(y) + \varepsilon\left[f(y,t) - \bar{f}(y) - \varepsilon D_y g \cdot f + \varepsilon D_y f \cdot g - (\mathbb{1} - \varepsilon D_y g) \cdot \frac{\partial g}{\partial t}\right] + O(\varepsilon^3),$$

and set
$$\frac{\partial g}{\partial t} = f(y,t) - \bar{f}(y) \quad \Rightarrow \quad g(y,t) = \int_0^t \left(f(y,s) - \bar{f}(y)\right)\mathrm{d}s,$$

which leaves
$$\dot{y} = \varepsilon \bar{f} + \varepsilon^2\left[D_y f \cdot g - D_y g \cdot \left(f - \frac{\partial g}{\partial t}\right)\right] + O(\varepsilon^3),$$

or
$$\dot{y} = \varepsilon \bar{f} + \varepsilon^2\left[D_y f \cdot g - D_y g \cdot \bar{f}\right] + O(\varepsilon^3).$$

Now introduce

$$h(y,t) = D_y f(y,t) \cdot g(y,t) - D_y g(y,t) \cdot \bar{f}(y)$$

so that

$$\dot{y} = \varepsilon \bar{f} + \varepsilon^2 h(y,t) + O(\varepsilon^3).$$

We now consider the related equation

$$\dot{v} = \varepsilon \bar{f}(v) + \varepsilon^2 h(v,t),$$

and the corresponding transformation

$$v = z + \varepsilon^2 J(z,t),$$

68

where J is yet unknown. We substitute this into our equation for $\dot{v}$,

$$\frac{\mathrm{d}z}{\mathrm{d}t} + \varepsilon^2\left(\frac{\partial J}{\partial t} + D_z J \cdot \frac{\mathrm{d}z}{\mathrm{d}t}\right) = \varepsilon \bar{f}(z + \varepsilon^2 J) + \varepsilon^2 h(z + \varepsilon^2 J, t)$$

We again expand the RHS in its Taylor series and rearrange the terms

$$(\mathbb{1} + \varepsilon^2 D_z J) \cdot \frac{\mathrm{d}z}{\mathrm{d}t} = \varepsilon \bar{f} + \varepsilon^3 D_z \bar{f} \cdot J + \varepsilon^2 h - \varepsilon^2 \frac{\partial J}{\partial t} + O(\varepsilon^4),$$

invert the operator on $\dot{z}$,

$$\dot{z} = \varepsilon(\mathbb{1} - \varepsilon^2 D_z J)\left[\bar{f} - \varepsilon\frac{\partial J}{\partial t} + \varepsilon h + \varepsilon^2 D_z \bar{f} \cdot J\right] + O(\varepsilon^4),$$

distribute the operator on the RHS, and add and subtract $\varepsilon^2 \bar{h}$,

$$\dot{z} = \varepsilon\left[\bar{f} + \varepsilon\bar{h} - \varepsilon\frac{\partial J}{\partial t} + \varepsilon h - \varepsilon\bar{h} + \varepsilon^2(D_z \bar{f} \cdot J - D_z J \cdot \bar{f})\right] + O(\varepsilon^4).$$

We next define J so that we have an expression for $\dot{z}$ given in increasing powers of the small parameter ε,

$$\frac{\partial}{\partial t} J(z, t) = h(z, t) - \bar{h}(z) \qquad J(z, t) = \int_0^t \left(h(z, s) - \bar{h}(z)\right) \mathrm{d}s,$$

which we can now write as

$$\dot{z} = \varepsilon\bar{f} + \varepsilon^2\bar{h} + \varepsilon^3(D_z\bar{f} \cdot J - D_z J \cdot \bar{f}) + O(\varepsilon^4).$$

Now consider

$$\dot{u} = \varepsilon\bar{f}(u) + \varepsilon^2\bar{h}(u),$$

and insert the solution to this equation into the near identity transformation of x

$$x \approx u + \varepsilon g(u, t).$$

69

For the initial value problem (3.2) with large $\omega \gg 1$, we will again proceed by writing in terms of $\tau = \omega t$, and letting a dot represent differentiation w.r.t. the new variable τ

$$\omega^2 \ddot{x} = 3\alpha p_m \kappa^2 (1 - \varepsilon_F^2 \sin \tau) x.$$

Now insert a new small parameter $\delta = \frac{1}{\omega^2} \ll 1$,

$$\ddot{x} = \delta 3\alpha p_m \kappa^2 (1 - \varepsilon_F^2 \sin \tau) x.$$

We write this as a system of two first order equations

$$\dot{x}_1 = x_2,$$

$$\dot{x}_2 = \delta 3\alpha p_m \kappa^2 (1 - \varepsilon_F^2 \sin \tau) x_1,$$

and then as a vector equation,

$$\underline{\dot{x}} = \delta \begin{pmatrix} 0 & 1/\delta \\ 3\alpha\kappa^2 p_m (1 - \varepsilon_F^2 \sin \tau) & 0 \end{pmatrix} \begin{pmatrix} x_1 \\ x_2 \end{pmatrix}, \qquad \underline{x} = \begin{pmatrix} x_1 \\ x_2 \end{pmatrix}.$$

Here the vector function f is given by

$$f(\underline{x}, \tau) = \begin{pmatrix} 0 & 1/\delta \\ 3\alpha\kappa^2 p_m (1 - \varepsilon_F^2 \sin(\tau)) & 0 \end{pmatrix} \begin{pmatrix} x_1 \\ x_2 \end{pmatrix},$$

and our initial value problem is written as

$$\underline{\dot{x}} = \delta f(\underline{x}, \tau), \qquad \underline{x}(\tau = 0) = \begin{pmatrix} \xi \\ (F - 1)\sqrt{\delta} \end{pmatrix}.$$

For the next order term we need $\bar{f}$, a time average of the function f,

$$\bar{f}(\underline{x}) = \begin{pmatrix} 0 & 1/\delta \\ 3\alpha\kappa^2 p_m & 0 \end{pmatrix} \begin{pmatrix} x_1 \\ x_2 \end{pmatrix}.$$

70

The vector function g is then given by the integral of $f - \bar{f}$,

$$g(\underline{y}, \tau) = \begin{pmatrix} 0 & 0 \\ 3\alpha p_m \kappa^2 \varepsilon_F^2 (\cos(\tau) - 1) & 0 \end{pmatrix} \begin{pmatrix} y_1 \\ y_2 \end{pmatrix},$$

and h by

$$h(\underline{y}, \tau) = \frac{1}{\delta} \begin{pmatrix} 3\alpha p_m \kappa^2 \varepsilon_F^2 (\cos(\tau) - 1) & 0 \\ 0 & 3\alpha p_m \kappa^2 \varepsilon_F^2 (1 - \cos(\tau)) \end{pmatrix} \begin{pmatrix} y_1 \\ y_2 \end{pmatrix}.$$

The average of h is then

$$\bar{h}(\underline{u}) = \frac{12\alpha\varepsilon^2}{\delta} \begin{pmatrix} -1 & 0 \\ 0 & 1 \end{pmatrix} \begin{pmatrix} u_1 \\ u_2 \end{pmatrix},$$

which allows us to write the equation

$$\dot{\underline{u}} = \begin{pmatrix} -12\alpha\delta\varepsilon^2 & 1 \\ 12\alpha\delta & 12\alpha\delta\varepsilon^2 \end{pmatrix} \begin{pmatrix} u_1 \\ u_2 \end{pmatrix}, \qquad \underline{u}(\tau = 0) = \begin{pmatrix} \xi \\ c_0\sqrt{\delta} \end{pmatrix},$$

which defines $\underline{u}$

$$\underline{u} = \exp\left(\begin{pmatrix} -3\alpha p_m \kappa^2 \delta\varepsilon^2 & 1 \\ 3\alpha p_m \kappa^2 \delta & 3\alpha p_m \kappa^2 \delta\varepsilon^2 \end{pmatrix} \tau \right) \begin{pmatrix} \xi \\ (F-1)\sqrt{\delta} \end{pmatrix}.$$

Our approximate solution is then

$$\left(\mathbb{1} + \delta \begin{pmatrix} 0 & 0 \\ 3\alpha p_m \kappa^2 \varepsilon^2 (\cos\tau - 1) & 0 \end{pmatrix} \right)$$

$$\cdot \exp\left(\begin{pmatrix} -3\alpha p_m \kappa^2 \delta\varepsilon^2 & 1 \\ 3\alpha p_m \kappa^2 \delta & 3\alpha p_m \kappa^2 \delta\varepsilon^2 \end{pmatrix} \tau \right) \begin{pmatrix} \xi \\ (F-1)\sqrt{\delta} \end{pmatrix},$$

and the next order of accuracy is given by

$$\underline{x} \approx \underline{u} + \delta g(\underline{u}, \tau) + \delta^2 J(\underline{u}, \tau),$$
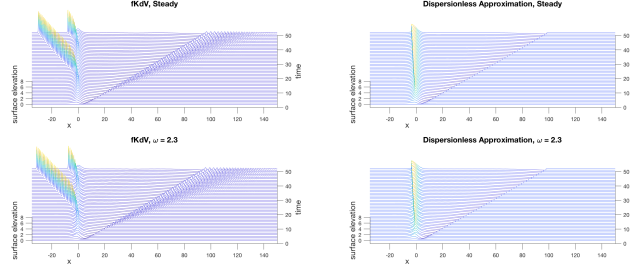
71

Figure 3.4: Waterfall plots of solutions to the fKdV equation (1.15) (left), and the dispersionless approximation to the fKdV equation (1.16) (right) for steady forcing (2.19) (top), and a forcing function with modulating amplitude (3.3) (bottom). Parameter values are $F = 2.6$, $\varepsilon = 0.2$, $\alpha = 2/3$, $dx = 0.0305176$, $dt = $ 1e-5, $p_m = 1.4$, $\kappa = 0.3$, $\varepsilon_F = 1$, and $\omega = 2.32966$.
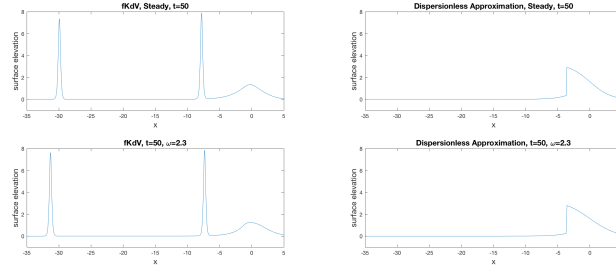

Figure 3.5: Numerical solutions to fKdV (1.15) (left) and the dispersionless approximation to fKdV (1.16) (right) at time $t = 50$. The solution obtained from a steady forcing function (2.5) is shown in the top plots. The bottom plots were generated using forcing function (3.3). Oscillations in this simulation are fast relative to the resonant oscillation frequency predicted by (2.29). Parameter values are $F = 2.6$, $\varepsilon = 0.2$, $\alpha = 2/3$, $dx = 0.0305176$, $dt = $ 1e-5, $p_m = 1.4$, $\kappa = 0.3$, $\varepsilon_F = 1$, and $\omega = 2.32966$.

where

$$J(z, t) = \int_0^t \left(h(z, s) - \bar{h}(z) \right) \mathrm{d}s.$$

High frequency oscillations in amplitude seem to offer the closest agreement with the case of steady forcing, as shown in Figures (3.1.2) and (3.1.2). An oscillation frequency of only $\omega = 2.32986$ (ten times the resonant frequency predicted by equation (2.29)) is qualitatively the same as the case of steady forcing.

3.1.3 Resonant Modulation

By oscillating the amplitude of the forcing function at a frequency such that the period of oscillation is equal to the expected period of soliton generation given by (2.29), the behaviors of the solutions of the forced KdV equation (1.15) and the dispersionless approximation (1.16) are significantly altered. In the dispersionless approximation the forming shock is prevented from
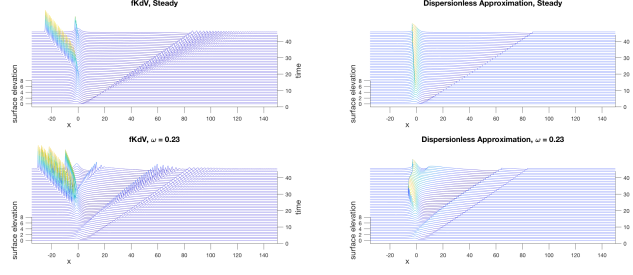
Figure 3.6: Waterfall plots of solutions to the fKdV equation (1.15) (left), and the dispersionless approximation to the fKdV equation (1.16) (right) for steady forcing (2.5) (top), and a forcing function with modulating amplitude (3.3). The frequency of modulation is such that the period of the oscillation of the forcing function is equal to the period of soliton generation as predicted by (2.29). Parameter values are $F = 2.6$, $\varepsilon = 0.2$, $\alpha = 2/3$, $dx = 0.030517$, $dt = $ 1e-5, $p_m = 1.4$, $\kappa = 0.3$, $\varepsilon_F = 1$, and $\omega = 0.232966$.
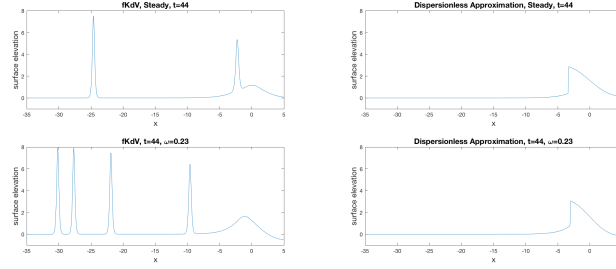

Figure 3.7: Numerical solutions to fKdV (1.15) (left) and the dispersionless approximation to fKdV (1.16) (right) at time $t = 44$. The solution obtained using a steady forcing function (2.5) is shown in the top plots. The bottom plots were generated using a forcing function with modulating amplitude (3.3). Parameter values are $F = 2.6$, $\varepsilon = 0.2$, $\alpha = 2/3$, $dx = 0.030517$, $dt = $ 1e-5, $p_m = 1.4$, $\kappa = 0.3$, $\varepsilon_F = 1$, and $\omega = 0.232966$.

propagating upstream and appears to be forced downstream for a period of time as it decreases in amplitude. The full fKdV equation generates more upstream propagating waves when forcing amplitude is modulated at what we expect to be a resonant frequency.

3.2   Position Modulation

We can also oscillate the position of the forcing function, which can also be thought of as modulating the speed of the fluid flow over the obstacle or of the obstacle moving through the fluid. We expect approaches similar to those employed in the previous section will yield analogous results. To explore the problem numerically we us the forcing function

$$f(x) = p_m \operatorname{sech}^2\Big(\kappa\big(x - \varepsilon_F \sin(\omega t)\big)\Big). \tag{3.5}$$
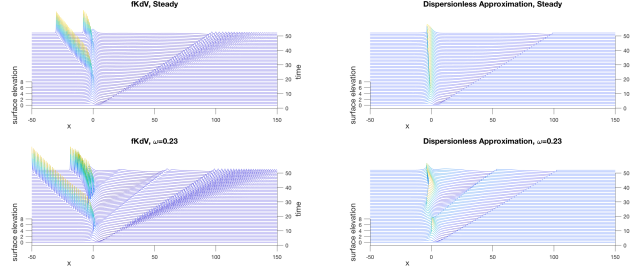
73

Figure 3.8: Waterfall plots of surface elevation from the fKdV equation (1.15) from time $t = 0$ to time $t = 50$ are shown in the left plots. The plots on the right show solutions to the dispersionless approximation to the fKdV equation (1.16). The top plots were generated using the forcing fucntion (2.5). Plots generated using the forcing function (3.5) are shown on the bottom. The forcing modulation frequency was set to $\omega = \frac{2\pi}{T_s}$ with T_s from equation (2.29). Parameter values $F = \varepsilon_F = 2.6$, $\varepsilon = 0.2$, $\alpha = 2/3$, $dx = 0.0305176$, $dt = 2\text{e-}5$, $p_m = 1.4$, $\kappa = 0.3$, and $\omega = 0.232966$.
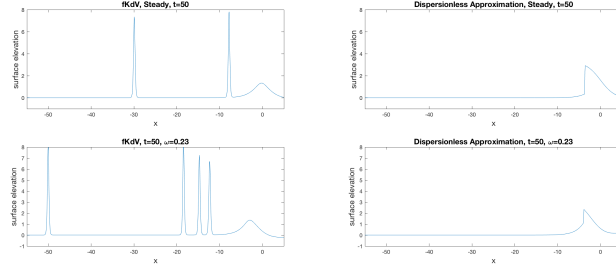

Figure 3.9: Surface elevation from fKdV (1.15) (left) and the dispersionless approximation to fKdV (1.16) (right) at time $t = 50$. The plots at the top of the figure were generated using (2.5), and bottom plots were generated using the forcing function (3.5). The forcing modulation frequency was set to $\omega = \frac{2\pi}{T_s}$ with T_s from equation (2.29). Parameter values $F = \varepsilon_F = 2.6$, $\varepsilon = 0.2$, $\alpha = 2/3$, $dx = 0.0305176$, $dt = 2\text{e-}5$, $p_m = 1.4$, $\kappa = 0.3$, and $\omega = 0.232966$.

Figures (3.2) and (3.2) show numerical solutions of equations (1.15) and (1.16) with time dependent forcing function (3.5). As is clear from figure (3.2), it is possible to prevent upstream shock propagation in (1.16) by oscillating the position of the forcing function at an amplitude equal to the Froude number and a resonant frequency $\frac{2\pi}{T_s}$, with T_s given by equation (2.29). However, the same forcing function applied to the full forced KdV equation (1.15) does not prevent the upstream propagation of solitons.

CHAPTER 4

Experiments

4.1 Flume Experiments

In a recirculating flume with a test section that is six inches wide, six inches tall, and 17.0625 inches long, an aluminum cylinder capped on the ends was partially submerged in flow moving at various rates. Linear wave theory agreed well with experimental observations.

4.1.1 Linear Wave Theory

Figure 4.1: The surface of constant background fluid flow is disturbed by a partially submerged cyllinder. Relatively short wavelength capillary waves are shown upstream (to the left) of the obstacle. Experimental observations agree well with predictions from linear wave theory.

In figure (4.1.1), as flow moves from left to right, the capillary waves upstream of the cylinder were measured at 5.5 millimeters. Linear wave theory predicts waves of 5.72 millimeters, at the given flow speed. Linear wave theory also predicts that longer wavelength stationary gravity waves will appear downstream of the obstacle. In figure (4.1.1), the gravity waves downstream of the cylinder were measured at 10.583 centimeters. Linear wave theory predicts a wavelength of 4.871
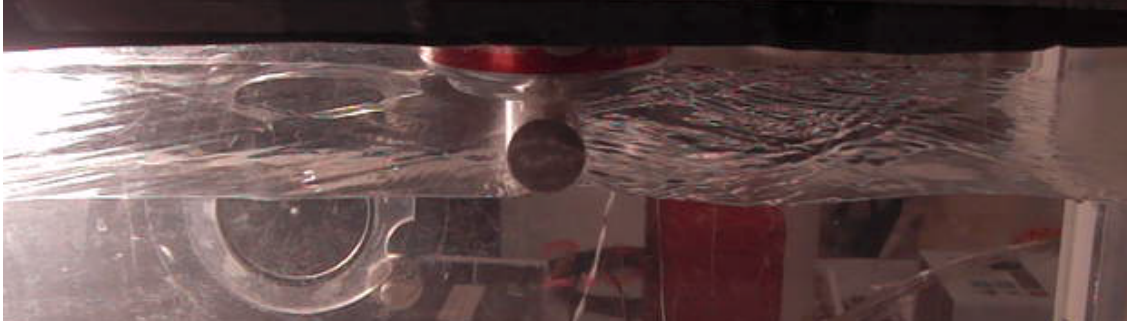
Figure 4.2: The surface of constant background fluid flow is disturbed by a partially submerged cyllinder. Relatively long wavelength gravity waves are shown downstream (to the right) of the obstacle. Due to the larger amplitude, experimental observations do not agree well with predictions from linear wave theory.

centimeters. It is clear in the images that the amplitudes of the downstream stationary gravity waves are much larger than those of the upstream capillary waves. Linear wave theory depends on a small-amplitude assumption. Here it is likely that nonlinearity plays a much greater role because of the larger amplitudes of the waves.

4.1.2 Capillary Accordions

Another fascinating phenomenon was observed for a range of flow speeds and a circular cylinder submerged just below the fluid surface or only partially submerged. The train of solitary waves that appears upstream of the obstacle appears to expand and contract, much like an accordion. The phenomenon can easily be observed with the naked eye, but is much more striking when recorded using a high speed camera and observed in slow motion. The accordion behavior is pictured in Figure (4.1.2). The images in Figure (4.1.2) are different frames from the same high speed video taken with the recirculating flume set to a constant flow rate. To make the wave forms more apparent, light was directed onto blue and yellow colored paper at an angle that would reflect onto the fluid surface and then into the camera. Color contrast was enhanced using Adobe Photoshop.

4.1.3 Upstream Propagating Solitary Waves

The forced KdV equation predicts upstream propagating solitary waves in certain parameter regimes. We seek to demonstrate this experimentally. In the recirculating flume described above, a semi-elliptic cylinder was attached to the bottom of the test section. The obstacle had a rectangular

Figure 4.3: Color enhanced images of a fluid surface at two times showing expansion and contraction of capillary waves excited by a cylindrical obstacle placed just below the surface of the fluid, which moved with a constant background flow speed.

base 150 mm wide and 72 mm across. At its highest point the topography was 12 mm tall. The recirculating flume was run at settings 3.7 Hertz to 3.9 Hertz. The depth of the water was 3.6 centimeters. A random dot pattern was attached to the transparent bottom of the flume in order to utilize the surface Schlieren technique described in [19]. A zoomed out top view of the test section is pictured in Figure (4.1.3). Though all upstream disturbances were of very small amplitude and barely visible to the naked eye, using this technique we are able to visualize the shape and estimate the dimensions of the apparent waves as they travel upstream. Results are pictured in Figure (4.1.3).

4.2 Wave Tank Experiments

Equivalently to generating fluid flow past a fixed obstacle, we can tow an obstacle through a stationary fluid. Figure (4.6) shows the tank.

Figure 4.4: Experimental image of a top view of a fluid recirculating flume with water moving from top to bottom in the image and a transparent bottom with a random do pattern attached below for use with the surface Schlieren technique described in [19].
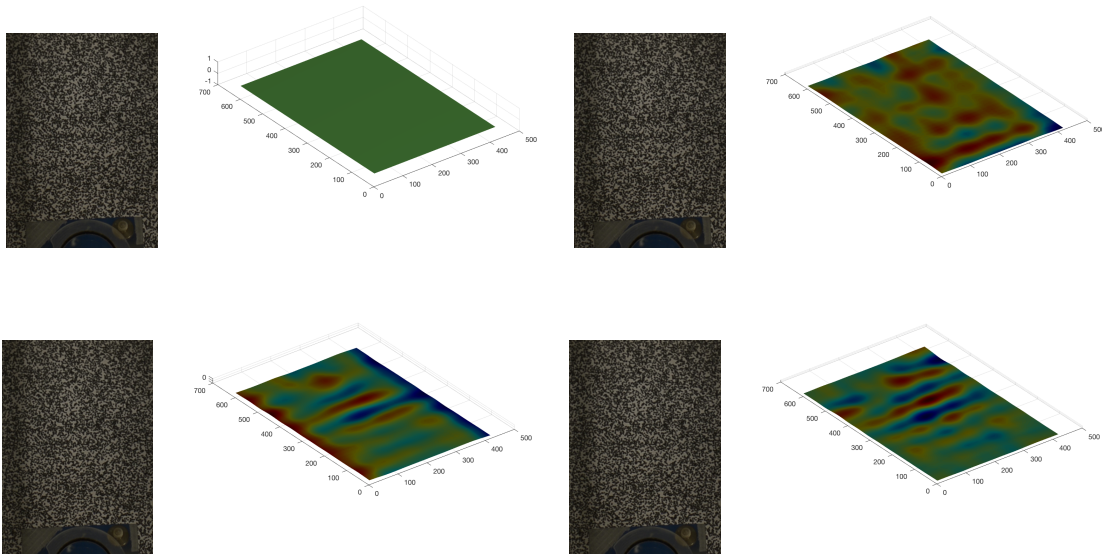

Figure 4.5: Experimental images of a random dot pattern viewed through a moving fluid, upstream of a semielliptical topography displayed with the reconstructed fluid surface using the surface Schlieren technique described in [19].

4.2.1 Upstream Propagating Solitary Waves

A two dimensional topography that spanned the width of the tank in the shape of a circular segment with a chord of 4.5 cm was towed along the length of the tank very near the bottom at various speeds between 48 and 114 cm per second in a water depth of 5.3 cm. The topography was rigidly fastened to a towing carriage by two thin vertical bars adjacent to the channel inner side walls. The apparatus is visible in Figure (4.6). Our setup was very similar to that of Lee et. al. When towed at appropriate speeds disturbances that resemble solitons can be seen propagating ahead of the topography. A train of these disturbances are visible in Figure (4.6), and Figure (4.2.1) shows a blown up image of one such wave.

We can compare our analytically obtained prediction and out numerical prediction with experimental data. A two dimensional topography that spanned the width of a tank 0.75 meters wide in the shape of a circular segment with a chord of 4.5 cm and a maximum height of 0.6 cm was towed along approximately 15 meters of the 27 meter length of the tank very near the bottom at 48.61 cm per second in a water depth of 5.3 cm. A high speed camera was positioned to track the position (and determine the speed) of the towing carriage used to move the topography. The topography was rigidly fastened to the towing carriage by two thin vertical bars adjacent to the channel inner side walls. Our setup was very similar to that of Lee et. al. in [17]. Image of the experiment are displayed in Figures 4.6 and 4.8. Disturbances that resemble solitons were observed propagating ahead of the topography.

In this experimental setup, two observed upstream propagating solitons travel at speeds of approximately 0.65 and 0.58 meters per second and maintain a spacing of approximately 1.0 meter over a time span of three seconds. The frequency of soliton generation could not be determined from collected data.

We can compare experimental results with the numerical solution of the forced KdV equation (1.15) using parameters to match the physical quantities of the experiment, i.e. $\alpha = 0.12$, $\varepsilon = 1.4$, $F = 0.67$, and a forcing function to match the obstacle $f_{\exp}(x) = \sqrt{4.5^2 - x^2} - 3.9$. We evolve a zero initial condition according to (1.15) with spatial grid point spacing $dx = 0.0457764$ and a time step $dt = $ 5e-4. From nondimensional time values $t = 150$ to $t = 300$ (a change in dimensional time of 9.4 seconds), the leading upstream propagating soliton travels at a speed (after converting back

Figure 4.6: A frame of video taken of the experimental setup described in this section. An obstacle 0.6 cm in height and 4.5 cm wide is towed at the bottom of 5.3 cm of water at a rate of 48.61 cm per second. Disturbances in the shape of solitary waves were observed propagating ahead of the obstacle.

to dimensional units) of 0.32 meters per second and the second soliton at a speed of 0.30 meters per second. At these time values the spacing of the solitons (in dimensional units) is 0.64 meters and 0.78 meters (respectively). From nondimensional time values $t = 252$ to $t = 300$ (a change in dimensional time of approximately 3 seconds) the distance between the leading two solitons corresponds to 74 cm and 78 cm.

Using the prediction in (2.29), we expect a new soliton to be generated every 6.3 seconds, with amplitude 3.7 cm (double the expected shock amplitude (2.18) in the hydraulic approximation (1.16)). An exact soliton solution to the free KdV equation (1.14) of this amplitude would travel at 25 cm per second. Thus we might expect solitons to be 160 cm apart.
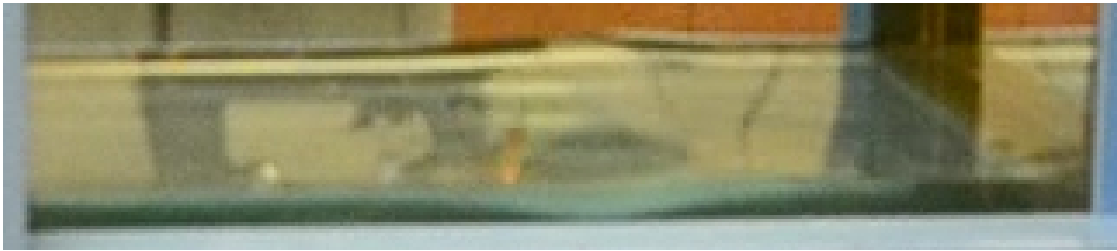

Figure 4.7: Zoomed in image of a single solitary wave. Wave generated in the experiment were of small amplitude but clearly observable through distortions in the image reflected off of the surface of the fluid.

80
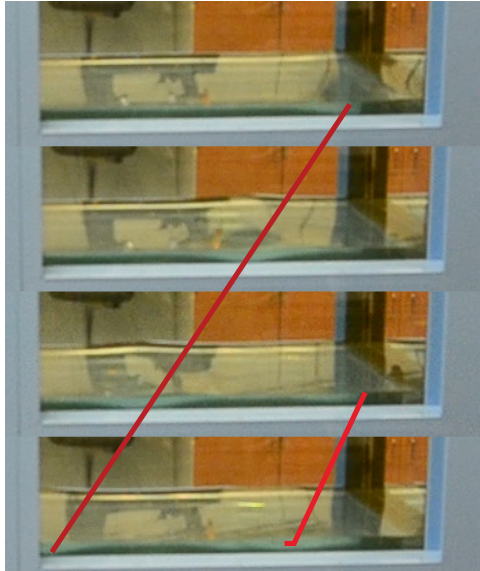
Figure 4.8: Zoomed in images of a single panel of the wave tank. Moving down the column shows the passage of a single solitary wave across the entire panel.

ETD-RK4 KdV SOURCE CODE

```cpp
// #include "DTSource.h"
#include "DTSaveError.h"

#include "DTArguments.h"
#include "DTDataFile.h"
#include "DTDictionary.h"
#include "DTPlot1D.h"
#include "DTProgress.h"
#include "DTSeriesGroup.h"

//////////////////////////////////////
//    DT_RetGroup
//////////////////////////////////////

struct DT_RetGroup {
    DTPlot1D full;
    DTPlot1D lin;
    DTPlot1D burg;

    void pinfo(void) const;
    void pinfoIndent(string) const;

    static void WriteStructure(DTDataStorage &,string);
};

void DT_RetGroup::pinfo(void) const
{
```

```
        pinfoIndent ("");
}


void DT_RetGroup :: pinfoIndent ( string pad ) const
{
        cerr << pad << " full = ";  full . pinfo ();
        cerr << pad << " lin = ";  lin . pinfo ();
        cerr << pad << " burg = ";  burg . pinfo ();
}


void DT_RetGroup :: WriteStructure ( DTDataStorage &output , string name )
{
        output . Save (" full " , name+" _1N ");
        output . Save (" Plot1D " , name+" _1T ");

        output . Save (" lin " , name+" _2N ");
        output . Save (" Plot1D " , name+" _2T ");

        output . Save (" burg " , name+" _3N ");
        output . Save (" Plot1D " , name+" _3T ");

        output . Save (3 , name+" _N ");
        output . Save (" Group " , name );
}


extern  void  Write ( DTDataStorage &, string  name , const  DT_RetGroup &);


void  Write ( DTDataStorage &output , string  name , const  DT_RetGroup &var )
{
```

```
    Write(output,name+"_full",var.full);

    Write(output,name+"_lin",var.lin);

    Write(output,name+"_burg",var.burg);

    Write(output,name,DTDoubleArray());

    // So that DataTank can see the variable.

}


////////////////////////////////////////
//      Main routine
////////////////////////////////////////


void Computation(int M,int N,double dt,double tmax,int stride,
                 DTSeriesGroup<DT_RetGroup> &computed);


int main(int argc,const char *argv[])
{
    DTSetArguments(argc,argv);


    DTDataFile inputFile("Input.dtbin",DTFile::ReadOnly);

    DTDataFile outputFile("Output.dtbin",DTFile::NewReadWrite);

    // Input variables.

    int M = int(inputFile.ReadNumber("M"));

    int N = int(inputFile.ReadNumber("N"));

    double dt = inputFile.ReadNumber("dt");

    double tmax = inputFile.ReadNumber("tmax");

    int stride = int(inputFile.ReadNumber("stride"));


    // Output series.

    DTSeriesGroup<DT_RetGroup> computed(outputFile,"Var");
```

```
if (DTArgumentIncludesFlag("saveInput"))
{ // Add -saveInput to the argument list to
// save the input in the output file.
    WriteOne(outputFile,"M",M);
    WriteOne(outputFile,"N",N);
    WriteOne(outputFile,"dt",dt);
    WriteOne(outputFile,"tmax",tmax);
    WriteOne(outputFile,"stride",stride);
}



// The computation.
clock_t t_before = clock();
Computation(M,N,dt,tmax,stride,computed);
clock_t t_after = clock();
double exec_time = double(t_after-t_before)/double(CLOCKS_PER_SEC);


// The execution time.
outputFile.Save(exec_time,"ExecutionTime");
outputFile.Save("Real Number","Seq_ExecutionTime");


// The errors.
DTSaveError(outputFile,"ExecutionErrors");
outputFile.Save("StringList","Seq_ExecutionErrors");


outputFile.SaveIndex();


return 0;
}
```

```
///////////////////////////////////
//     Computational routine
///////////////////////////////////

void Computation(int M, int N, double dt, double tmax, int stride,
                 DTSeriesGroup<DT_RetGroup> &computed);




///////////////////////////////////
//     Computational routine
///////////////////////////////////

#include <cmath>
#include <iostream>
#include <complex>
#include <iterator>
#include <vector>
#include <fstream>
#include <string>
#include <cstdio>
#include <ctime>
#include <sstream>

using namespace std;


typedef complex<double> cx;
```

```
void KCfft(cx [], cx []);
void KCifft(cx [], cx []);
void flux(double [], double []);
void dFlux(double [], double []);
void KurgTadm(double, double [], cx [], double []);
void minmod(double [], double[], double []);


const int N = 512;
const int m = log2(N);
const int nplots = 50;
const cx J = cx(0,1);


// Forcing parameters
double pm = 0.25;                    // forcing amplitude
double xi = 0.3;


// KdV equation parameters
double alpha = alphaIn.0 * 0.001;    // nonlinearity
double eps = epsIn.0 * 0.001;        // dispersion
double Fr = froudeIn.0 * 0.01;       // Froude number


#include "DTDoubleComplexArray.h"
#include "DTArray.h"


inline DTDoubleComplex conj(const DTDoubleComplex &c)
{return DTDoubleComplex(c.real,-c.imag);}


DTPlot1D ConvertToPlot(const double *x,const cx *y,int N);
DTPlot1D ConvertToPlot(const double *x,const double *y,int N);
```

```
DTPlot1D ConvertToPlot(const double *x,const cx *y,int N)
{
    DTMutableDoubleArray returnArray(2,N+1);
    returnArray(0,0) = 0;
    returnArray(1,0) = N;
    int i;
    for (i=0;i<N;i++) {
        returnArray(0,i+1) = x[i];
        returnArray(1,i+1) = real(y[i]);
    }


    return DTPlot1D(returnArray);
}


DTPlot1D ConvertToPlot(const double *x,const double *y,int N)
{
    DTMutableDoubleArray returnArray(2,N+1);
    returnArray(0,0) = 0;
    returnArray(1,0) = N;
    int i;
    for (i=0;i<N;i++) {
        returnArray(0,i+1) = x[i];
        returnArray(1,i+1) = y[i];
    }


    return DTPlot1D(returnArray);
}
```

```
void Computation(int M, int N, double dt, double tmax, int stride,
                 DTSeriesGroup<DT_RetGroup> &computed)
{
    DTProgress progress;

    std::clock_t start;
    double duration;

    start = clock();

    // spatial domain info
    double xmax = 400.0;    // domain length
    double dx = xmax/N;        // spatial step size
    double x[N];                // spatial domain

    // loop to assign values to spatial domain
    for (int i=0; i<N; ++i)
        x[i] = (i+1)*dx - xmax/2;

    // frequency domain info
    cx *k = new cx[N];                    // frequency domain
    // loops to assign values to frequency domain
    for (int i=0; i <= N/2; i++)
        k[i] = i*(2*M_PI/xmax);
    for (int i=-N/2+1; i <= -1; i++)
        k[i+N] = i*(2*M_PI/xmax);

    // time info
    double t = 0.0;          // initial time value
```

```
// declare variables for surface elevation
// and forcing with their Fourier transforms
cx *u = new cx[N];
cx *u_hat = new cx[N];
cx *forcing = new cx[N];
cx *f_hat = new cx[N];
cx *u_lin = new cx[N];
cx *u_lin_hat = new cx[N];
double u_burg[N];


DT_RetGroup state;


// zero initial condition
for (int i=0; i<N; i++){
    u[i] = 0.0;
    u_lin[i] = 0.0;
    u_burg[i] = 0.0;
}


state.full = ConvertToPlot(x,u,N);
state.lin = ConvertToPlot(x,u_lin,N);
state.burg = ConvertToPlot(x,u_burg,N);
computed.Add(state,0);


// fft of initial condition
KCfft(u, u_hat);
KCfft(u_lin, u_lin_hat);
```

```cpp
// loop to assign values to derivative of forcing function f
for (int i=0; i<N; i++) {
    forcing[i] = -2.0*pm*xi*pow(1/cosh(xi*x[i]),2)*tanh(xi*x[i]);
}


KCfft(forcing, f_hat); // fft of derivative of forcing function


cout << "alpha = " << alpha << ", epsilon = " << eps
<< ", Froude = " << Fr << ", dt = " << dt;
cout << ", pm = " << pm << ", xi = " << xi;//
<< ", osc_amp = " << osc_amp << ", omega = " << omega;
cout <<
", f_x(x) = -2.0*pm*xi*pow(1/cosh(xi*x[i]),2)*tanh(xi*x[i])\n\n";


cx L[N], E[N], E2[N];
for (int i=0; i<N; i++) {
    L[i] = J*k[i]*(1-Fr) - eps/6*J*pow(k[i],3);
    E[i] = exp(dt*L[i]);
    E2[i] = exp(dt*L[i]/2.);
}


const int M = 64;           // no. of points for complex means
cx r[M], mean, f1[N], f2[N], f3[N];
double Q[N];
DTMutableArray<cx> LR(N,M);


for (int i=0; i<M; i++) {
```

```cpp
        // roots of unity
        r[i] = exp(J*M_PI*((double)(i+1.)-.5)/(double)M);


        for (int j=0; j<N; j++) {
            LR(j,i) = dt*conj(L[j]) + r[i];
        }
    }


    cx LRjii;
    double scale = 1.0/(double)M;
    for (int j=0; j<N; j++) {
        mean = 0;
        for (int ii=0; ii<M; ii++)
            mean += (exp(LR(j,ii)/2.0)-1.0)/LR(j,ii);


        mean = mean/(double)M;


        Q[j] = dt * real(mean);


        mean = 0;
        for (int ii=0; ii<M; ii++) {
            LRjii = LR(j,ii);
            mean += (-4.-LRjii+exp(LRjii)*(4.-3.*LRjii+LRjii*LRjii))
            /pow(LRjii,3)*scale;
        }
        f1[j] = dt * real(mean);


        mean = 0;
        for (int ii=0; ii<M; ii++) {
```

```
            LRjii = LR(j,ii);
            mean += (2.+LRjii+exp(LRjii)*(-2.+LRjii))
            /pow(LRjii,3)*scale;
        }
        f2[j] = dt * real(mean);


        mean = 0;
        for (int ii=0; ii<M; ii++) {
            LRjii = LR(j,ii);
            mean += (-4.-3.*LRjii-pow(LRjii,2)+exp(LRjii)*(4.-LRjii))
            /pow(LRjii,3)*scale;
        }
        f3[j] = dt * real(mean);

}


// data for y axis of waterfall plot
double tdata[nplots+1];
tdata[0] = t;
// declare variables to calculate and store
// result of full and linearized KdV
cx uu[nplots+1][N], g[N], non[N], a[N], b[N], c[N], Na[N], Nb[N];
cx uu_lin[nplots+1][N], Nc[N];
// declare variables to calculate and
// store result of dispersionless case
double uu_burg[nplots+1][N];
double eff1[N], eff2[N], eff3[N], eff4[N], place_hold[N];



for (int i=0; i<N; i++) {
```

```
        g[i] = 3.0/4.0*alpha*J*k[i];
}


double filter = floor(N/3);
if (fmod(filter,2)==0)
    filter = filter − 1;


// Main time stepping loop
int iteration = 0;
while (t<tmax){
    t = t + dt;        // update time variable
    iteration++;



    //Filter
    for (int j=N/2+1−(filter −1)/2−1; j<=N/2+(filter −1)/2; j++)
        u_hat[j] = 0;


    KCifft(u_hat,u);



    for (int j=0; j<N; j++)
        u[j] = pow(real(u[j]),2);
    KCfft(u, non);
    for (int j=0; j<N; j++)
        non[j] = g[j] * non[j] + f_hat[j];


    for (int j=0; j<N; j++)
        a[j] = E2[j] * u_hat[j] + Q[j] * non[j];
```

```
KCifft (a, u);
for (int j=0; j<N; j++)
    u[j] = pow(real(u[j]),2);
KCfft(u,Na);
for (int j=0; j<N; j++)
    Na[j] = g[j] * Na[j] + f_hat[j];


for (int j=0; j<N; j++)
    b[j] = E2[j]*u_hat[j] + Q[j]*Na[j];
KCifft (b, u);
for (int j=0; j<N; j++)
    u[j] = pow(real(u[j]),2);
KCfft(u,Nb);
for (int j=0; j<N; j++)
    Nb[j] = g[j]*Nb[j] + f_hat[j];


for (int j=0; j<N; j++)
    c[j] = E2[j]*a[j] + Q[j]*(2.0*Nb[j]-non[j]);
KCifft (c, u);
for (int j=0; j<N; j++)
    u[j] = pow(real(u[j]),2);
KCfft(u,Nc);
for (int j=0; j<N; j++)
    Nc[j] = g[j]*Nc[j] + f_hat[j];


for (int j=0; j<N; j++)
    u_hat[j] = E[j]*u_hat[j] + non[j]*f1[j]
        + 2.0*(Na[j]+Nb[j])*f2[j] + Nc[j]*f3[j];
```

```
KCifft(u_hat,u);




// Solving the linear problem (i.e. g = 0)
// filter
for (int j=N/2+1-(filter-1)/2-1; j<=N/2+(filter-1)/2; j++)
    u_lin_hat[j] = 0;
KCifft(u_lin_hat,u_lin);


for (int j=0; j<N; j++){
    u_lin[j] = pow(real(u_lin[j]),2);
    non[j] = f_hat[j];
}


for (int j=0; j<N; j++)
    a[j] = E2[j] * u_lin_hat[j] + Q[j] * non[j];
KCifft(a,u_lin);
for (int j=0; j<N; j++){
    u_lin[j] = pow(real(u_lin[j]),2);
    Na[j] = f_hat[j];
}


for (int j=0; j<N; j++)
    b[j] = E2[j]*u_lin_hat[j] + Q[j]*Na[j];
KCifft(b,u_lin);
for (int j=0; j<N; j++){
    u_lin[j] = pow(real(u_lin[j]),2);
    Nb[j] = f_hat[j];
```

```
}

for ( int  j=0;  j<N;  j++)
    c [ j ]  =  E2 [ j ]∗ a [ j ]  +  Q[ j ]∗ ( 2.0 ∗Nb[ j]−non [ j ] ) ;
KCifft ( c , u_lin ) ;
for ( int  j=0;  j<N;  j++){
    u_lin [ j ]  =  pow( real ( u_lin [ j ] ) , 2 ) ;
    Nc[ j ]  =  f_hat [ j ] ;
}

for ( int  j=0;  j<N;  j++)
    u_lin_hat [ j ]  =  E[ j ]∗ u_lin_hat [ j ]
        +  non [ j ]∗ f1 [ j ]  +  2.0 ∗(Na[ j]+Nb[ j ] ) ∗ f2 [ j ]  +  Nc[ j ]∗ f3 [ j ] ;

KCifft ( u_lin_hat , u_lin ) ;

// Solving  the  dispersionless  problem
KurgTadm(dx , u_burg , forcing , eff1 ) ;
for ( int  j=0;  j<N;  j++)
    place_hold [ j ]  =  u_burg [ j ]  +  dt /2.0  ∗  eff1 [ j ] ;
KurgTadm(dx , place_hold , forcing , eff2 ) ;
for ( int  j=0;  j<N;  j++)
    place_hold [ j ]  =  u_burg [ j ]  +  dt /2.0  ∗  eff2 [ j ] ;
KurgTadm(dx , place_hold , forcing , eff3 ) ;
for ( int  j=0;  j<N;  j++)
    place_hold [ j ]  =  u_burg [ j ]  +  dt∗ eff3 [ j ] ;
KurgTadm(dx , place_hold , forcing , eff4 ) ;
```

```
        for (int j=0; j<N; j++)
            u_burg[j] = u_burg[j]
                + dt/6.0 * (eff1[j] + 2.0*eff2[j]
                + 2.0*eff3[j] + eff4[j]);



        if (iteration%stride==0) {
            state.full = ConvertToPlot(x,u,N);
            state.lin = ConvertToPlot(x,u_lin,N);
            state.burg = ConvertToPlot(x,u_burg,N);
            computed.Add(state,t);

        }

    }



    duration = ( std::clock() - start ) / (double) CLOCKS_PER_SEC;


    std::cout<<"printf: "<< duration <<'\n';


}



//Kincaid & Cheney fft
void KCfft(cx zeta[], cx zeta_hat[])
{
    cx u, v, w = exp(-2*M_PI*J/ (double)N);
    cx Z[N], D[N];


    for (int k=0; k<N; k++)
```

```
{
    Z[k] = pow(w,k);

    zeta_hat[k] = zeta[k];

}


for (int n=0; n<m; n++)

{
    for (int k=0; k<pow(2.0,m-n-1); k++)

    {
        for (int j=0; j<pow(2.0,n); j++)

        {
            u = zeta_hat[(int)pow(2.0,n)*k+j];
            v = Z[j*(int)pow(2.0,m-n-1)]

                *zeta_hat[(int)pow(2.0,n)*k+(int)pow(2.0,m-1)+j];
            D[(int)pow(2.0,n+1)*k+j] = (u+v)/2.;
            D[(int)pow(2.0,n+1)*k+j+(int)pow(2.0,n)] = (u-v)/2.;

        }

    }
    for (int j=0; j<N; j++)

        zeta_hat[j] = D[j];

}


for(int n=0; n<N; n++)

    zeta_hat[n] *= N;

}
```

```
//Inverse fft
void KCifft(cx zeta_hat[], cx zeta[])
{
    cx u, v, w = exp(2*M_PI*J/(double)N);
    cx Z[N], D[N];


    for (int k=0; k<N; k++)
    {
        Z[k] = pow(w,k);
        zeta[k] = zeta_hat[k];
    }


    for (int n=0; n<m; n++)
    {
        for (int k=0; k<pow(2.0,m-n-1); k++)
        {
            for (int j=0; j<pow(2.0,n); j++)
            {
                u = zeta[(int)pow(2.0,n)*k+j];
                v = Z[j*(int)pow(2.0,m-n-1)]
                    *zeta[(int)pow(2.0,n)*k+(int)pow(2.0,m-1)+j];
                D[(int)pow(2.0,n+1)*k+j] = (u+v)/2.;
                D[(int)pow(2.0,n+1)*k+j+(int)pow(2.0,n)] = (u-v)/2.;
            }
        }
        for (int j=0; j<N; j++)
            zeta[j] = D[j];
    }
```

```
}




// Kurganov Tadmor scheme for numerically capturing propagating shocks
void KurgTadm(double dx, double u[], cx force[], double kt[])
{
    double a[N], b[N], c[N], dm[N], dp[N], u_x[N], u_plus[N];
    double u_minus[N], x;


    a[0] = (u[0] - u[N-1])/dx;
    b[N-1] = (u[0] - u[N-1])/dx;
    for(int i=1; i<N; i++){
        a[i] = (u[i] - u[i-1])/dx;
        b[i-1] = (u[i]-u[i-1])/dx;
    }


    minmod(a,b,u_x);


    for (int i=0; i<N; i++){
        u_plus[i] = u[i] - dx/2.0*u_x[i];
        u_minus[i] = u[i]+dx/2.0*u_x[i];
    }


    x = u_minus[N-1];
    for (int i=N-1; i>0; i--)
        u_minus[i] = u_minus[i-1];
```

```
u_minus[0] = x;


dFlux(u_minus, dm);
dFlux(u_plus, dp);


//spectral radius of the Jacobian of F(u)
for (int i=0; i<N; i++)
    a[i] = !(abs(dm[i])>abs(dp[i])) ? abs(dp[i]):abs(dm[i]);


b[N-1] = u_plus[0];
for (int i=0; i<N-1; i++)
    b[i] = u_plus[i+1];


flux(b,u_x);


b[N-1] = u_minus[0];
for (int i=0; i<N-1; i++)
    b[i] = u_minus[i+1];


flux(b,c);


for (int i=0; i<N; i++)
    u_x[i] = u_x[i] + c[i];


flux(u_plus,c);


for (int i=0; i<N; i++)
    u_x[i] = u_x[i] - c[i];
```

```
flux (u_minus, c);


for (int i=0; i<N; i++){
    u_x[i] = u_x[i] - c[i];
    u_x[i] = -u_x[i]/(2.0*dx);
}


b[N-1] = u_minus[0];
c[N-1] = u_plus[0];
b[N-1] = c[N-1] - b[N-1];
for (int i=0; i<N-1; i++){
    b[i] = u_minus[i+1];
    c[i] = u_plus[i+1];
    b[i] = c[i] - b[i];
}


c[N-1] = a[0];
b[N-1] = b[N-1]*c[N-1];
for (int i=0; i<N-1; i++){
    c[i] = a[i+1];
    b[i] = b[i]*c[i];
}


for (int i=0; i<N; i++){
    a[i] = a[i]*(u_plus[i] - u_minus[i]);
    b[i] = (b[i] - a[i])/(2.0*dx);
    kt[i] = u_x[i] + b[i] + real(force[i]);
}
}
```

```
// Minmod
void minmod(double a[], double b[], double u[])
{
    double c, d;

    for (int i=0; i<N; i++){
        if (a[i] == 0)
            c = 0;
        else
            c = a[i]/abs(a[i]);
        if (b[i] == 0)
            d = 0;
        else
            d = b[i]/abs(b[i]);
        u[i] = ((c)+(d))/2.0
            *(!(abs(b[i])<abs(a[i]))?abs(a[i]):abs(b[i]));
    }
}



// Flux
```

```
void flux(double f[], double y[])
{
    for (int i=0; i<N; i++)
        y[i] = (Fr - 1)*f[i] - 3.0*alpha*pow(f[i],2)/4.0;
}




// dFlux
void dFlux(double f[], double y[])
{
    for (int i=0; i<N; i++)
        y[i] = (Fr - 1) - 3.0*alpha*f[i]/2.0;
}
```

REFERENCES

[1] Carl M Bender and Steven A Orszag. *Advanced mathematical methods for scientists and engineers I: Asymptotic methods and perturbation theory.* Springer Science & Business Media, 2013.

[2] R Camassa and T Yao-tsu Wu. Stability of forced steady solitary waves. *Phil. Trans. R. Soc. Lond. A*, 337(1648):429–466, 1991.

[3] Steven M Cox and Paul C Matthews. Exponential time differencing for stiff systems. *Journal of Computational Physics*, 176(2):430–455, 2002.

[4] Gr Dagan and MP Tulin. Two-dimensional free-surface gravity flow past blunt bodies. *Journal of Fluid Mechanics*, 51(3):529–543, 1972.

[5] Arnaud Debussche and Jacques Printems. Effect of a localized random forcing term on the korteweg-de vries equation. *Journal of Computational Analysis and Applications*, 3(3):183–206, 2001.

[6] GA El, RHJ Grimshaw, and NF Smyth. Transcritical shallow-water flow past topography: finite-amplitude theory. *Journal of Fluid Mechanics*, 640:187–214, 2009.

[7] GA El, Roger HJ Grimshaw, and Noel F Smyth. Unsteady undular bores in fully nonlinear shallow-water theory. *Physics of Fluids*, 18(2):027104, 2006.

[8] Lawrence K Forbes. Free-surface flow over a semicircular obstruction, including the influence of gravity and surface tension. *Journal of Fluid Mechanics*, 127:283–297, 1983.

[9] S Grandison and J-M Vanden-Broeck. Truncation approximations for gravity-capillary free-surface flows. *Journal of engineering mathematics*, 54(1):89, 2006.

[10] RHJ Grimshaw and N Smyth. Resonant flow of a stratified fluid over topography. *Journal of Fluid Mechanics*, 169:429–464, 1986.

[11] TH Havelock. The method of images in some problems of surface waves. *Proceedings of the Royal Society of London. Series A, Containing Papers of a Mathematical and Physical Character*, 115(771):268–280, 1927.

[12] TH Havelock. The vertical force on a cylinder submerged in a uniform stream. *Proceedings of the Royal Society of London. Series A, Containing Papers of a Mathematical and Physical Character*, 122(790):387–393, 1929.

[13] Motonori Hirata, Shinya Okino, and Hideshi Hanazaki. Numerical simulation of capillary gravity waves excited by an obstacle in shallow water. *Proceedings of the Estonian Academy of Sciences*, 64(3):278, 2015.

[14] Aly-Khan Kassam and Lloyd N Trefethen. Fourth-order time-stepping for stiff pdes. *SIAM Journal on Scientific Computing*, 26(4):1214–1233, 2005.

[15] Alexander Kurganov and Eitan Tadmor. New high-resolution central schemes for nonlinear conservation laws and convection–diffusion equations. *Journal of Computational Physics*, 160(1):241–282, 2000.

[16] Horace Lamb. *Hydrodynamics*. Cambridge university press, 1932.

[17] Seung-Joon Lee, George T Yates, and T Yaotsu Wu. Experiments and analyses of upstream-advancing solitary waves generated by moving disturbances. *Journal of Fluid Mechanics*, 199:569–593, 1989.

[18] PA Milewski and J-M Vanden-Broeck. Time dependent gravity-capillary flows past an obstacle. *Wave Motion*, 29(1):63–79, 1999.

[19] Frédéric Moisy, Marc Rabaud, and Kévin Salsac. A synthetic schlieren method for the measurement of the topography of a liquid interface. *Experiments in Fluids*, 46(6):1021, 2009.

[20] Alan C Newell. *Solitons in mathematics and physics*, volume 48. Siam, 1985.

[21] DH Peregrine. Interaction of water waves and currents. In *Advances in applied mechanics*, volume 16, pages 9–117. Elsevier, 1976.

[22] NF Smyth. Modulation theory solution for resonant flow over topography. *Proc. R. Soc. Lond. A*, 409(1836):79–97, 1987.

[23] EO Tuck. The effect of non-linearity at the free surface on flow past a submerged cylinder. *Journal of Fluid Mechanics*, 22(2):401–414, 1965.

[24] Gerald Beresford Whitham. *Linear and nonlinear waves*, volume 42. John Wiley & Sons, 2011.

[25] T Yao-Tsu Wu. Generation of upstream advancing solitons by moving disturbances. *Journal of fluid mechanics*, 184:75–99, 1987.